AUBURN

SAMUEL GINN
COLLEGE OF ENGINEERING

Research Report

CRACKING TENDENCY OF LIGHTWEIGHT CONCRETE

Submitted to

The Expanded Shale, Clay, and Slate Institute

Prepared by

Benjamin E. Byard and Anton K. Schindler

DECEMBER 2010

Highway Research Center
Harbert Engineering Center
Auburn, Alabama 36849

www.eng.auburn.edu/research/centers/hrc.html

Report No.	2. Government Accession No.	Recipient Catalog No.
Title and Subtitle Cracking Tendency of Lightweight Concrete		**Report Date** December 2010 **Performing Organization Code**
Author(s) Benjamin E. Byard and Anton K. Schindler		**8. Performing Organization Report No.**
Performing Organization Name and Address Highway Research Center 238 Harbert Engineering Center Auburn University, AL 36830		**Work Unit No. (TRAIS)** **Contract or Grant No.**
Sponsoring Agency Name and Address The Expanded Shale, Clay, and Slate Institute 230E Ohio Street, Suite 400 Chicago, IL 60611-3265		**Type of Report and Period Covered** Technical Report **Sponsoring Agency Code**

Supplementary Notes

Abstract

Early-age cracking in bridge decks is a severe problem that may reduce functional life of the structure. In this project, the effect of using lightweight aggregate on the cracking tendency of bridge deck concrete was evaluated by cracking frame testing techniques. Cracking frames measure the development of stresses due to thermal and autogenous shrinkage effects from setting until the onset of cracking. Expanded shale, clay, and slate lightweight coarse and fine aggregates were used to produce internal curing, sand-lightweight, and all-lightweight concretes to compare their behavior relative to a normalweight concrete in a bridge deck application. Specimens were tested under isothermal curing conditions and match-cured conditions that simulate summer and fall placement scenarios.

Increasing the amount of pre-wetted lightweight aggregate in the concrete systematically decreases the density, modulus of elasticity, coefficient of thermal expansion, and thermal diffusivity of the concrete. The use of pre-wetted lightweight aggregates in concrete can reduce or eliminate the stress development caused by autogenous shrinkage. The decrease in autogenous stresses is due to internal curing, because water is desorbed from the lightweight aggregates to fill capillary voids formed by chemical shrinkage. When compared to a normalweight control concrete, the use of lightweight aggregates in concrete effectively delays the occurrence of cracking at early ages in bridge deck applications.

Key Words	Distribution Statement		
Concrete bridge deck, cracking, lightweight aggregate, internal curing, internal curing, cracking tendency, coefficient of thermal expansion.	No restrictions.		
Security Classification (of this report) Unclassified	**Security Classification (of this page)** Unclassified	**No. of pages** 82	**Price**

Form DOT F 1700.7 (8-72)

Research Report

Cracking Tendency of Lightweight Concrete

Prepared by:
Benjamin E. Byard
Anton K. Schindler

Highway Research Center
and
Department of Civil Engineering
at
Auburn University

December 2010

DISCLAIMERS

The contents of this report reflect the views of the authors, who are responsible for the facts and the accuracy of the data presented herein. The contents do not necessarily reflect the official views or policies of Auburn University. This report does not constitute a standard, specification, or regulation.

NOT INTENDED FOR CONSTRUCTION, BIDDING, OR PERMIT PURPOSES

Anton K. Schindler, Ph.D., P.E.
Research Supervisor

ACKNOWLEDGEMENTS

The authors wish to express their gratitude to the Expanded Shale, Clay, and Slate Institute (ESCSI) for funding this research project. The authors appreciate the cement and chemical admixtures donated by TXI, Inc. and BASF Construction Chemicals, LLC, respectively. The authors would like to thank the following individuals for their cooperation and assistance towards this research effort:

John P. Ries	ESCSI, Cottonwood Heights, Utah
Kenneth S. Harmon	Carolina Stalite Company, Salisbury, North Carolina
Reid W. Castrodale	Carolina Stalite Company, Salisbury, North Carolina
Jody Wall	Carolina Stalite Company, Salisbury, North Carolina
Ernest Cubit	TXI, Inc., Houston, Texas
George Grygar	TXI, Inc., Sandy, Utah
Don Reeves	TXI, Inc., Houston, Texas
Andrew Mackie	Buildex, Inc., Ottawa, Kansas
Rickey Swancey	BASF Construction Chemicals, LLC, Birmingham, Alabama

ABSTRACT

Early-age cracking in bridge decks is a severe problem that may reduce functional life of the structure. In this project, the effect of using lightweight aggregate on the cracking tendency of bridge deck concrete was evaluated by cracking frame testing techniques. Cracking frames measure the development of stresses due to thermal and autogenous shrinkage effects from setting until the onset of cracking. Expanded shale, clay, and slate lightweight coarse and fine aggregates were used to produce internal curing, sand-lightweight, and all-lightweight concretes to compare their behavior relative to a normalweight concrete in a bridge deck application. Specimens were tested under isothermal curing conditions and match-cured conditions that simulate summer and fall placement scenarios.

Increasing the amount of pre-wetted lightweight aggregate in the concrete systematically decreases the density, modulus of elasticity, coefficient of thermal expansion, and thermal diffusivity of the concrete. The use of pre-wetted lightweight aggregates in concrete can reduce or eliminate the stress development caused by autogenous shrinkage. The decrease in autogenous stresses is due to internal curing, because water is desorbed from the lightweight aggregates to fill capillary voids formed by chemical shrinkage. When compared to a normalweight control concrete, the use of lightweight aggregates in concrete effectively delays the occurrence of cracking at early ages in bridge deck applications.

TABLE OF CONTENTS

LIST OF TABLES

LIST OF FIGURES

Chapter 1

Introduction

1.1 BACKGROUND

Early-age cracking of concrete bridge decks, typically caused by thermal effects, drying shrinkage, and autogenous shrinkage can have detrimental effects on long-term behavior and durability. Darwin and Browning (2008) recently reported that "by controlling early age cracking, the amount of cracking at later ages should remain low," and that early-age cracking can significantly increase the rate and amount of chloride penetration (from deicing salts), which may accelerate the corrosion rate of embedded reinforcing steel. Transverse cracking occurs in most geographical locations and climates, and in many types of bridge superstructures (Krauss and Rogalla 1996). The National Cooperative Highway Research Program (NCHRP) Report 380 (Krauss and Rogalla 1996) reported results of a survey sent to all U.S. Departments of Transportation (DOTs) and several transportation agencies overseas to evaluate the extent of deck cracking. Sixty-two percent of the responding agencies considered early-age transverse cracking to be problematic. A survey conducted by the Federal Highway Administration (FHWA) found that more than 100,000 bridges suffer from early-age cracking (FHWA 2008). Given the abundance of cracking observed in bridge decks, and the impact of early-age cracking on long-term performance and durability, it is imperative that bridge deck concrete be proportioned and placed to minimize early-age cracking.

Cracking of hardening concrete occurs when the induced tensile stress exceeds the tensile strength of the concrete. The development of in-place stresses is affected by the shrinkage, coefficient of thermal expansion, setting characteristics, restraint conditions, stress relaxation (creep-adjusted modulus of elasticity), and temperature history of the hardening concrete. The tensile strength (and strain capacity) increases as the hydration of the cementitious system progresses. The tensile strength is impacted by the cementitious materials, the water-cementitious materials ratio, the aggregate type and gradation, the degree of curing (internal/external) provided, and the temperature history of the hardening concrete. Quantification of many of the mechanisms mentioned above is quite complicated at early ages, and many of these variables have complex interactions.

In this project, the effect that the use of lightweight aggregate (LWA) has on the cracking tendency was evaluated by cracking frame testing techniques. Cracking frames can measure the development of stresses due to thermal and autogenous shrinkage effects from setting until cracking (Mangold 1998). The combined effect of modulus elasticity, creep/relaxation, coefficient of thermal expansion, thermal conductivity, autogenous shrinkage, and tensile strength on the

cracking potential in a specific application is thus directly captured and quantified by this unique test setup. Since the specimen is sealed against water loss, the effect of drying shrinkage is not measured with this setup.

A rigid cracking frame as developed by Dr. Rupert Springenschmid at the Technical University of Munich, Germany was utilized in this research project. The two rigid cracking frames used at Auburn University during this project are shown in Figure 1-1. These cracking frames were designed to produce restraint for 6 x 6 x 50 in. concrete specimens from placement to approximately 6 days. Each cracking frame consists of two crossheads and a pair of stiff Invar sidebars. The crossheads are designed to grip the concrete specimen while the sidebars provide restraint as the concrete hardens. The Invar bars are sized to provide approximately 80% restraint to movement for the hardened concrete and strain gauges are used to continuously measure the stress state in the concrete specimen as it hardens in the frame. The frame is designed to allow fresh concrete to be cast into temperature-controlled formwork within the frame. With this unique formwork, the concrete can be subjected to a variety of temperature profiles that simulate in-place conditions of bridge decks, elevated slabs, pavements, mass concrete structures, etc.

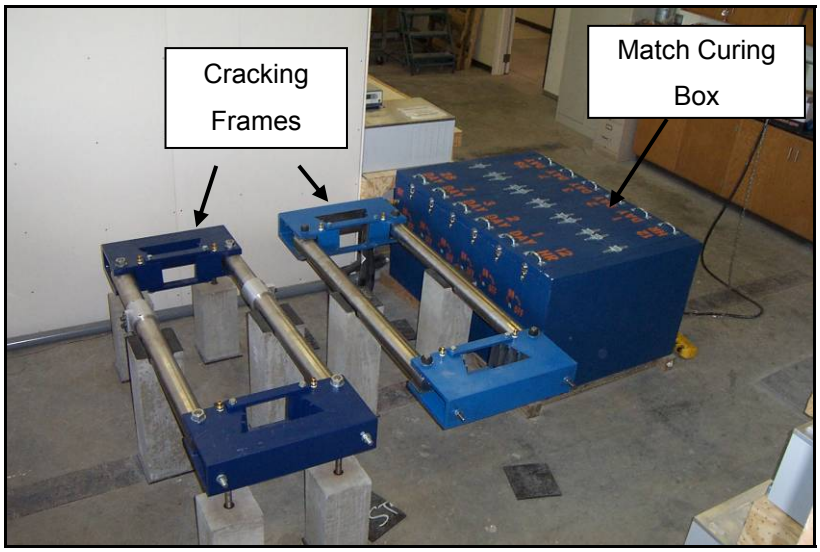

Figure 1-1: Test equipment to assess the cracking potential of concrete mixtures

Due to increased insulation ability of lightweight aggregate, its use in concrete mixtures has been reported to increase the temperature rise due to hydration measured during the construction of the New Benecia-Martinez Bridge (Maggenti 2007). This increase in temperature rise may not translate to increased thermal cracking risk, simply since thermal cracking risk is a function of the concrete strength and stress development. Lightweight concrete has a lower modulus of elasticity, lower coefficient of thermal expansion and provides internal curing to the

concrete and these characteristics may reduce the stress and counter the effects caused by its increased temperature development (Byard, Schindler, and Barnes 2010).

1.2 LIGHTWEIGHT AGGREGATES

Rotary kilns are commonly used to produce LWA under controlled conditions (Chandra and Berntsson 2002). Historically, LWA have been used to reduce the density of concrete. However, LWA can be used to alter more than just the density of concrete. Because lightweight aggregates have high absorption capacities when compared to conventional aggregates, they provide internally stored water that may become available, if needed. These internal water supplies can provide additional water for hydration as well as reduce the effects of self-desiccation and thus autogenous shrinkage effects (Henkensiefken 2008). Limited work has been done to determine cracking tendency of bridge deck concrete with lightweight aggregate. It is thus necessary to determine the effect of lightweight aggregate on the cracking tendency of bridge deck concrete.

1.3 PROJECT OBJECTIVES

The primary objective of the study documented in this report is to evaluate the influence of lightweight aggregates on the development of stresses and the occurrence of cracking at early ages for bridge deck concrete. The primary objectives of the research described in this report are as follows:

- Develop and evaluate the cracking tendency of three types of lightweight aggregate bridge deck concretes relative to a typically used normalweight concrete mixture,
- Evaluate the effect of placement and curing temperature on the cracking tendency of concrete,
- Evaluate the modulus of elasticity, splitting tensile strength, compressive strength, coefficient of thermal expansion, and thermal diffusivity of lightweight concretes and determine their effect on the early-age cracking tendency,
- Evaluate the effect of three different source aggregates (shale, clay, and slate) on the development of mechanical properties and the cracking tendency of bridge deck concrete, and
- Determine the effectiveness of pre-wetted lightweight aggregate to provide internal curing moisture to mitigate autogenous stress development.

Secondary objectives of this study include:

- Compare the measured modulus of elasticity values to those estimated by the expression recommended by ACI 318 (2008) and the AASHTO LRFD Bridge Design Specifications (2007), and

- Compare the measured splitting tensile strength to those estimated by the expression recommended by ACI 207.2R (1995) and ACI 207.1R (1996), and evaluate the applicability of the ACI 318 (2008) lambda coefficient.

1.4 RESEARCH APPROACH

The cracking tendency of the concrete mixtures was determined using rigid cracking frame testing techniques. Three lightweight aggregate sources were evaluated by producing three different concretes with each of these lightweight aggregates and one concrete mixture with normalweight aggregate. Each concrete mixture was subjected to two types of controlled temperature histories while measuring the stress development from setting until the onset of cracking. To assess the effect of placing temperature, each mixture was placed at summer and fall placement conditions. Match-cured concrete cylinders were produced to determine the development of mechanical properties of each concrete mixture under various controlled temperature histories. The effect of the supplied internal curing water from lightweight aggregate was assessed by measuring the restrained stress development of concrete specimens cured under isothermal conditions. In addition, the coefficient of thermal expansion of the hardened concrete was assessed.

1.5 REPORT OUTLINE

A summary of literature reviewed pertaining to early-age cracking, lightweight aggregates, properties of lightweight aggregate concrete, autogenous shrinkage, internal curing, and methods to assess early-age concrete behavior is presented in Chapter 2. The experimental testing program used to assess the early-age stress development of concrete is presented in Chapter 3. In addition, Chapter 3 contains the method used to model bridge deck temperatures, and the methods used to assess the fresh and hardened properties of the lightweight and normalweight concretes. The properties of the lightweight aggregates and the other raw materials are also presented in Chapter 3. The results of the experimental work performed for this project are presented in Chapter 4. A discussion and synthesis of the results are presented in Chapter 5. Conclusions and recommendations resulting from the work documented in this report are presented in Chapter 6.

Chapter 2

Literature Review

The results of a literature review of early-age cracking, autogenous shrinkage, chemical shrinkage, lightweight aggregate production, and lightweight aggregate properties are presented in this chapter. In addition, internal curing and methods for proportioning lightweight aggregate for internal curing purposes in concrete are reviewed in this chapter. Finally, test methods to assess early-age concrete behavior are reviewed and are presented herein.

2.1 EARLY-AGE CRACKING

2.1.1 Thermal Effects

The development of thermal stresses can be calculated using the expression presented in Equation 2-1. For an accurate estimate of thermal stress, creep effects during early ages and over the structure's life should be accounted for in Equation 2-1 (Schindler and McCullough 2002).

$$\text{Thermal Stress} = \sigma_T = \Delta T \times \alpha_t \times E_c \times K_r \quad \text{. . . . . Equation 2-1}$$

where,
- ΔT = temperature change = $T_{zero\text{-}stress}$ - T_{min} (°F),
- α_t = coefficient of thermal expansion (strain/°F),
- E_c = creep-adjusted modulus of elasticity (lb/in^2),
- K_r = degree of restraint factor,
- $T_{zero\text{-}stress}$ = concrete zero-stress temperature (°F), and
- T_{min} = minimum concrete temperature (°F).

An illustration of the development of concrete temperatures and thermal stresses over time under summer placement conditions for freshly placed concrete is presented in Figure 2-1. In terms of stress development, the final-set temperature is the temperature at which the concrete begins to resist stresses that result from the restraint of external volume changes. In Figure 2-1, it can be seen that hydration causes the concrete temperature to increase beyond the setting temperature, time (A). Because the expansion of the concrete caused by the temperature rise is restrained, the concrete will be in compression when the peak temperature, time (B), is reached. When the peak temperature is reached, the hydrating paste is still developing structure, its strength is low, and high amounts of early-age relaxation may occur when the concrete is subjected to high compressive stress (Emborg 1989). The phenomenon of gradual decrease in stress when a material is subjected to sustained strain is called stress relaxation (Mehta and Monteiro 2006).

As the concrete temperature subsequently decreases, the compressive stress is gradually relieved until the stress condition changes from compression to tension, time (C). The temperature at which this transient stress-free condition occurs is denoted the "zero-stress temperature". Due to the effects of relaxation, the zero-stress temperature may be significantly higher than the final-set temperature (Emborg 1989). If tensile stresses caused by a further temperature decrease exceed the tensile strength of the concrete, cracking will occur, time (D). Because the thermal stress is proportional to the difference between the zero-stress temperature and the cracking temperature, thermal cracking can be minimized by decreasing the zero-stress temperature. This in turn can be accomplished by (1) minimizing the final-set temperature, (2) minimizing the peak temperature achieved during the high-relaxation phase, or (3) delaying the attainment of the peak temperature.

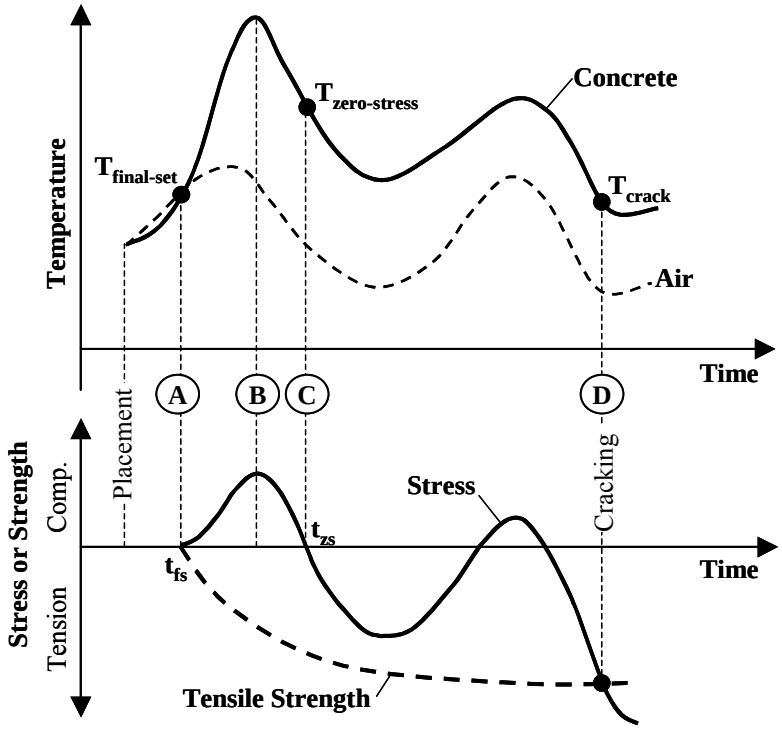

Figure 2-1: Development of early-age thermal stresses (Schindler and McCullough 2002)

2.1.2 Autogenous and Chemical Shrinkage Effects

The reaction products formed from cement hydration are smaller than the initial components. The reduction of the absolute volume of the reactants due to hydration is chemical shrinkage. Before setting, this phenomenon results in a volumetric change but generates no stress as the concrete is still plastic (Holt 2001). At setting, enough hydration products have formed to provide a self-supporting skeletal framework in the paste matrix. In between the framework of solids are water filled capillary voids. As water is consumed by the ongoing hydration process, the voids

empty and capillary tensile stresses are generated, which results in a volumetric shrinkage. The concrete volume change that occurs without moisture transfer to the environment and temperature change is called autogenous shrinkage. Before setting, chemical shrinkage and autogenous shrinkage are equal (Holt 2001). The addition of pre-wetted LWA helps mitigate stress due to autogenous stresses by desorbing water from the aggregate particles into the hydrated cement paste pore structure and relieving some or all of the capillary tension (Henkensiefken 2008). Generally, autogenous shrinkage and stress development is not a concern at water-cementitious materials (w/cm) ratios above 0.42 (Mindess, Young, and Darwin 2002; Mehta and Monteiro 2006).

Holt (2001) provided the graphic depiction in Figure 2-2 of the composition change of a sealed paste due to the cement hydration reactions, where C is the cement volume, W is the volume of water, H_y is the volume of the hydration products and V is the volume of voids. This figure relates how the autogenous shrinkage is a portion of the chemical shrinkage. After set, the chemical shrinkage is an internal volume reduction, whereas the autogenous shrinkage is an external volume change.

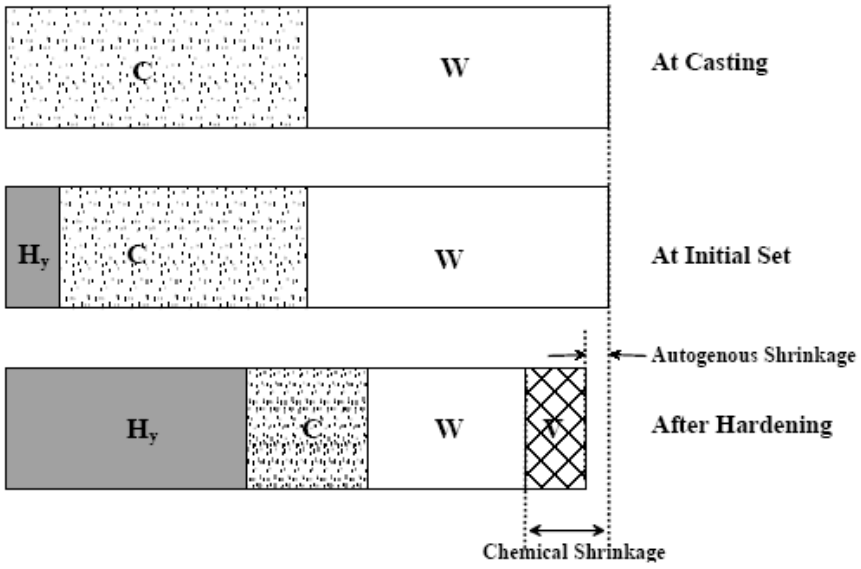

Figure 2-2: Volume reduction due to autogenous shrinkage (Holt 2001)

2.2 LIGHTWEIGHT AGGREGATE

LWA can be classified as natural or manufactured. Natural LWAs include pumice, scoria, and tuff. Most LWA used in concrete in the United State are manufactured. Manufacturing provides regional availability and more consistency than natural LWA (Chandra and Berntsson 2002). Manufactured LWA includes expanded shale, clay, and slate. In addition to manufactured LWA, some byproducts can serve as LWA including sintered fly ash, expanded slag, and bed ash.

2.2.1 Production

The manufacture of LWA by rotary kiln methods are produced as described in the ESCSI Reference Manual (ESCSI 2007) and illustrated in the flow diagram shown in Figure 2-3. The aggregate is collected from its source by mining in the case of harder materials like slate or shale or by scraping for softer materials like clays. The raw materials are then prepared for the kiln by crushing and sizing. Vibratory screens then size the crushed material. The material is then fed into the upper end of the rotary kiln and it travels down the kiln in 30-60 minutes. The travel time depends on the length, diameter, and rotational speed of the kiln. Kiln lengths vary from 60 to 225 ft with diameters of 6 to 12 ft. Heating of the material is gradual for the first 2/3 of the kiln length, but increases rapidly to the maximum in the last 1/3 of kiln length. Maximum kiln temperatures vary between 1920 and 2190 °F. The heating of the particle interiors cause gasses to be liberated. The plastic state of the material allows the gasses to form disconnected pores within the material and expansion occurs. As the expanded material cools, the pores remain giving the aggregate its relatively low density and increased ability to absorb water. The materials is then crushed and sieved to various sizes to obtain the desired gradations.

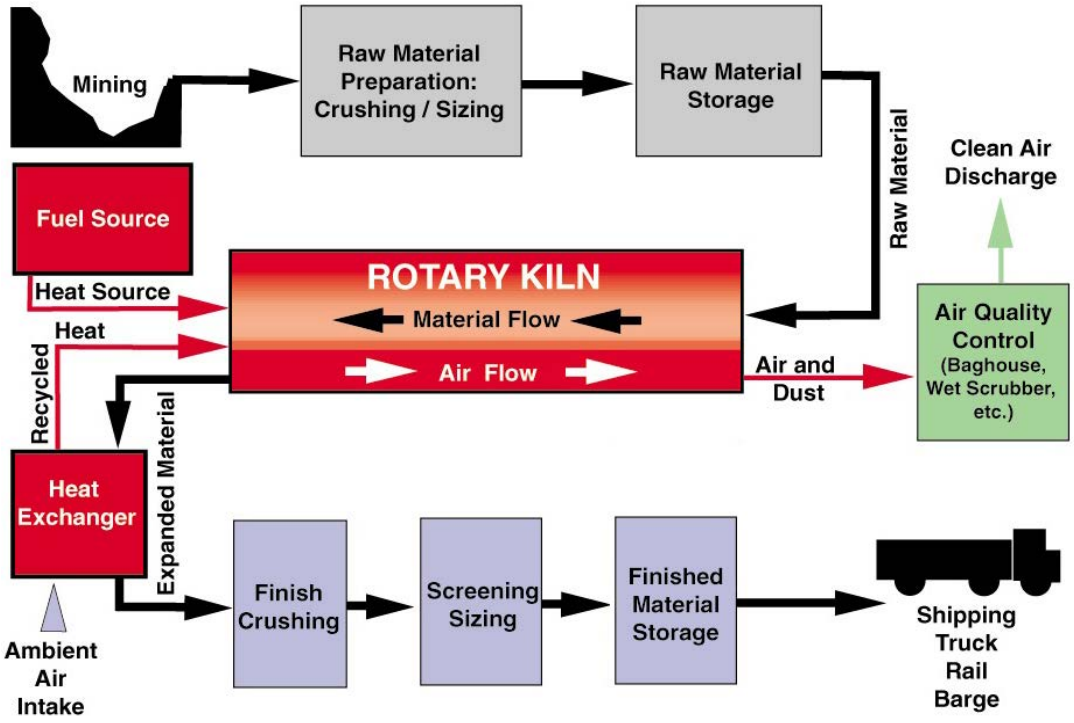

Figure 2-3: Production of rotary kiln lightweight aggregate (ESCSI 2007)

2.2.2 Properties

The impact of using LWA on concrete's coefficient of thermal expansion (α_t), modulus of elasticity, thermal conductivity, and tensile strength are discussed in this section.

2.2.2.1 Coefficient of Thermal Expansion

The coefficient of thermal expansion of concrete is primarily affected by the coefficient of thermal expansion of the aggregate, because the aggregate makes up the bulk of the concrete (Mindess, Young, and Darwin 2002). LWAs are reported to have a lower coefficient of thermal expansion compared to siliceous gravel; therefore, concrete made with LWA has a lower coefficient of thermal expansion than its siliceous normalweight counterpart (Mehta and Monteiro 2006).

2.2.2.2 Modulus of Elasticity

The modulus of elasticity of the concrete depends heavily on the stiffness of the aggregate (Mehta and Monteiro 2006). LWA has a lower modulus of elasticity because of its increased porosity. Consequently, lightweight concrete has lower modulus of elasticity compared to normalweight concrete (Mindess, Young, and Darwin 2002). Equation 2-2 (ACI 318 2008) can be used to estimate the modulus of elasticity from a known density and compressive strength. This expression indicates that the modulus of elasticity is directly proportional to the density to the 1.5 power and the square root of the compressive strength. This expression also reveals that the concrete's modulus of elasticity will decrease as more LWA is introduced into the mixture.

$$E_c = 33 w_c^{1.5} \sqrt{f_c} \quad \text{.....Equation 2-2}$$

where, E_c = modulus of elasticity (lb/in^2),

w_c = density of normal concrete or equilibrium density of lightweight concrete (lb/ft^3), and

f_c = concrete compressive strength (psi).

2.2.2.3 Thermal Conductivity

Due to LWA's increased porosity, it has a lower thermal conductivity or greater insulating ability compared to normalweight concrete (Mehta and Montero 2006; Mindess, Young, Darwin, 2002; Chandra and Berntsson 2002). Maggenti (2007) measured the temperature development in mass concrete piers, and concluded that LWA concrete has a greater temperature rise due to hydration compared to normalweight concrete with identical cementing materials, water, and fine aggregate contents.

2.2.2.4 Tensile Strength

Tensile strength of concrete develops due to the same factors as compressive strength; however, concrete's tensile strength is much lower than its compressive strength, due to ease of crack propagation under tensile stresses (Mindess, Young, and Darwin 2002). The rate of development and magnitude of the tensile strength play an important role in early-age cracking.

Aggregate characteristics influence the tensile strength of concrete (Mehta and Monteiro 2006). Aggregate texture has a substantial impact on the tensile strength of concrete. Concretes

with rough textured or crushed aggregates have been shown to have higher tensile strengths, especially at early ages, than smoother aggregates (Mehta and Monteiro 2006).

The Interfacial Transition Zone (ITZ) is formed when water films form around aggregate particles in the fresh concrete leading to an increased water to cement ratio in the hydrated paste surrounding the aggregate particles (Mehta and Monteiro 2006). The ITZ is primarily composed of the porous, weak, water-soluble calcium hydroxide (CH). The ITZ is the strength-limiting phase in concrete (Mehta and Monteiro 2006). LWAs have been shown to improve the quality of the ITZ, because of their slight pozzolanic surface, which consumes the CH, and their absorptive surface that reduces the water film around the aggregate (Chandra and Berntsson 2002).

Equation 2-3 (ACI 207.2R 1995) and Equation 2-4 (ACI 207.1R 1996) can be used to estimate the splitting tensile strength from a known compressive strength.

$$f_{ct} = 6.7\sqrt{f_c} \quad \text{.....Equation 2-3}$$

$$f_{ct} = 1.7(f_c)^{2/3} \quad \text{.....Equation 2-4}$$

where, f_{ct} = splitting tensile strength (psi), and

f_c = concrete compressive strength (psi).

ACI 318 (2008) provides a lightweight modification factor (λ), presented in Equation 2-5, as a multiplier of the square root of the design compressive strength (f'_c) in all applicable design equations. The AASHTO LRFD Bridge Design Specifications (AASHTO 2007) contains a similar approach to account for the effect lightweight aggregate on the concrete strength. For sand-lightweight and all-lightweight mixtures, λ is set equal to 0.85 and 0.75, respectively. Linear interpolation between 0.85 and 1.0 is permitted for mixtures with a blend of normalweight and lightweight coarse aggregate. If the splitting tensile strength of the lightweight concrete is known or specified, λ can be calculated as follows:

$$\lambda = \frac{f_{ct}}{6.7\sqrt{f'_c}} \quad \text{..... Equation 2-5}$$

where, λ = lightweight modification factor (unitless),

f_{ct} = splitting tensile strength (psi), and

f'_c = design compressive strength of concrete (psi).

2.3 INTERNAL CURING

Historically, LWA have been used to reduce the density of concrete. In recent years; however, LWAs have been added to concrete to take advantage of the high absorption capacity of the aggregates, which may provide internal water for hydration.

When cement hydrates, capillary pores are created. As the water in the capillary pores is consumed by continuing hydration or by atmospheric desiccation, the internal relative humidity decreases and stresses are induced. Pre-wetted high absorption particles can desorb water into the cement pore structure, thus reducing capillary stresses and providing water for hydration. The process of providing additional water for capillary pore stress reduction and additional cement hydration through pre-wetted particles is called *internal curing*.

High absorption materials such as perlite, wood pulp, super-absorbent particles (SAP), and LWA are some materials that have been used in concrete for internal curing purposes. Materials like perlite, wood pulp, and SAP provide no load carrying capacity in the concrete matrix, whereas LWA does have load carrying capacity. Because of LWA's structural performance and market availability, it is used more frequently as an internal curing material (Delatte et al. 2008).

Lightweight fine aggregates are generally used for internal curing purposes due to their greater dispersion compared to coarse aggregates. It has been shown that water from LWA can move 0.07 in. into paste around the aggregate particle (Henkensiefken 2008).

Bentz (Bentz, Lura, and Roberts 2005) provides a simplified method for proportioning lightweight fine aggregate for internal curing purposes as shown in Equation 2-6. The unit chemical shrinkage is calculated based on the composition of the cement and the densities of the hydration products is then normalized with water's density. The coefficients suggested by Bentz, Lura, and Roberts (2005) for chemical shrinkage due to cement hydration are presented in Table 2-1. The total chemical shrinkage is determined by using the cement content and maximum degree of hydration of the mixture. The maximum degree of hydration can be estimated as w/cm/0.36 if the w/cm is less than or equal to 0.36. For w/cm greater than 0.36, the maximum degree of hydration is assumed to be 1.0. Next, the volume of water equal to the total chemical shrinkage is determined and this amount water is provided by the lightweight aggregate. The volume of water provided by the lightweight fine aggregate is calculated using the absorption capacity of the aggregate and the saturation of the aggregate. This volume of water prevents the capillary voids from emptying, which should prevent capillary stresses from developing.

$$M_{LWA} = \frac{C_f \times CS \times \alpha_{\max}}{S \times \phi_{LWA}} \quad \text{..... Equation 2-6}$$

where, M_{LWA} = oven-dry weight of lightweight aggregate (lb),

C_f = cement content for the mixture (lb/yd^3),

CS = chemical shrinkage (lb of water/lb of cement),

α_{max} = maximum degree of cement hydration,

S = degree of saturation of aggregate (0 to 1), and

Φ_{LWA} = absorption of lightweight aggregate (lb water / lb dry LWA).

Table 2-1: Coefficients for chemical shrinkage (Bentz, Lura, and Roberts 2005)

Cement Phase	Coefficient (Pound of water / Pound of solid cement phase)
C_2S	0.0704
C_3S	0.0724
C_3A	0.115*
C_4AF	0.086*

* assuming total conversion of the aluminate phases to monosulfate.

Equation 2-6 uses the volume of absorbed water within the LWA as internal curing water to balance the anticipated chemical shrinkage demand. It is known that not all the absorbed water within the LWA will be desorbed for early-age internal curing (RILEM TC 196 2007). The amount of water desorbed from the LWA will be a function of the aggregate pore size distribution, the spacing of the LWA in the concrete, the pore size distribution of the paste matrix, permeability of the paste and the internal relative humidity around the aggregate particle (RILEM TC 196 2007).

As cement hydrates and consumes water from capillary pores in the paste matrix capillary tensile stresses develop. Water is then desorbed from the pores of the LWA into the paste capillary pores. Available water is more easily removed from larger pores than from smaller pores. LWA with large amounts of smaller pores do not as readily release their internal water. The lower limit of useful pore size may be considered around 100 nm (RILEM TC 196). Due to different pore size distribution within various LWAs, they can have significantly different desorption properties. For internal curing purposes, the desorption properties are more important than absorption properties (Lura 2003; Bentz, Lura, and Roberts 2005).

It is necessary that the lightweight aggregate release moisture at a high relativity humidity so the moisture will be available at early-ages within the concrete. Castro et al. (2011) tested the desorption of a variety of lightweight materials at 93% relative humidity. A summary some of the desorption coefficients relevant to the LWA tested in this study are presented in Table 2-2. The desorption response is thus different for the expanded shale, clay, and slate and this needs to be accounted for when determining the amount of internal curing water available from these LWAs.

Table 2-2: Desorption coefficients at 93% relativity humidity (Castro et al. 2011)

Item	Lightweight Aggregate Type		
	Slate	Clay	Shale
Supplier	Stalite	TXI	Buildex
Source	Gold Hill, NC	Frazier Park, CA	New Market, MO
Desorption coefficient at 93% relative humidity	0.962	0.887	0.976

2.4 METHODS TO ASSESS EARLY-AGE CONCRETE BEHAVIOR

2.4.1 Restrained Stress Development

The rigid cracking frame (RCF), shown in Figure 2-4, is comprised of two mild steel crossheads and two 4 in. diameter Invar sidebars. The test setup was adapted from the configuration developed by Dr. Rupert Springenschmid as documented by RILEM Technical Committee 119 (1998).

a)

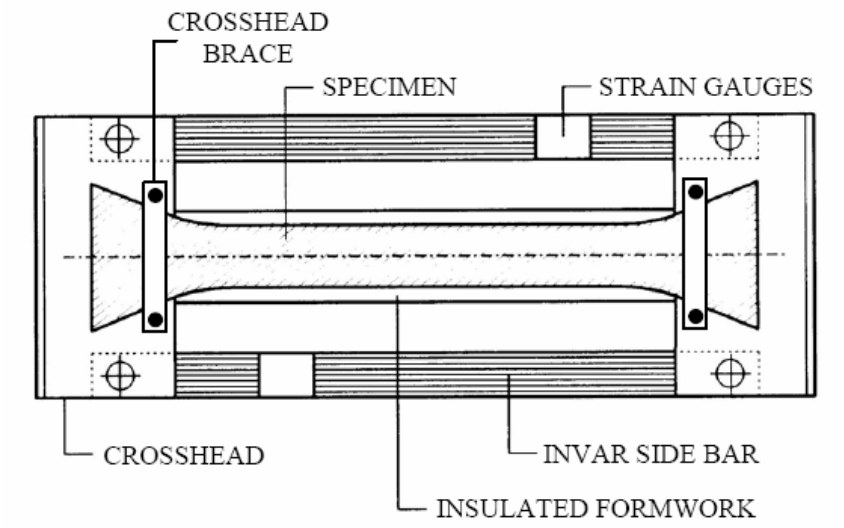

b)

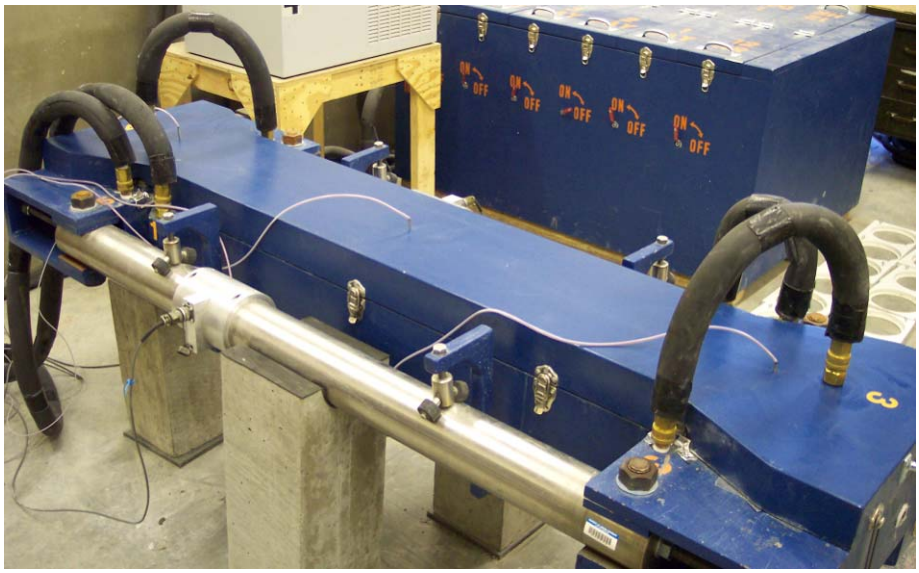

Figure 2-4: Rigid cracking frame test setup: a) Schematic of test (Mangold 1998) b) Actual equipment used

Fresh concrete is consolidated in the RCF, and its stress development is measured continuously until cracking occurs. The 6 × 6 × 49 in. concrete specimen is restrained by dovetailed crossheads at each end. The dovetail is gradually tapered to reduce stress

concentrations and is lined with teeth that grip the concrete. To further prevent slippage of the concrete, crosshead braces are used at the end of the crosshead to restrain opening of the crosshead as the concrete goes into tension. The formwork shown includes 0.5 in. diameter copper tubing throughout. A mixture of water and ethylene glycol is circulated from a temperature-controlled water bath through the formwork to control the curing temperature of the concrete sample. The formwork of the RCF is lined with sheeting to reduce friction between the concrete and the form and to seal the concrete specimen on all surfaces. Because of the presence of the sealed plastic layer around the concrete specimen, no moisture is lost and drying shrinkage effects do not contribute to the stress development while the forms are in place.

When concrete in the RCF starts to hydrate and volume changes due to temperature and autogenous shrinkage effects develop, the Invar bars provide restraint against movement and stress develops in the concrete. The concrete's stress development is monitored using strain gauges mounted on the Invar bars, that are calibrated to the bar forces, which equilibrate the concrete stresses.

The stress developed by the RCF under an isothermal condition is a function of the modulus of elasticity, the autogenous shrinkage, and the relaxation. The stress developed by the RCF under a match-cured condition is a function of the concrete's coefficient of thermal expansion, temperature history, modulus of elasticity, autogenous shrinkage, and relaxation.

It been observed that the cracking frame stress at failure is less than the splitting tensile strength measured on molded concrete cylinders (Meadows 2007). This is due to the test specimen size, the rate of loading and the type of loading (Meadows 2007). The section of concrete subjected to the highest tensile stress is much larger in the cracking frame than in a 6 x 12 in. cylinder. The larger volume of concrete subjected to the highest tensile stress in the cracking frame provides a higher probability of a flaw in the sample and therefore it has a lower apparent strength. In addition, the rate of loading can affect the strength results. Slow load rates yield lower apparent strength and conversely higher load rates yield higher apparent strength (Wight and MacGregor 2009). The splitting tensile strength specimens were loaded to failure in less than 5 minutes, whereas the cracking frames were loaded for 23-109 hours, thus the concrete in the cracking frame will exhibit a lower apparent tensile strength. In addition, the cracking frame is a direct tension test; where as the splitting tension is an indirect tensions test. Meadows (2007) reports that the ratio of cracking frame stress at failure to splitting tensile strength generally falls between 50 to 80 percent.

2.4.2 Unrestrained Length Change Assessment

Bjøntegaard (1999) developed a free shrinkage frame (FSF) to determine the unrestrained uniaxial strain of a curing *concrete* specimen. A FSF similar to the one developed by Bjøntegaard was constructed by Auburn University and is shown in Figure 2-5.

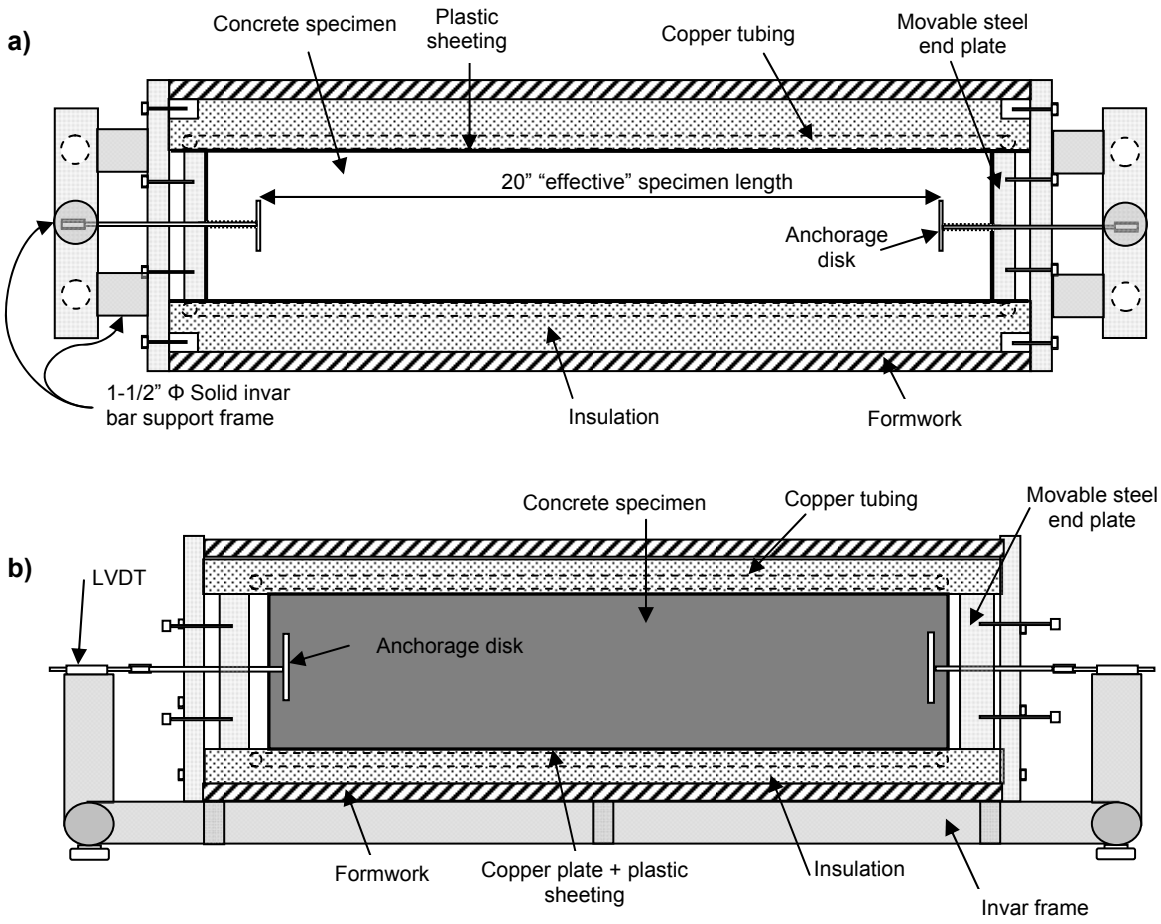

Figure 2-5: Free shrinkage frame test setup: a) Plan view schematic of test equipment, b) Section view schematic, and c) Actual equipment used

The FSF consists of a box that is thermally controlled with 0.5 in. diameter copper tubing, and a supporting Invar steel frame. The box serves as the formwork for the freshly placed concrete and the system to match cure the concrete to any temperature profile. A 6 × 6 × 24 in. concrete

specimen is cast with two sacrificial steel plates connected with an Invar rod to a linear variable displacement transducer (LVDT) to measure linear expansion and contraction. The fresh concrete is placed on a double layer of plastic sheeting with a lubricant in between to minimize friction, which facilitates free movement of the concrete specimen. Plastic sheeting is also used to seal the concrete specimen on all surfaces. When concrete in the FSF is cured to a specified temperature history, the measured strain is a function of thermal and autogenous effects. The test specimen is entirely sealed with a plastic layer, so no moisture is lost. Therefore drying shrinkage effects do not contribute to the free movement measured in the FSF. When the concrete is placed, the movable steel end plates support the fresh concrete ends. When initial set is reached, the movable end plates are released and moved back to allow expansion beyond the initial specimen size. Initial set is determined from penetration resistance as per ASTM C 403. The mortar sample for setting is match-cured to the same temperature history of the FSF. The end plates in position prior to placement is shown in Figure 2-4a and the end plates drawn back after setting is shown in Figure 2-4b.

2.4.3 Coefficient of Thermal Expansion

AASHTO T 336 (2009) can be used to determine the coefficient of thermal expansion of the hardened concrete. For this test, a cylindrical concrete specimen is placed in a frame and submerged in water. A schematic of a typical test frame and specimen are shown in Figure 2-6. A spring-loaded linear variable displacement transformer (LVDT), mounted on a frame, is placed in contact with the top surface of the concrete specimen. The temperature of the water is cycled over a range of 50 °F to 122 °F ± 2 °F, and the subsequent length change of the concrete specimen is measured. From the measured displacement over the known temperature change, the concrete specimen's coefficient of thermal expansion is calculated.

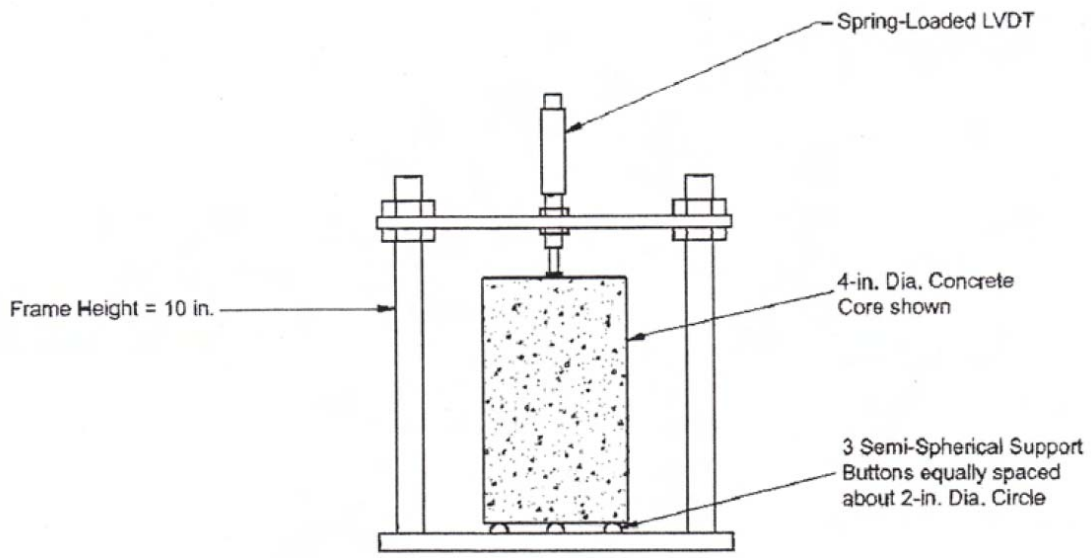

Figure 2-5: Front view of coefficient of thermal expansion test setup (AASHTO T 336 2009)

2.4.4 Semi-Adiabatic Calorimetry

Under adiabatic conditions, a specimen is sealed in a chamber and no heat loss is permitted to occur. Under semi-adiabatic conditions, a small amount of heat loss systematically occurs over time and the heat lost is accounted for by calibration.

Hydration of portland cement is an exothermic reaction. Determining the amount and rate of heat evolved by a particular mixture is essential when modeling early-age in-place temperatures. Semi-adiabatic calorimetry provides an indirect, convenient means of measuring the heat released during hydration of a concrete sample (Schindler and Folliard 2005). Each concrete mixture has a unique heat of heat of hydration development. Without knowing the rate and amount of heat evolved from a concrete mixture, modeling the early-age in-place temperature is impossible.

Semi-adiabatic calorimetry testing generally involves placing the fresh concrete in an insulated vessel or calorimeter. The calorimeter must be calibrated with a material of known thermal properties to determine the rate that the calorimeter dissipates thermal energy. Normally hot water is used for calibration. Temperature probes are used to measure the concrete temperature and the ambient temperature around the calorimeter. The difference between the ambient temperature and temperature inside the calorimeter affects the rate the calorimeter dissipates thermal energy. As the cement hydrates, the heat evolution is captured by the temperature probe positioned in the concrete specimen. Knowing the amount and rate of heat loss from the calorimeter, the amount of heat evolved from the concrete can be calculated. A schematic view of the semi-adiabatic calorimeter used on this project is shown in Figure 2-7.

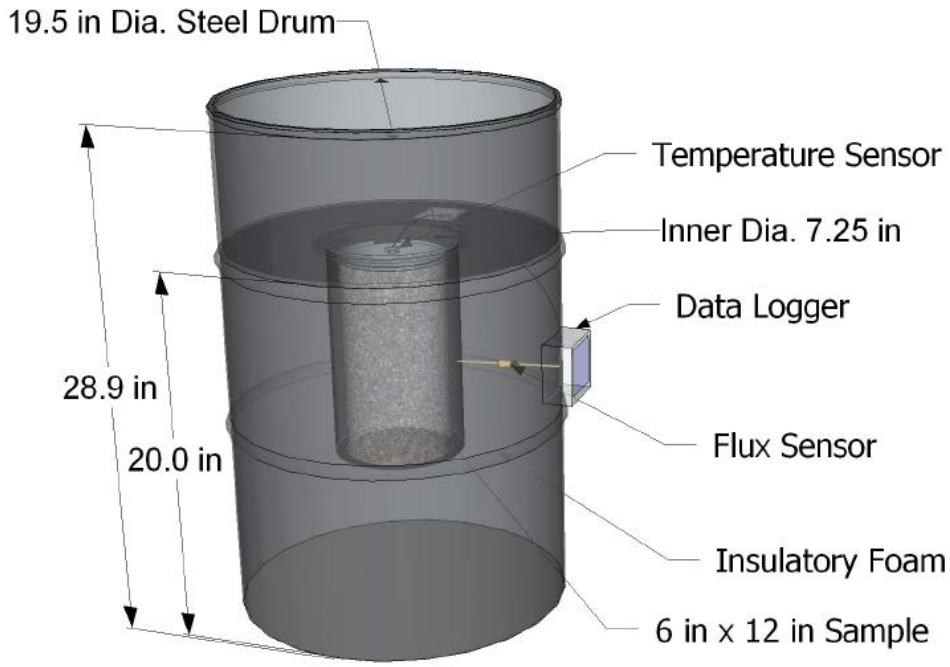

Figure 2-7: Semi-adiabatic calorimeter (adapted from Weakley 2009)

Chapter 3

Experimental Work

3.1 Experimental Program

Concretes proportioned with varying amounts and types of lightweight aggregates were tested to determine their cracking tendency compared to a control mixture using rigid cracking frame (RCF) testing techniques. A mixture using river gravel was tested as a control concrete and all mixtures were proportioned for bridge deck applications. Temperature profiles were modeled to determine the temperature history that concrete in an 8-in thick bridge deck would experience in both summer and fall placement scenarios with the mixtures used. Two rigid cracking frames were used for match-cured and isothermal temperature conditions as schematically shown in Figures 3-1 and 3-2, respectively. Additional tests that were performed on match-cured concrete specimens are shown in Figure 3-1.

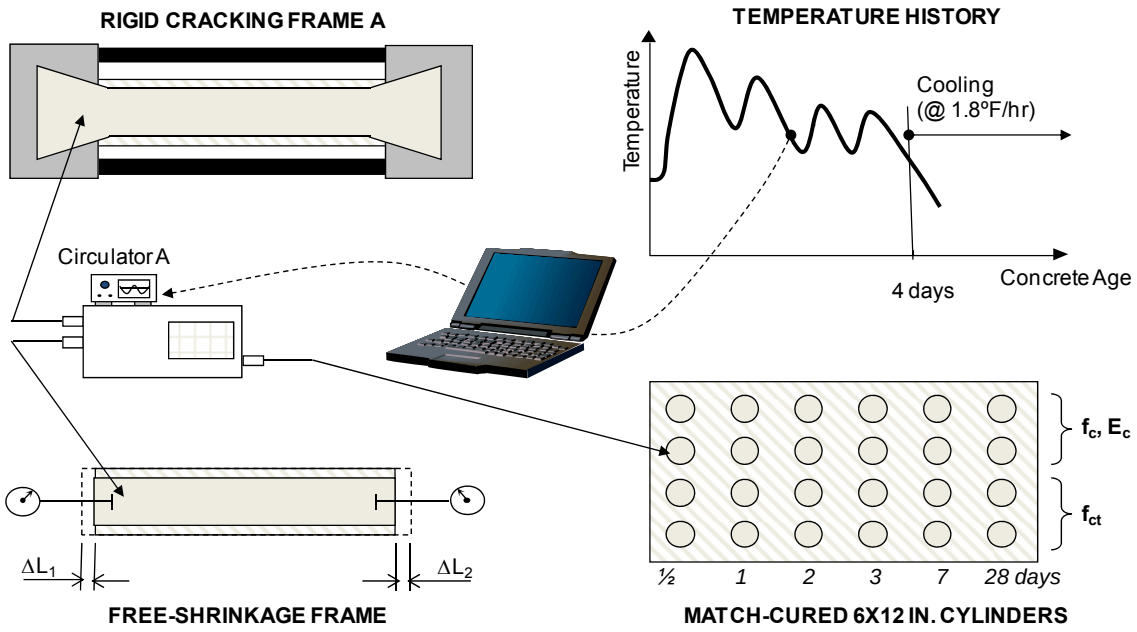

Figure 3-1: Match curing testing setup

Concrete in RCF A was *match cured* (Figure 3-1) to the modeled bridge deck temperature profiles to determine the concrete stress generated due to thermal effects and autogenous shrinkage effects. A free shrinkage frame (FSF) was also used to determine the free strain of the mixtures. The FSF was tested using the same *match-cured* temperature profile that simulates bridge deck conditions to determine the free strain due to thermal and autogenous effects.

Molded cylinders were also *match cured* to the modeled bridge deck temperature to determine the concrete strength and modulus of elasticity development. Concrete in RCF B was cured under *isothermal* temperatures (Figure 3-2) and the stress generated is due to only autogenous shrinkage effects.

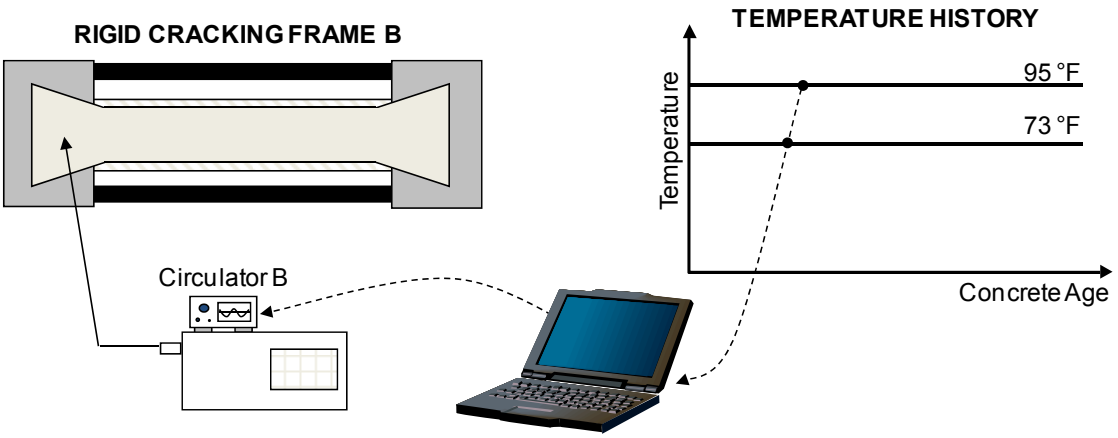

Figure 3-2: Isothermal curing testing setup

Curing temperatures have a major impact on the rate of hydration, rate of development of mechanical properties, and the rate of stress development in concrete. Cracking tendency data collected at typical laboratory temperatures often do not represent the worst-case scenario, as it is well known that early-age cracking is exacerbated under warm-weather conditions (Schindler and McCullough 2002). Each mixture was thus tested under the following two placement scenarios:

- **Summer placement scenario**: Concrete placement temperature ≈ 95 °F, and ambient air temperature cycling between 85 and 95 °F.
- **Fall placement scenario**: Concrete placement temperature ≈ 73 °F, and ambient air temperature cycling between 70 and 77 °F.

The use of these two placement scenarios allows one to determine the effect of placement and curing temperature on the cracking sensitivity of the lightweight and control concrete mixtures. The ConcreteWorks software program (Poole et al. 2006) was used to predict the concrete temperature history of each specific mixture as it would develop in an 8-in. thick bridge deck for both summer and fall placement scenarios. The development of the temperature profile is discussed in Section 3.5.

All constituent materials for the summer placement scenario were placed in an environmental chamber and preconditioned so that the fresh concrete temperature would be approximately 95 °F. All the constituent materials for the fall placement scenario were conditioned at room temperature so that the fresh concrete temperature would be approximately 73 °F.

After 96 hours, the modeled temperature profile essentially followed the prevailing diurnal cycle typical of the simulated placement month. The temperature peaks and valleys were the same from day-to-day, because the effect of the cement hydration had dissipated and only environmental effects affect the temperature change. Therefore, if cracking had not occurred before 96 hours it would not likely occur without additional temperature decrease. If cracking had not occurred at 96 hours, the temperature was decreased by 1.8 °F/hr until the onset of cracking, which is also the practice used by Breitenbücher and Mangold (1994).

3.2 LIGHTWEIGHT AGGREGATES

3.2.1 Sources

Expanded shale, clay, and slate lightweight coarse and fine aggregates were evaluated. The lightweight aggregates were selected to represent those available in different regions of the United States and to include the three raw materials used in the United States for LWA: shale, clay, and slate. The type and source of LWA used in the experimental work are shown in Table 3-1. It should be noted that two gradations of *clay* fine aggregates were used; the coarser gradation will be called "*Maximizer*" as per the terminology used by this supplier. In addition, two *slate* fine aggregates were used. The coarser fine aggregate will be called "D Tank" and the other will be called "MS 16" Fine aggregate. Suppliers directly shipped all of the lightweight aggregates to Auburn University's Concrete Materials Laboratory.

Table 3-1: Lightweight material source type, location, and properties

Item		Lightweight Aggregate Type				
		Slate		**Clay**		**Shale**
Supplier		Stalite		TXI		Buildex
Source		Gold Hill, NC		Frazier Park, CA		New Market, MO
Coarse Aggregate	Gradation	#4 to 3/4 in.		#4 to 3/8 in.		#4 to 1/2 in.
	Pre-wetted Absorption §	6.4 %		25.5 %		32.0 %
	Relative Density*	1.52		1.72		1.59
Fine Aggregate	Gradation	0 to #4	0 to #4	0 to #4	0 to 3/8 in.	0 to #4
	Pre-wetted Absorption §	9.0 %	9.0 %	19.0 %	19.0 %	19.3 %
	Relative Density *	1.84	1.84	1.81	1.81	1.80
	Fineness Modulus	2.83	3.37	3.07	4.32	2.99

Note: * Relative density at surface dry state after 7 days of soaking in water for slate and clay aggregates and 14 days of soaking for shale aggregates.

§ Measured water absorbed after pre-wetting aggregates for either 7 or 14 days.

3.2.2 Properties

The lightweight aggregates were shipped in super sacks and were stored in Auburn University's Structural Engineering laboratory. Upon arrival, the aggregates were sampled and sieve analyses were performed to obtain the gradations as per ASTM C 136. The specific gravity and pre-wetted absorption of the coarse and fine aggregate were determined in accordance with ASTM C 127 and ASTM C 128, respectively. The materials were pre-wetted for 7 or 14 days prior to absorption and relative density testing. The slate and clay samples were pre-wetted for 7 days and the shale for 14 days. For the lightweight fine aggregates, Provisional Method 2 of ASTM C 128 (the rubber mat method) was used to determine when the sample was at surface dry condition. The sieve analysis, pre-wetted absorption, relative density, and fineness modulus results are presented in Table 3-1. The gradations for all aggregates are listed in Appendix A.

3.2.3 Lightweight Aggregate Preconditioning

The lightweight aggregates were placed in plastic barrels and submerged in water for moisture preconditioning. The preconditioning time for the materials was based on recommendations provided by each supplier. The slate and clay materials were preconditioned for at least 7 days and the shale material for at least 14 days prior to batching. Valves were installed in the bottom of plastic, 55-gallon barrels to allow the water to be drained from the aggregates. For the lightweight fine aggregate materials, a 6-in. thick filter layer of normalweight coarse aggregate was placed in the bottom to prevent clogging of the valve during draining. Illustrations of the barrel setup are shown in Figure 3-3. After the material was preconditioned, it was drained slowly to reduce the amount of fines lost. The lightweight coarse and fine aggregate material were then shoveled onto a clean plastic sheet in separate piles where the excess surface moisture was allowed to run out. Then the aggregates were shoveled into separate 5-gallon buckets for temperature conditioning and batching.

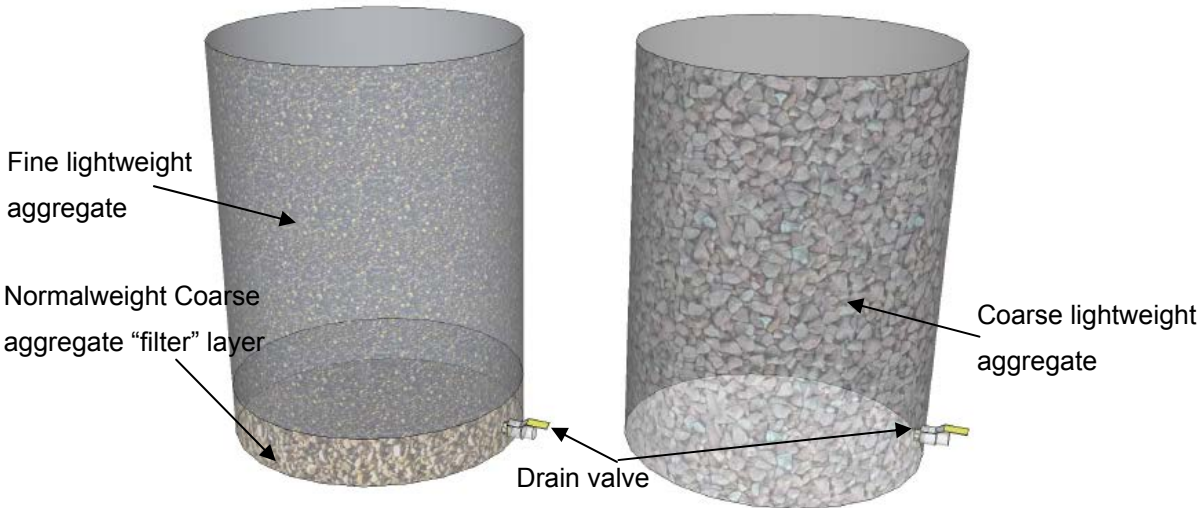

Figure 3-3: Illustration of barrel setup used for lightweight aggregate preconditioning

Temperature preconditioning was achieved by placing the sealed 5-gallon buckets at room temperature or in a heated environmental chamber for the fall or summer placement scenarios, respectively. On the morning of mixing, after 24 hours of temperature preconditioning, samples of aggregates were taken to assess their moisture contents to allow moisture corrections to be made for batching. Once the final moisture-adjusted batch weights were determined, the 5-gallon buckets of materials were taken from the temperature preconditioning area and weighed for mixing.

3.3 MIXTURE PROPORTIONS

Normalweight (CTRL), internal curing (IC), sand-lightweight (SLW), and all-lightweight (ALW) concretes were evaluated. The mixture proportions used for testing the shale, clay, and slate lightweight aggregates are shown in Tables 3-2, 3-3, and 3-4, respectively. For comparison purposes, the mixture proportions for the normalweight concrete are also shown in these tables. Because LWA may never reach a state of saturation, the term saturated surface dry (SSD) is not used with LWA. Therefore, the LWA batch weights are for the pre-wetted surface dry (SD) condition. Pre-wetting of the aggregates is described in Section 3.2.3.

For convenience, a mixture identification system is used in this report to refer to a specific type of LWA, mixture type, and simulated placement season. The identification system used is as follows:

LWA Type	-	Mixture Type	-	Simulated Placement Season
Slate		CTRL		Fall (Fall *match-cured* conditions)
Clay		IC		Sum (Summer *match-cured* conditions)
Shale		SLW		73°F (Fall *isothermal* temperature)
		ALW		95°F (Summer *isothermal* temperature)

Example: **Slate SLW (Fall)**, represents the sand-lightweight concrete with slate LWA that is made and cured under *match-cured* fall conditions.

Table 3-2: Expanded slate and normalweight mixture proportions and properties

Item	CTRL	Slate IC	Slate SLW	Slate ALW
Water Content (lb/yd^3)	260	260	276	276
Cement Content (lb/yd^3)	620	620	658	658
SSD Normalweight Coarse Aggregate (lb/yd^3)	1,761	1,761	0	0
SD Slate Lightweight Coarse Aggregate (lb/yd^3)	0	0	875	896
SSD Normalweight Fine Aggregate (lb/yd^3)	1,210	818	1,381	0
SD Slate Lightweight D Tank Fine Aggregate (lb/yd^3)	0	276	0	0
SD Slate Lightweight MS 16 Fine Aggregate (lb/yd^3)	0	0	0	945
Water-Reducing Admixture (oz/yd^3)	31.0	34.1	0.0	0.0
High-Range Water-Reducing Admixture (oz/yd^3)	0.0	0.0	39.5	8.2
Rheology-Controlling Admixture (oz/yd^3)	0.0	0.0	0.0	52.6
Air-Entraining Admixture (oz/yd^3)	0.8	0.8	6.6	7.4
Target Total Air Content (%)	5.5	5.5	5.5	5.5
Water-cement ratio (w/c)	0.42	0.42	0.42	0.42

Table 3-3: Expanded clay and normalweight mixture proportions and properties

Item	CTRL	Clay IC	Clay SLW	Clay ALW
Water Content (lb/yd^3)	260	260	276	276
Cement Content (lb/yd^3)	620	620	658	658
SSD Normalweight Coarse Aggregate (lb/yd^3)	1,761	1,761	0	0
SD Clay Lightweight Coarse Aggregate (lb/yd^3)	0	0	1,029	948
SSD Normalweight Fine Aggregate (lb/yd^3)	1,210	878	1,316	0
SD Clay Lightweight Maximizer (lb/yd^3)	0	230	0	0
SD Clay Lightweight Fine Aggregate (lb/yd^3)	0	0	0	998
Water-Reducing Admixture (oz/yd^3)	31.0	31.0	0.0	0.0
High-Range Water-Reducing Admixture (oz/yd^3)	0.0	0.0	52.6	34.5
Rheology-Controlling Admixture (oz/yd^3)	0.0	0.0	0.0	26.3
Air-Entraining Admixture (oz/yd^3)	0.8	0.8	19.7	2.5
Target Total Air Content (%)	5.5	5.5	5.5	5.5
Water-cement ratio (w/c)	0.42	0.42	0.42	0.42

Table 3-4: Expanded shale and normalweight mixture proportions and properties

Item	CTRL	Shale IC	Shale SLW	Shale ALW
Water Content (lb/yd^3)	260	260	276	276
Cement Content (lb/yd^3)	620	620	658	658
SSD Normalweight Coarse Aggregate (lb/yd^3)	1,761	1,761	0	0
SD Shale Lightweight Coarse Aggregate (lb/yd^3)	0	0	933	948
SSD Normalweight Fine Aggregate (lb/yd^3)	1,210	878	1,354	0
SD Shale Lightweight Fine Aggregate (lb/yd^3)	0	230	0	908
Water-Reducing Admixture (oz/yd^3)	31.0	31.0	0.0	0.0
High-Range Water-Reducing Admixture (oz/yd^3)	0.0	0.0	39.5	16.5
Rheology-Controlling Admixture (oz/yd^3)	0.0	0.0	0.0	79.0
Air-Entraining Admixture (oz/yd^3)	0.8	0.8	6.6	2.9
Target Total Air Content (%)	5.5	5.5	5.5	5.5
Water-cement ratio (w/c)	0.42	0.42	0.42	0.42

The normalweight mixture is a typical bridge deck mixture used in Alabama that meets the specification requirements of the Alabama Department of Transportation. The IC mixture is similar to the normalweight mixture, except that a fraction of the normalweight fine aggregate was replaced with lightweight fine aggregate. The IC mixture was initially proportioned using the method described in Section 2.3 proposed by Bentz, Lura, and Roberts (2005). However, it was found that the ASTM C 567 calculated equilibrium density of the IC mixture was below 135 lb/ft^3, which did not allow the mixture to be classified as "normalweight concrete" as per the AASHTO LRFD Bridge Design Specifications (2007). It was desired that the mixture be in the "normalweight concrete" category as per AASHTO LRFD Bridge Design Specifications (2007). Because of this, the maximum replacement of normalweight fine aggregate with lightweight fine aggregate was determined to obtain a calculated equilibrium density of 135 lb/ft^3. The IC mixtures thus contained *less* LWA than required by the method proposed by Bentz, Lura, and Roberts (2005).

The SLW mixture was proportioned using lightweight coarse aggregate and normalweight fine aggregate. The ALW mixture used both lightweight fine and coarse aggregate. The cement content for the SLW and ALW mixtures was increased to increase the paste content to improve the workability and pumpability of these lightweight concrete mixtures.

The slump and air contents were specified to be 4.0 ± 1.0 in. and 5.5 ± 1.5 %, which are typical values for bridge deck construction in the southeastern region of the United States. For this project, the measured density of the concrete was produced to be ± 1 lb/ft^3 of the calculated density after correcting for the measured air content of each batch.

As discussed in Section 2-3, not all of the absorbed water will be available for internal curing purposes, because the water held in the smaller pores will not be available for internal

curing. The amount of water required by Bentz, Lura, and Roberts (2005) in Equation 2-6 to fill the voids created by chemical shrinkage is presented in Table 3-5 along with the total amount of internal curing water available in the lightweight aggregates for each mixture. The total amount of available water is calculated using the absorption capacity in Table 3-1 and the desorption coefficients presented in Table 2-2. It was further assumed that the normalweight aggregates do not provide water for internal curing, which matches current normalweight concrete proportioning practice (ACI 211.1R 1991). The data in Table 3-5 reveal that the internal curing slate, clay, and shale concretes provide 44%, 23%, and 16% *less* internal curing water, respectively than required by the method proposed by Bentz, Lura, and Roberts (2005). All SLW and ALW concretes tested in this study provide more internal curing water than required by the method proposed by Bentz, Lura, and Roberts (2005).

Table 3-5: Total absorbed water available from LWA and water required by Equation 2-6

Concrete Type	Internal Curing Water Available From LWA (lb/yd^3)			Water Required by Equation 2-6 (lb/yd^3)
	Slate	Clay	Shale	
Internal curing	24	33	36	43
Sand-lightweight concrete	49	185	221	47
All-lightweight concrete	134	312	367	47

3.4 TEST METHODS

3.4.1 Restrained Stress Development

Each mixture was placed in the RCF and was cured to a temperature profile developed to reflect the temperature profile of an 8-in. thick concrete bridge deck constructed under summer or fall placement conditions. The development of the temperature profile is discussed in Section 3.5. The mixture was also placed in a RCF that was cured at an isothermal condition at 95 °F or 73 °F for a summer or fall placement conditions, respectively. If the specimen had not cracked after 96 hours, the concrete was cooled at a rate of 1.8 °F/hr to induce cracking, which is also the practice used by Breitenbücher and Mangold (1994). Since the response of the specimen was still measured after cooling was started, this approach still allows one to assess the behavior of the concrete up until cracking occurs.

The stress development of a specimen in the RCF cured under an isothermal curing condition is a function of its modulus of elasticity, autogenous shrinkage, and relaxation. The stress development of a specimen in the RCF cured under match-cured conditions is a function of its coefficient of thermal expansion, temperature history, modulus of elasticity, autogenous shrinkage, and relaxation.

3.4.2 Unrestrained Length Change Assessment

Each mixture was tested in the FSF and cured using the same match-cured temperature profile that was used for the RCF A, as shown in Figure 3-1. The FSF captured the strain the concrete would experience if it were unrestrained. The strain measured is a function of autogenous shrinkage, coefficient of thermal expansion, and temperature history.

3.4.3 Mechanical Properties

For each mixture and placement scenario, 24 - 6 × 12 in. cylinders were cast as per ASTM C 192. The cylinders were match-cured using the same temperature history as the RCF A and the FSF, as shown in Figure 3-1. The cylinders were tested for compressive strength, splitting tensile strength, and modulus of elasticity as per ASTM C 39, ASTM C 496, and ASTM C 469, respectively at ½ , 1, 2, 3, 7, and 28 days. Two cylinders were first tested to determine the splitting tensile strength of the concrete. From the splitting tensile strength, 40% of the compressive strength was estimated, which was used for modulus of elasticity testing. The same two cylinders used for modulus of elasticity testing were used for compressive strength testing. After the modulus of elasticity testing was completed, the two cylinders were then tested to failure to determine the compressive strength of the concrete. In no instance was the upper load limit used for modulus of elasticity testing greater than 40% of the actual compressive strength of the tested sample.

3.4.4 Coefficient of Thermal Expansion

While the development of coefficient of thermal expansion is difficult to test at very early ages, a test setup similar to the one described in AASHTO T 336 (2009) was used to determine the coefficient of thermal expansion of the hardened concrete after 28 days of standard curing. The modified AASHTO T 336 setup used for testing is shown in Figure 3-4.

The coefficient of thermal expansion test setup used in this study matched the configuration required by AASHTO T 336 (2009) specification; however, slight modifications were made to improve the repeatability of the test. Ceramic inserts were used to provide insulation between the heated components and the LVDT, which reduces the effect of temperature on the readings of the LVDT. Specifically, a smaller ceramic disk was used under the tip of the LVDT and a ceramic collar was used to mount the LVDT to the frame. The purpose of the ceramic collar was to limit the temperature transferred to the LVDT through the mounting crossbar. Additionally, an Invar steel spacer was added on top of the concrete specimen to create additional height above the specimen for fluctuations in water level and to limit heat transfer from the heated water to the crossbar. The disks and collar were used in the calibration procedure, thus their effects were accounted for in the calibration method of AASHTO T 336 (2009).

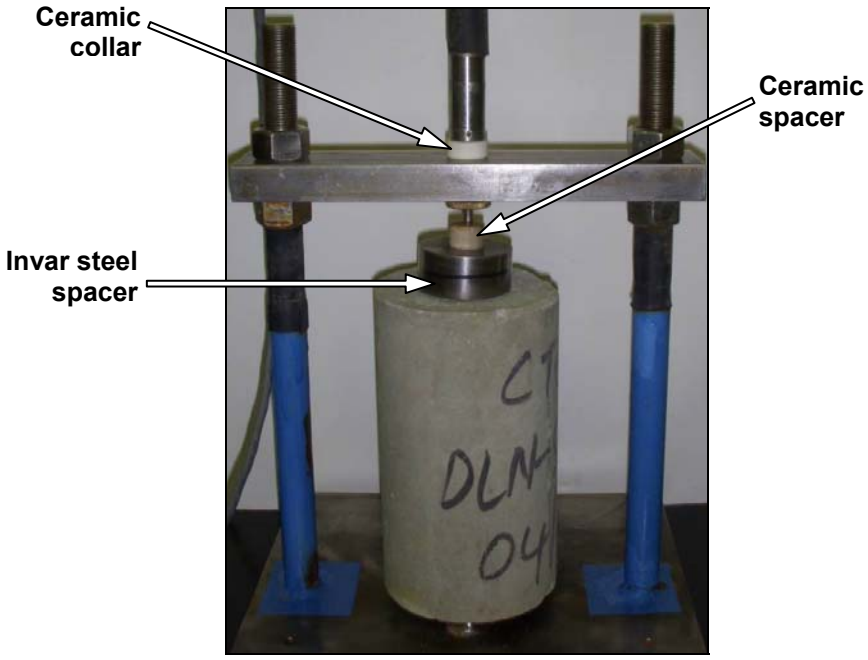

Figure 3-4: Modified AASHTO T 336 setup used for coefficient of thermal expansion testing

3.4.5 Semi-Adiabatic Calorimetry

Semi-adiabatic testing is used to characterize the heat of hydration development of each mixture (Schindler and Folliard 2005). The semi-adiabatic calorimeter (SAC) test equipment used during this project was supplied by Digital Site Systems, Inc., Pittsburgh, Pennsylvania. Since no standardized ASTM test method exists for this procedure, a RILEM draft test procedure was followed (RILEM 119-TCE 1998). The SAC consisted of an insulated 55-gallon drum that uses a 6 x 12 in. cylindrical concrete sample. Probes are used to record the concrete temperature, heat loss through the calorimeter wall, and air temperature surrounding the test setup. The heat loss through the calorimeter was determined by a calibration test performed by using heated water.

3.4.5.1 Heat of hydration characterization

Trial batches were produced to ensure the slump, total air content, and yield of the concrete met the project requirements. After a trial batch met the slump, air and yield criteria, a 6 × 12 in. cylinder was produced, weighed, and placed in the SAC. The cylinder was cured in the SAC for at least five days. The heat of hydration parameters were determined from the SAC data (Schindler and Folliard 2005).

3.4.5.2 Thermal diffusivity assessment

After about 7 days of curing a cylinder produced from the sand-lightweight concrete trial batch was placed in an oven, heated to approximately 160 °F, and placed in the SAC. The heat decay was measured over four to five days and the thermal diffusivity of the concrete back-calculated.

With the specific heat of the constituents except the lightweight coarse aggregate known (Lamond and Pielert 2006), the thermal diffusivity of the coarse aggregate was back-calculated to fit the measured temperature decay in the SAC. Now with the thermal diffusivity of the coarse aggregate known, the same process was used to determine the thermal diffusivity of the lightweight fine aggregate in the all-lightweight concrete mixture. With the adiabatic heat curve and the thermal diffusivities known, two temperature profiles were generated with the ConcreteWorks software package (Poole et al. 2006). One temperature profile simulates the temperature history a concrete bridge deck would experience during summer placement conditions (95°F) and the other was for fall placement conditions (73°F).

3.4.6 Setting Testing

Setting of concrete is the gradual transition from liquid to solid. Final setting of concrete relates to the point where stress and stiffness start to develop in freshly placed concrete. It is caused by the formation of sufficient hydration products (Schindler 2003). According to ASTM C 403, initial set is achieved when the concrete paste reaches a penetration resistance of 500 psi, and final set is achieved when the concrete paste reaches a penetration resistance of 4,000 psi.

In this project, one - 6 x 8 in. container was filled with mortar that was wet-sieved from the concrete. This specimen was placed in a chamber that is match-cured to the temperature profile of the free shrinkage frame. Penetration resistance testing is performed on this specimen in accordance with ASTM C 403. When initial setting is reached, the supporting plates in the free shrinkage frame are released to allow free movement to occur.

3.4.7 Other Fresh Quality Control Tests

All concrete was mixed as per ASTM C 192 under laboratory conditions. The temperature, slump, and density of the fresh concrete were measured as per ASTM C 1064, ASTM C 143, and ASTM C 138, respectively, for each batch of concrete. The total air content for the all normalweight aggregate mixtures was measured by the pressure method as per ASTM C 231. The total air content for all mixtures containing lightweight aggregate was measured by the volumetric method as per ASTM C 173. All ASTM tests were performed by a technician certified as an ACI Field Testing Technician - Grade I.

3.5 CONCRETE TEMPERATURE MODELING

The temperature profile that an in-place concrete element experiences is a function of the geometry of the element, the concrete mixture proportions, the chemical composition of the cementing materials, the placement temperature, the thermal conductivity of the aggregate, and environmental effects such as ambient temperature, wind speed, and incoming solar radiation.

To assess the effect of placement and curing temperature, the concrete modeling software ConcreteWorks (Poole et al. 2006) was used to determine the temperature profile that an 8-in thick bridge deck constructed on stay-in-place metal forms would experience. Two placement scenarios were investigated: summer and fall conditions. Bridge deck temperatures for summer and fall placements were determined for Montgomery, Alabama on construction dates of August 15 and October 15. Semi-adiabatic calorimetry was used to determine the hydration parameters of each mixture (Schindler and Folliard 2005). Using the hydration parameters, as well as the placement date, city, bridge geometry, aggregate type, thermal diffusivity, mixture proportions, placement temperature, wind speed, ambient relative humidity, and percent cloud cover, two concrete temperature profiles were generated for each simulated placement season. Note that this practice captures the unique temperature profile that each mixture would experience due to its own heat of hydration and thermal properties should it be placed in an 8-in. thick bridge deck. The match-cured temperature profile used for each mixture is thus unique to that mixture.

The mixtures were tested at each of the temperature scenarios to evaluate the effect of placement temperature and curing temperature on time to initial cracking. When summer scenarios mixtures were tested, the raw materials were placed in an environmental chamber and conditioned to obtain fresh concrete temperatures of approximately 95 °F.

3.6 OTHER RAW CONCRETE MATERIALS

3.6.1 Portland Cement

An adequate quantity of Type I portland cement was donated by TXI to complete all testing associated with this project. The properties of the portland cement are shown in Table 3-6.

Table 3-6: Portland cement properties

C_3S	C_2S	C_3A	C_4AF	Free CaO	SO_3	MgO	Blaine Fineness
60.3 %	18.2 %	5.4 %	11.3 %	0.9 %	2.6 %	1.3 %	351 (m^2/kg)

3.6.2 Normalweight Coarse and Fine Aggregates

The coarse aggregate for the project was an ASTM C 33 No. 67 siliceous river gravel. The fine aggregate used throughout the project was siliceous river sand. Both aggregate types were obtained from the quarry of Martin Marietta Materials located in Shorter, Alabama. The aggregates were sampled and sieve analyses were performed to obtain the gradations as per ASTM C 136. Samples were also obtained for specific gravity and absorption capacity testing of the coarse and fine aggregate as per ASTM C 127 and ASTM C 128, respectively. The sieve analysis results are presented in Appendix A. The specific gravity and absorption capacity for the

normalweight coarse and fine aggregates were 2.63, 0.52% and 2.61, 0.41%, respectively. The fineness modulus of the normalweight sand was 2.45.

3.6.3 Chemical Admixtures

Chemical admixtures were used as needed in the concrete mixtures to control the slump and the total air content of the fresh concrete. All chemical admixtures were supplied by BASF Admixtures, Inc.

The air-entraining admixture (AEA) used for this research was MB AE 90 which meets the requirements of ASTM C 260. The AEA dosage was determined based on multiple trial batches to obtain the target total air content.

The normal-range water-reducing admixture was Pozzolith 322N which meets the requirements for an ASTM C 494 Type A admixture. A polycarboxylate-based high-range water-reducing (HRWR) admixture was also used for some mixtures as shown in Tables 3-2 to 3-4. The HRWR admixture was Polyheed 1025, which meets the requirements for an ASTM C 494 Type F admixture. The dosages of the water-reducing admixtures were determined by trial batches to obtained fresh concrete that met the project slump requirements.

For the ALW mixtures, a rheology-controlling admixture was used. Without the rheology-controlling admixture, the slump test of all ALW mixtures exhibited a shear failure and this concrete was very harsh. Representatives of BASF Admixtures, Inc. recommended the use of Navitas 33 to counter the harshness of the ALW mixtures and this admixture did significantly improve the workability of these mixtures. The rheology-controlling admixture can be classified as an ASTM C 494 Type S admixture.

Chapter 4

Experimental Results

The results collected from the experimental work performed in this project are presented in this chapter. A discussion and synthesis of the results are provided in Chapter 5. Three lightweight aggregates were tested: expanded slate, expanded clay, and expanded shale. The mixture proportions, thermal properties, fresh properties, temperature profiles, restrained stress development, unrestrained length change, and mechanical property development for both the summer and fall placement scenarios were evaluated for each mixture. The results for concretes made with expanded shale, clay, and slate aggregates are compared to the normalweight aggregate concrete mixture in Sections 4.1, 4.2, and 4.3, respectively.

4.1 EXPANDED SLATE RESULTS

4.1.1 Mixture Gradations and Proportions

Three concretes containing expanded slate LWA were produced and tested at two temperature scenarios. The three concretes used were an internal curing (IC), a sand-lightweight (SWL), and an all-lightweight (ALW) concrete. The proportions for the concretes made with this LWA are shown in Table 3-2. The combined aggregate gradations for the mixtures are presented on a 0.45 power curve in Figures 4-1 and 4-2. The 0.45 power curve gives an indication of the particle packing of a blended aggregate gradation (Mindess, Young, and Darwin 2002).

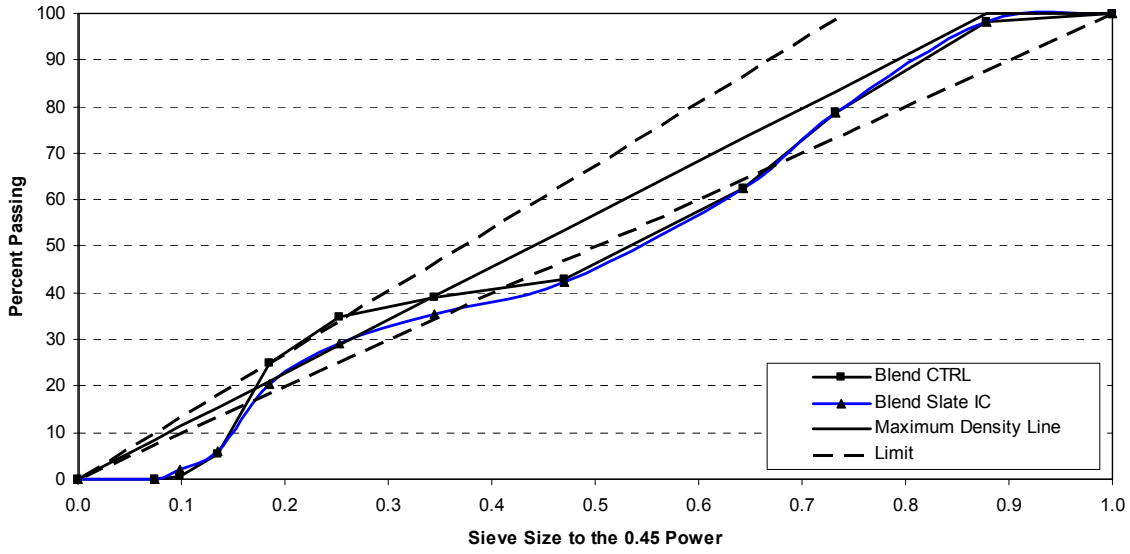

Figure 4-1: Combined gradation of CTRL and Slate IC mixtures on the 0.45 power curve

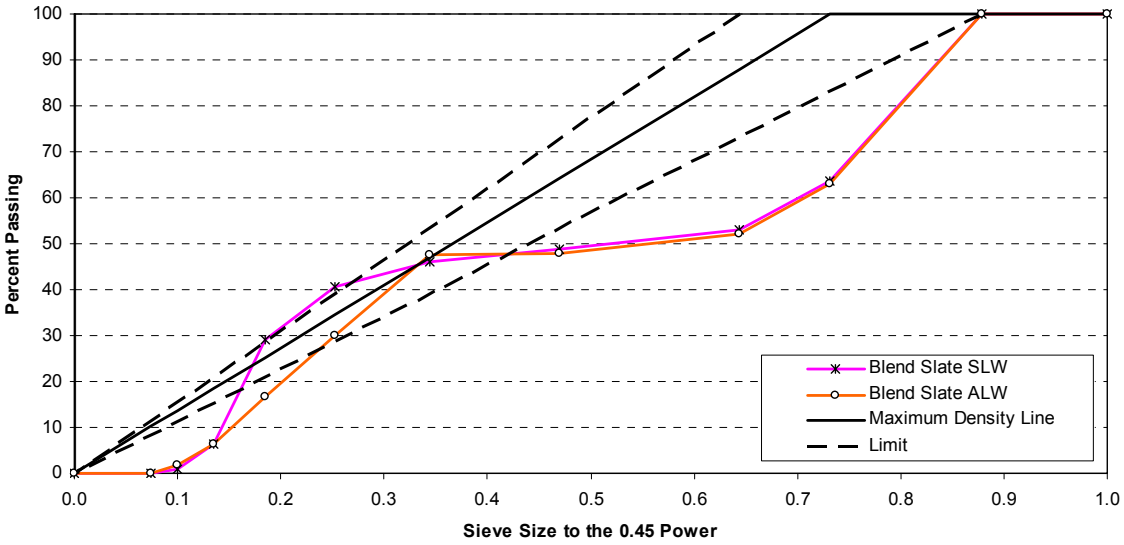

Figure 4-2: Combined gradation of Slate SLW and ALW mixtures on the 0.45 power curve

4.1.2 Fresh Concrete Properties

For each mixture and placement scenario, two batches were produced. The first batch was used to produce the concrete cylinders for mechanical property testing and the second batch was for RCF and FSF testing. The fresh properties for each mixture, batch, and placement scenario are presented in Table 4-1. The "Δ Density" column in Table 4-1 is the difference between the measured density and the calculated density after correcting for the measured air content of each batch. A positive sign for the "Δ Density" indicates the measured density was greater than the calculated density and visa versa.

4.1.3 Miscellaneous Properties

The calculated equilibrium density as per ASTM C 567, coefficient of thermal expansion measured from the modified AASHTO T 336 setup, and the thermal diffusivity determined from semi-adiabatic calorimetry are summarized in Table 4-2.

4.1.4 Curing Temperatures

The curing temperature profiles for the fall and summer placement scenarios for the expanded slate aggregate concretes and the normalweight control concrete are presented in Figure 4-3. The temperature profiles are truncated at the time of cracking.

Table 4-1: Measured fresh concrete properties of expanded slate and control mixtures

Mixture and Placement Scenario	Batch No.	Fresh Concrete Test Results				Calculated
		Slump (in.)	Temp. (°F)	Air (%)	Density (lb/ft^3)	Δ Density (lb/ft^3)
CTRL (Fall)	1	3.25	74	5.0	143.8	0.3
	2	4.5	73	6.25	141.9	0.6
CTRL (Sum)	1	2.5	100	4.75	143.0	-0.3
	2	2.0	100	5.25	141.9	-0.6
Slate IC (Fall)	1	3.25	74	5.75	137.8	-0.2
	2	3.5	75	5.75	138.6	0.6
Slate IC (Sum)	1	2.0	97	4.5	140.6	0.8
	2	2.5	97	4.75	140.1	0.8
Slate SLW (Fall)	1	3.5	74	4.5	119.0	0.3
	2	3.75	74	4.5	119.2	0.1
Slate SLW (Sum)	1	2.0	97	4.25	119.8	0.2
	2	2.5	95	4.25	120.0	0.4
Slate ALW (Fall)	1	5.0	70	5.0	104.0	0.8
	2	4.5	68	5.25	103.8	0.8
Slate ALW (Sum)	1	2.25	92	4.5	104.3	0.6
	2	2.5	95	4.25	104.8	0.8

Table 4-2: Miscellaneous properties of expanded slate and control mixtures

Property	CTRL	Slate IC	Slate SLW	Slate ALW
Calculated Equilibrium Density (lb/ft^3)	140.0	135.0	113.6	95.5
Coefficient of Thermal Expansion (με/°F)	6.2	5.9	5.1	4.3
Thermal Diffusivity (ft^2/hr)	0.046	0.042	0.033	0.029

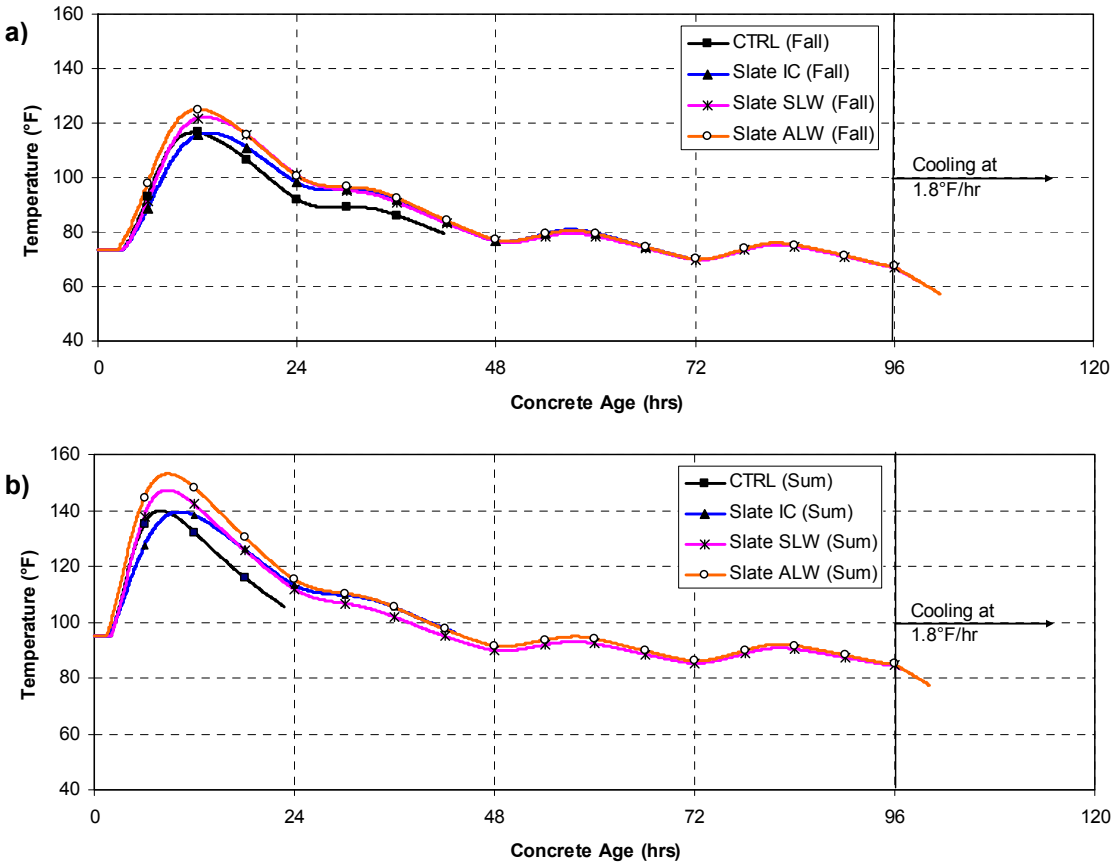

Figure 4-3: Modeled temperature profile for slate and control mixtures:
a) Fall and b) Summer placement scenarios

4.1.5 Restrained Stress Development

The restrained stress development is presented in Figure 4-4 and Figure 4-5 for the match cured and isothermal cured conditions, respectively. The restrained stress development data for the match-cured condition end at the time of cracking. The restrained stress development for the isothermal curing conditions was measured for 96 hours.

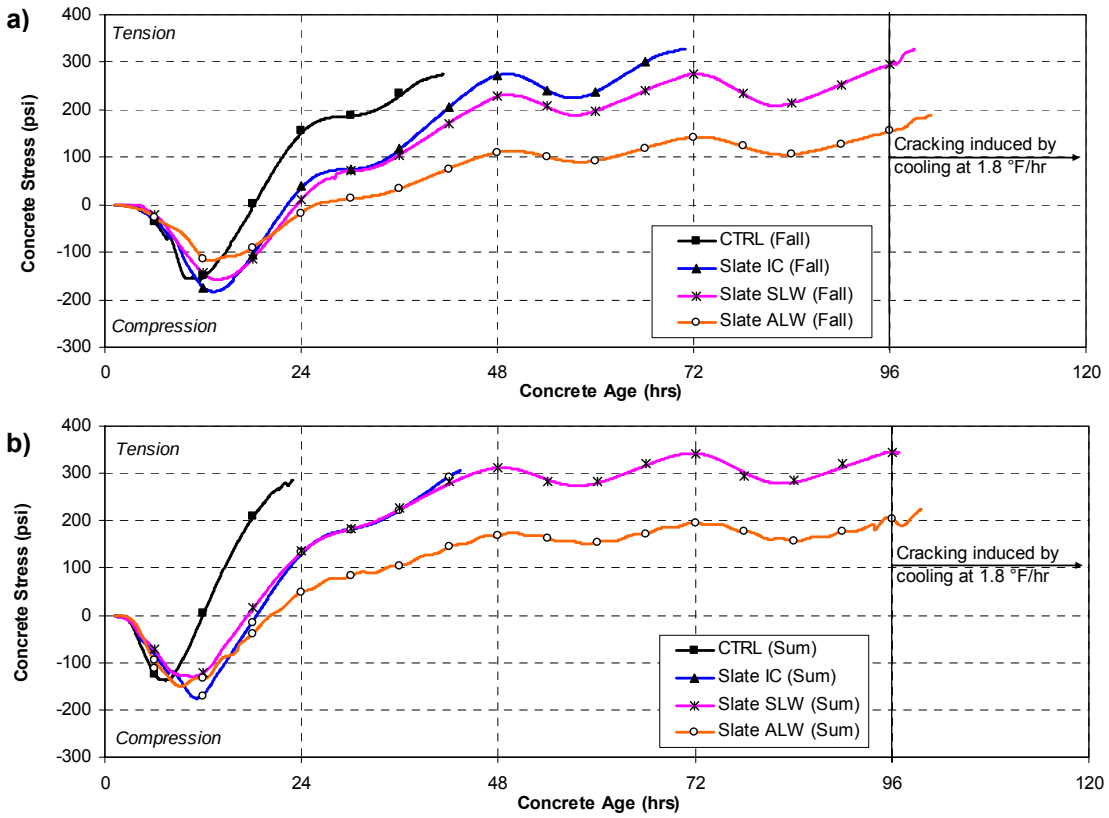

Figure 4-4: Restrained stress development for slate and control mixtures: a) Fall and b) Summer placement scenarios

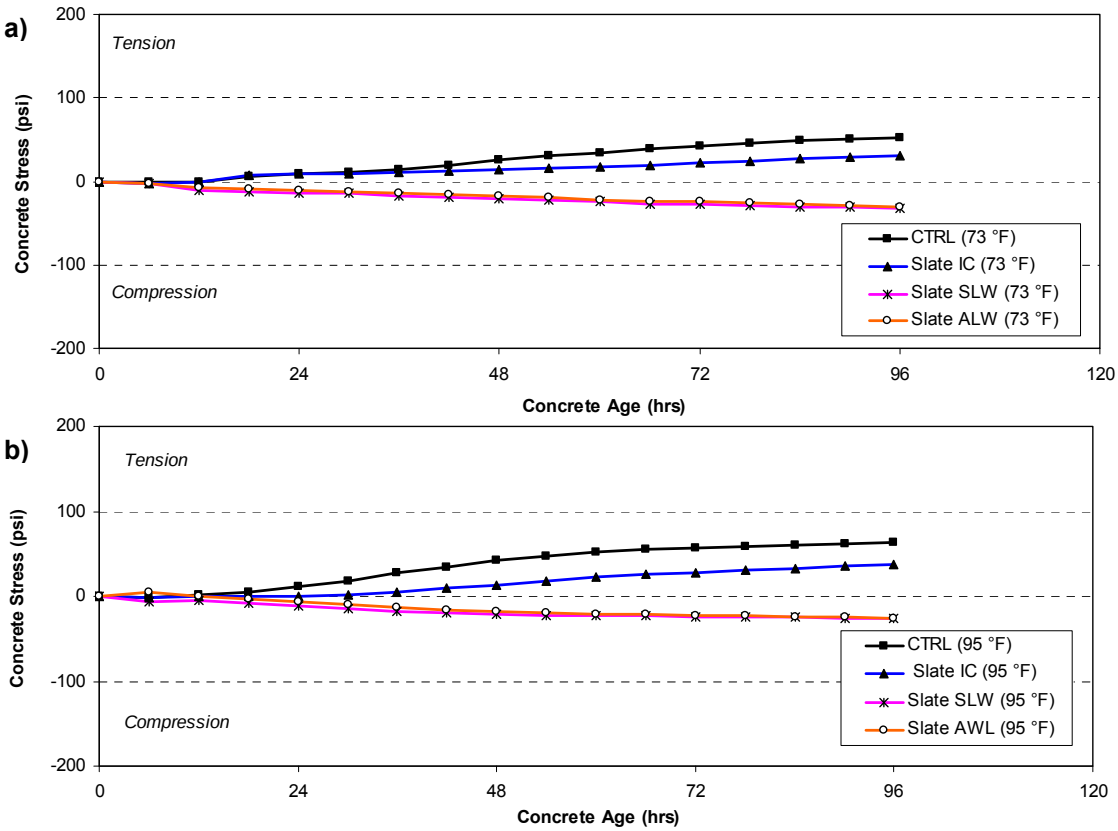

Figure 4-5: Restrained stress development for slate and control mixtures under: a) 73 °F and b) 95 °F isothermal conditions

4.1.5.1 Time to zero stress and cracking

The time and temperature to the zero stress and cracking condition for each mixture and curing scenario are summarized in Table 4-3.

Table 4-3: Time and temperature at zero stress and cracking of slate and control mixtures

Mixture	Zero Stress		Cracking	
	Time (hrs)	Temp. (°F)	Time (hrs)	Temp. (°F)
CTRL (Fall)	18.7	104.8	41.7	79.5
CTRL (Sum)	12.4	131.0	22.8	105.5
Slate IC (Fall)	22.3	101.6	70.8	70.6
Slate IC (Sum)	18.4	125.1	43.3	96.4
Slate SLW (Fall)	23.3	102.5	98.9 *	61.9
Slate SLW (Sum)	17.4	127.3	96.9 *	82.8
Slate ALW (Fall)	23.5	101.6	100.3 *	59.7
Slate ALW (Sum)	17.9	131.0	99.6*	78.5

* Note: Cracking induced by cooling at 1.8 °F/hr after 96 hours

4.1.6 Measured Unrestrained Length Change

The strain measurements from the unrestrained specimens in the FSF are presented in Figure 4-6. The concrete specimens were match cured using the modeled temperature profile of the 8-in. thick bridge deck. The data are truncated at the time of cracking to help illustrate the strain developed in concrete until cracking occurred.

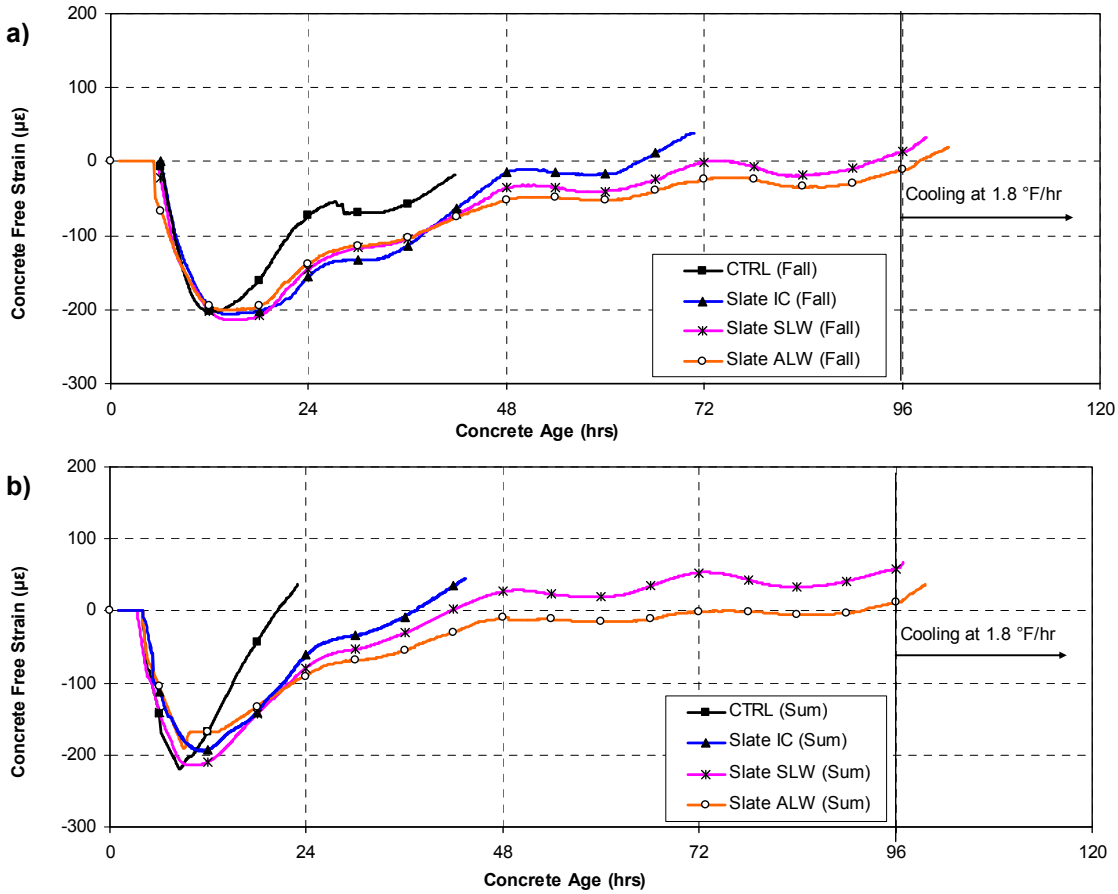

Figure 4-6: Free shrinkage strains for slate and control mixtures:
a) Fall and b) Summer placement scenarios

4.1.7 Mechanical Properties

The compressive strength, splitting tensile strength, and modulus of elasticity development were measured by testing cylinders match cured to the bridge deck temperature profile for each mixture and placement scenario. A regression analysis was performed on the discrete data points with the exponential function recommended by ASTM C 1074. The resulting best-fit curves for each property are shown in Figures 4-7 and 4-8 for fall and summer placement scenarios, respectively. The average of the two test cylinders for each mechanical property is summarized in Appendix B.

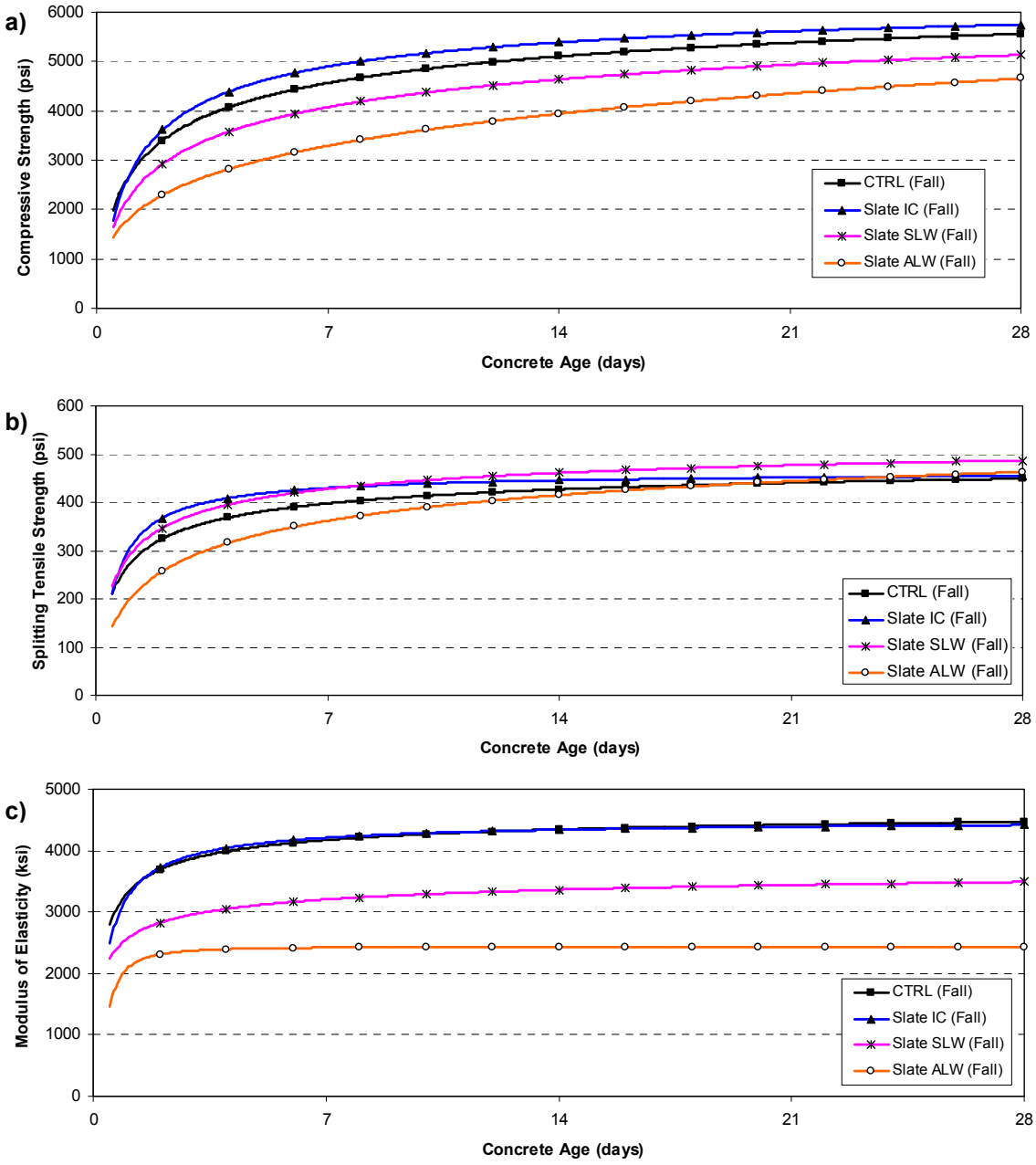

Figure 4-7: Fall placement scenario for slate and control mixtures: a) Compressive strength, b) Splitting tensile strength, and c) Modulus of elasticity development

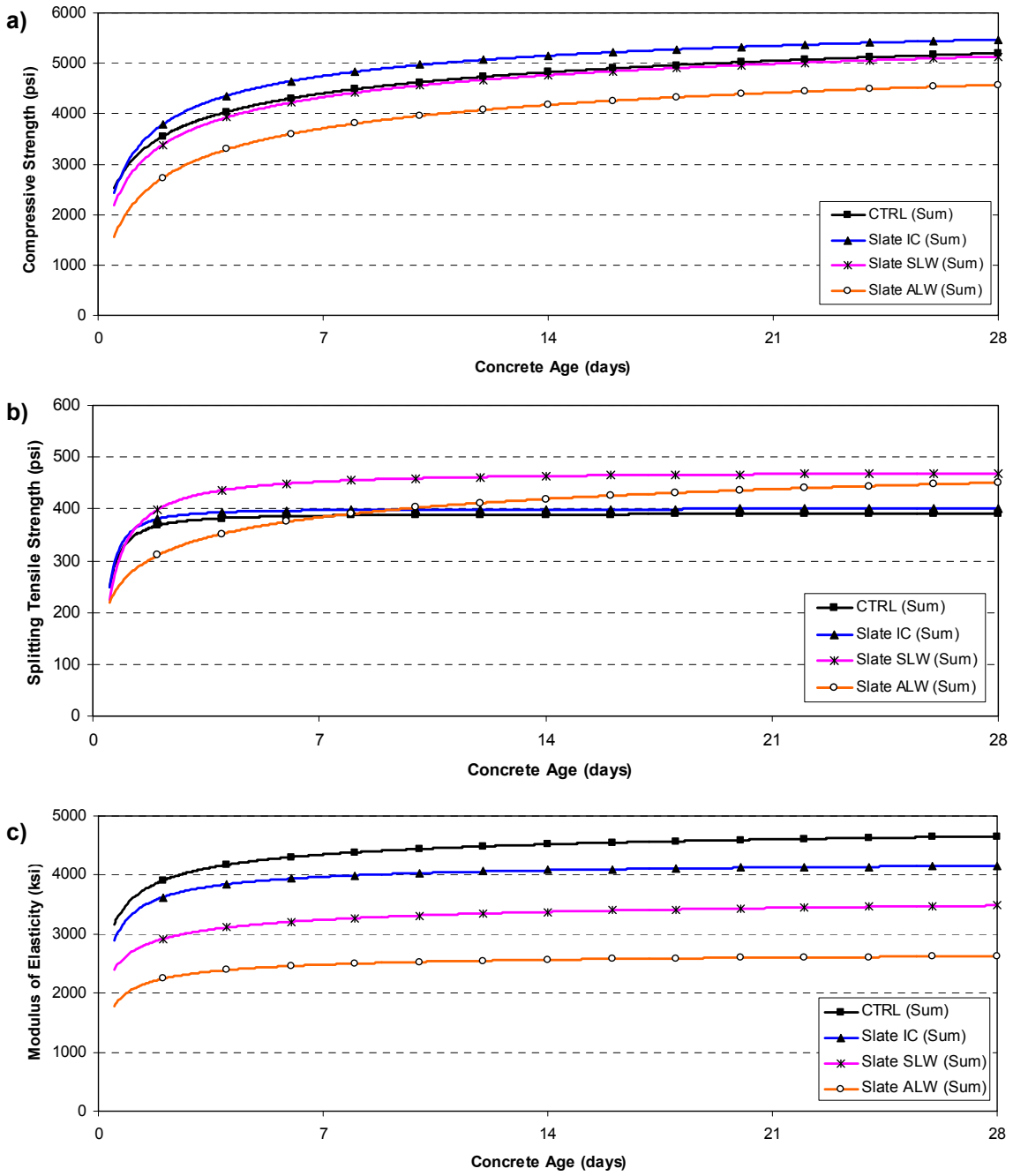

Figure 4-8: Summer placement scenario for slate and control mixtures: a) Compressive strength, b) Splitting tensile strength, and c) Modulus of elasticity development

4.2 EXPANDED CLAY RESULTS

4.2.1 Mixture Gradations and Proportions

Three concretes containing expanded clay LWA were produced and tested at two temperature scenarios. The three concretes were an internal curing (IC), a sand-lightweight (SWL) and an all-lightweight (ALW) concrete. The proportions for the concretes made with this LWA are shown in Table 3-3. The combined aggregate gradations of each mixture presented on a 0.45 power curve are presented in Figures 4-9 and 4-10.

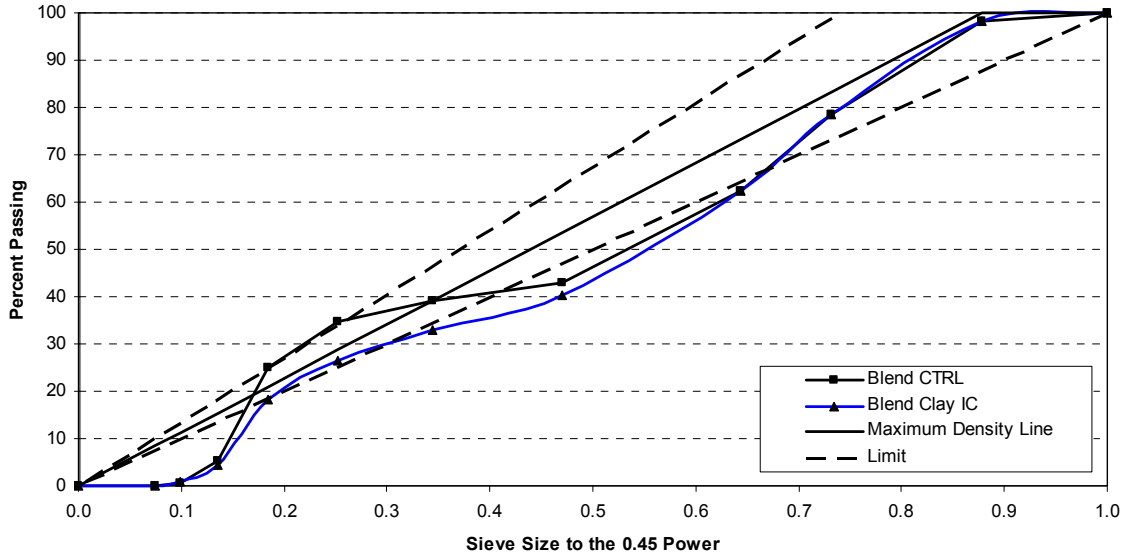

Figure 4-9: Combined gradation of CTRL and Clay IC mixtures on the 0.45 power curve

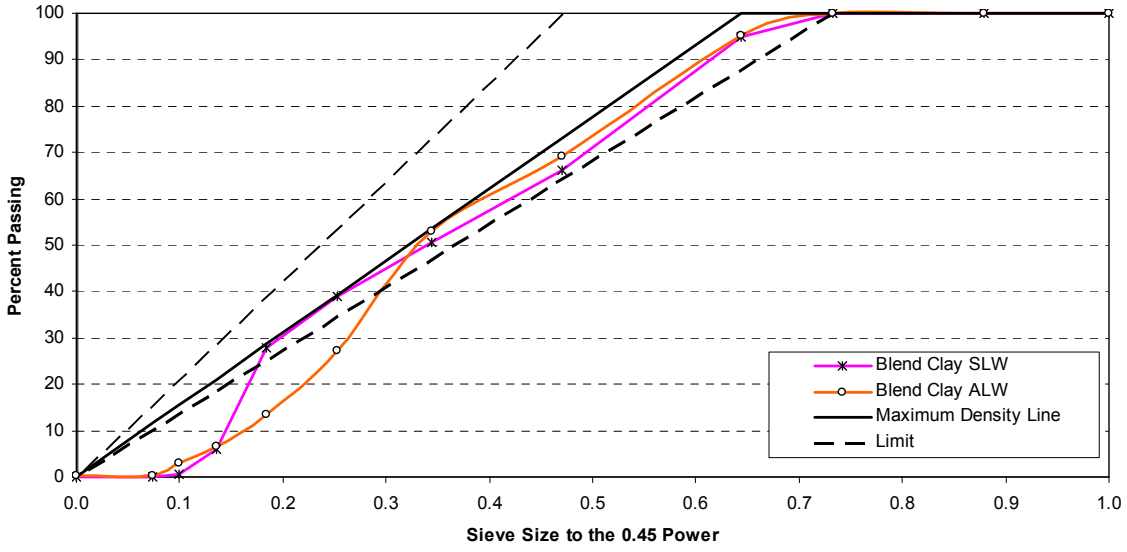

Figure 4-10: Combined gradation of Clay SLW and ALW mixtures on 0.45 power curve

4.2.2 Fresh Concrete Properties

For each mixture and placement scenario, two batches were produced. The first batch was used to produce the concrete cylinders for mechanical property testing and the second batch was for RCF and FSF testing. The fresh properties for each mixture, batch, and placement scenario are presented in Table 4-4. As mentioned previously, the "Δ Density" column in Table 4-4 is the difference between the measured density and the calculated density after correcting for the measured air content of each batch.

Table 4-4: Measured fresh concrete properties of expanded clay and control mixtures

Mixture and Placement Scenario	Batch No.	Fresh Concrete Test Results				Calculated
		Slump (in.)	Temp. (°F)	Air (%)	Density (lb/ft^3)	Δ Density (lb/ft^3)
CTRL (Fall)	1	3.25	74	5.0	143.8	0.3
	2	4.5	73	6.25	141.9	0.6
CTRL (Sum)	1	2.5	100	4.75	143.0	-0.3
	2	2.0	100	5.25	141.9	-0.6
Clay IC (Fall)	1	3.25	73	4.5	140.4	0.1
	2	4.75	73	5.25	136.4	0.2
Clay IC (Sum)	1	2.25	95	4.25	141.4	0.8
	2	2.5	96	4.5	140.6	0.3
Clay SLW (Fall)	1	3.75	74	5.0	122.1	0.0
	2	4.0	74	5.25	121.7	0.1
Clay SLW (Sum)	1	2.5	97	5.0	122.8	0.7
	2	2.25	97	4.5	123.4	0.7
Clay ALW (Fall)	1	3.0	73	6.0	105.6	0.6
	2	3.5	72	6.5	106.5	0.3
Clay ALW (Sum)	1	2.0	95	4.5	108.6	0.8
	2	2.25	95	4.75	107.4	-0.1

4.2.3 Miscellaneous Properties

The calculated equilibrium density as per ASTM C 567, coefficient of thermal expansion measured from the modified AASHTO T 336 setup, and the thermal diffusivity determined from semi-adiabatic calorimetry are summarized in Table 4-5.

Table 4-5: Miscellaneous properties of expanded clay and control mixtures

Property	CTRL	Clay IC	Clay SLW	Clay ALW
Calculated Equilibrium Density (lb/ft^3)	140.0	135.0	111.2	91.3
Coefficient of Thermal Expansion (με/°F)	6.2	5.8	5.1	4.0
Thermal Diffusivity (ft^2/hr)	0.046	0.042	0.035	0.030

4.2.4 Curing Temperatures

The curing temperature profiles for fall and summer placement scenarios for the expanded clay aggregate concretes and the normalweight aggregate control concrete are presented in Figure 4-11. The temperature profiles are truncated at the time of cracking.

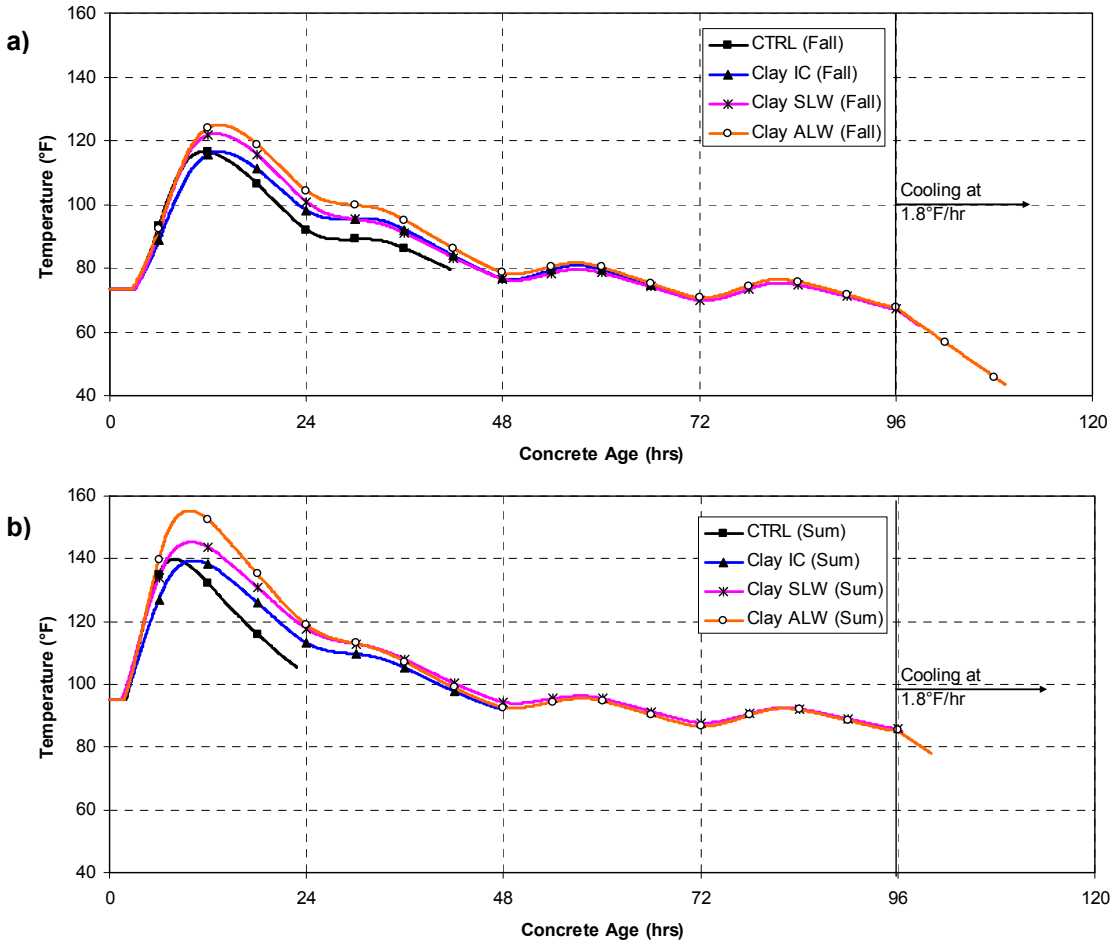

Figure 4-11: Modeled temperature profile for clay and control mixtures: a) Fall and b) Summer placement scenarios

4.2.5 Restrained Stress Development

The restrained stress development is presented in Figure 4-12 and Figure 4-13 for the match cured and isothermal cured conditions, respectively. The restrained stress development data for the match-cured condition end at the time of cracking. The restrained stress development for the isothermal curing conditions was measured for 96 hours.

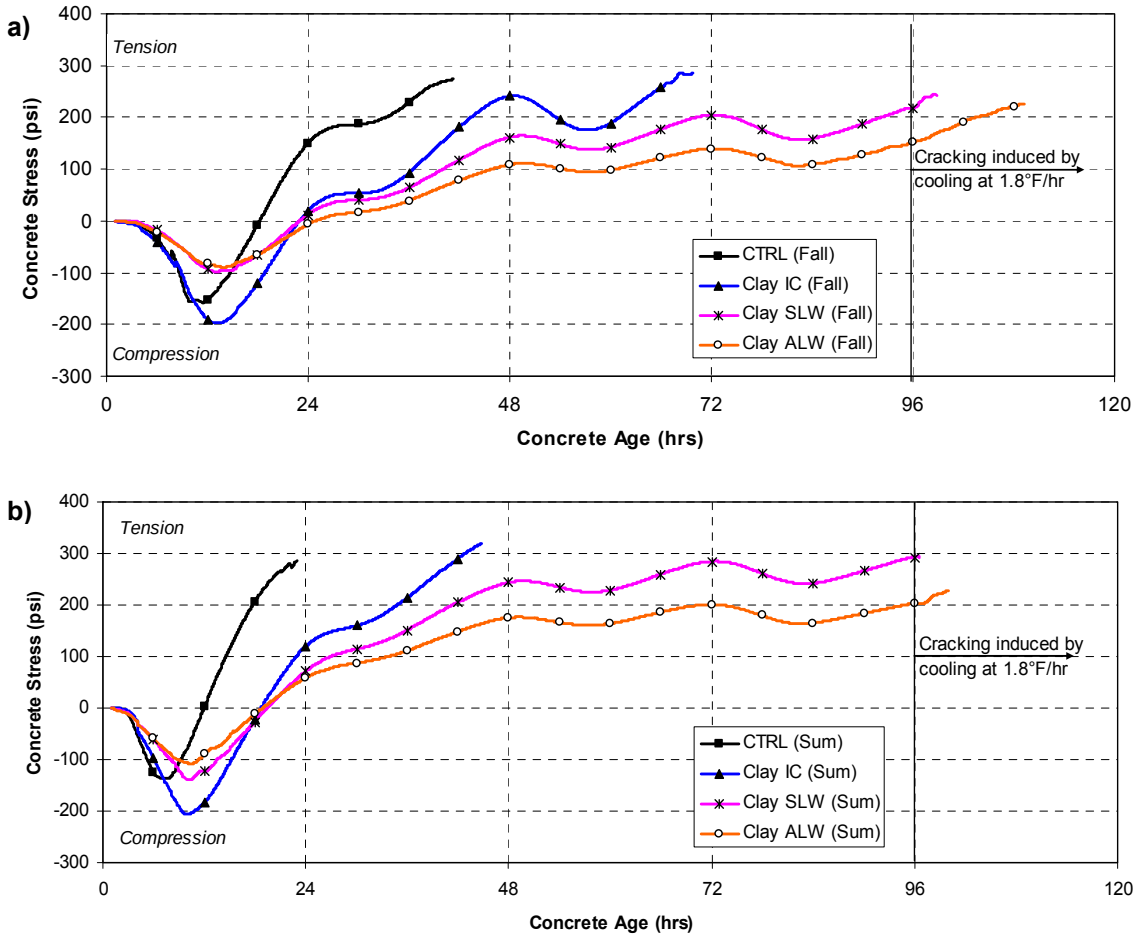

Figure 4-12: Restrained stress development for clay and control mixtures: a) Fall and b) Summer placement scenarios

4.2.5.1 Time to Zero Stress and Cracking

The time and temperature to the zero stress and cracking for each mixture and curing scenario is presented in Table 4-6.

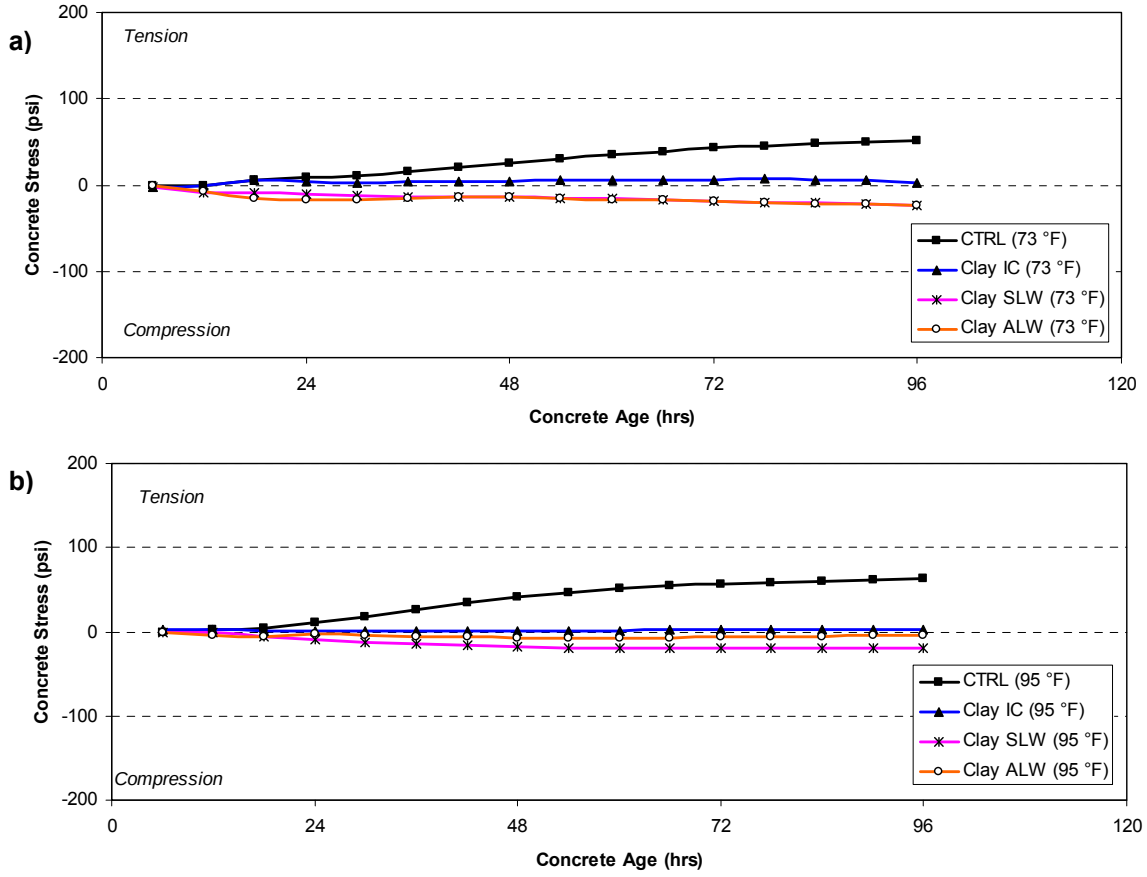

Figure 4-13: Restrained stress development for clay and control mixtures under: a) 73 °F and b) 95 °F isothermal conditions

Table 4-6: Time and temperature at zero stress and cracking of clay and control mixtures

Mixture	Zero Stress		Cracking	
	Time (hrs)	Temp. (°F)	Time (hrs)	Temp. (°F)
CTRL (Fall)	18.7	104.8	41.7	79.5
CTRL (Sum)	12.4	131.3	22.8	105.5
Clay IC (Fall)	22.8	100.3	69.8	71.4
Clay IC (Sum)	18.8	124.3	44.8	94.7
Clay SLW (Fall)	22.5	104.3	98.8 *	62.0
Clay SLW (Sum)	19.5	127.4	96.6 *	85.0
Clay ALW (Fall)	24.8	103.0	109.3 *	43.5
Clay ALW (Sum)	18.9	132.5	100.0 *	78.0

* Note: Cracking induced by cooling at 1.8 °F/hr after 96 hours

4.2.6 Measured Unrestrained Length Change

The strain measurements from the unrestrained specimens in the FSF are presented in Figure 4-14. The concrete specimens were match cured to the modeled temperature profile of the 8-in. thick bridge deck. The data are truncated at the time of initial cracking to help illustrate the strain developed in concrete until cracking occurred.

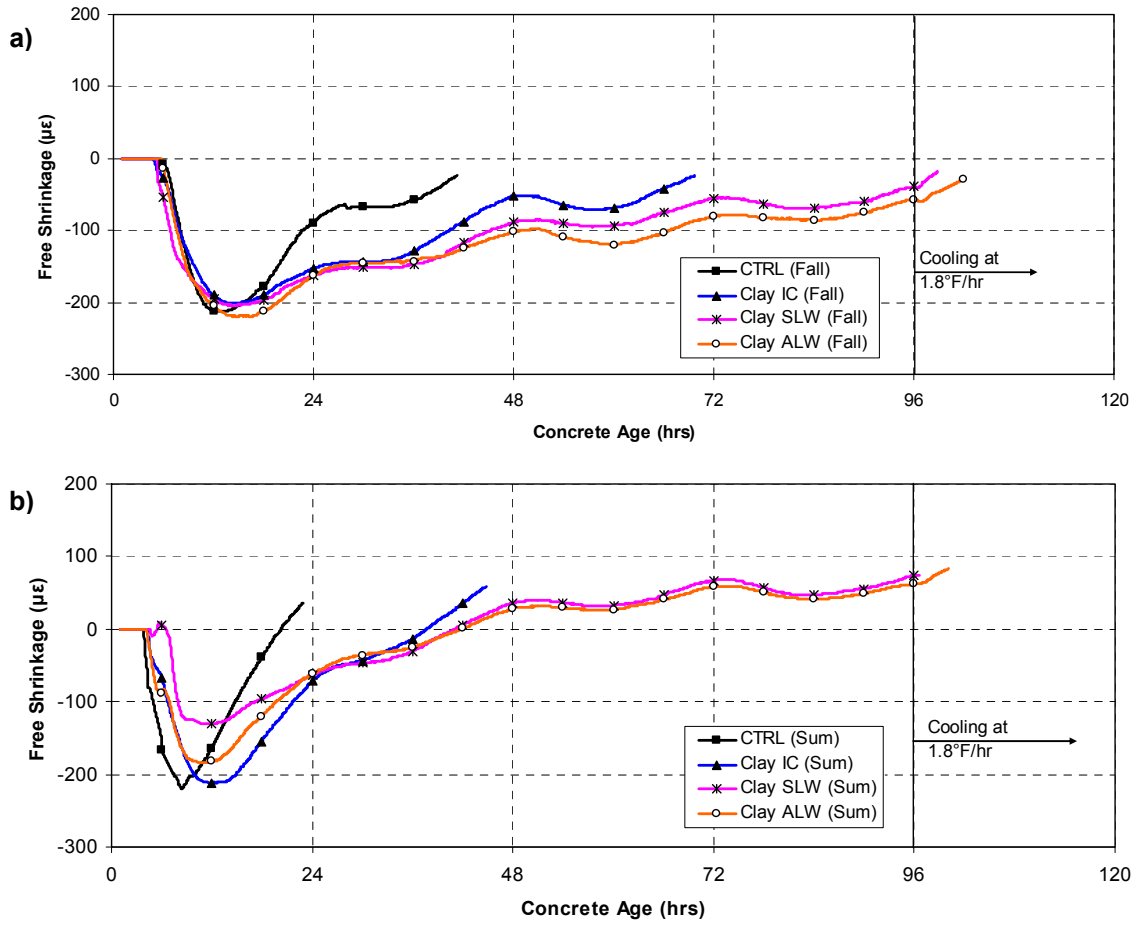

Figure 4-14: Free shrinkage strains for clay and control mixtures:
a) Fall and b) Summer placement scenarios

4.2.7 Mechanical Properties

The compressive strength, splitting tensile strength, and modulus of elasticity development were measured by testing cylinders match cured to the bridge deck temperature profile for each mixture and placement scenario. A regression analysis was performed on the discrete data points with the exponential function recommended by ASTM C 1074. The resulting best-fit curves for each property are shown in Figures 4-15 and 4-16 for fall and summer placement scenarios, respectively. The average of the two test cylinders for each mechanical property is summarized in Appendix B.

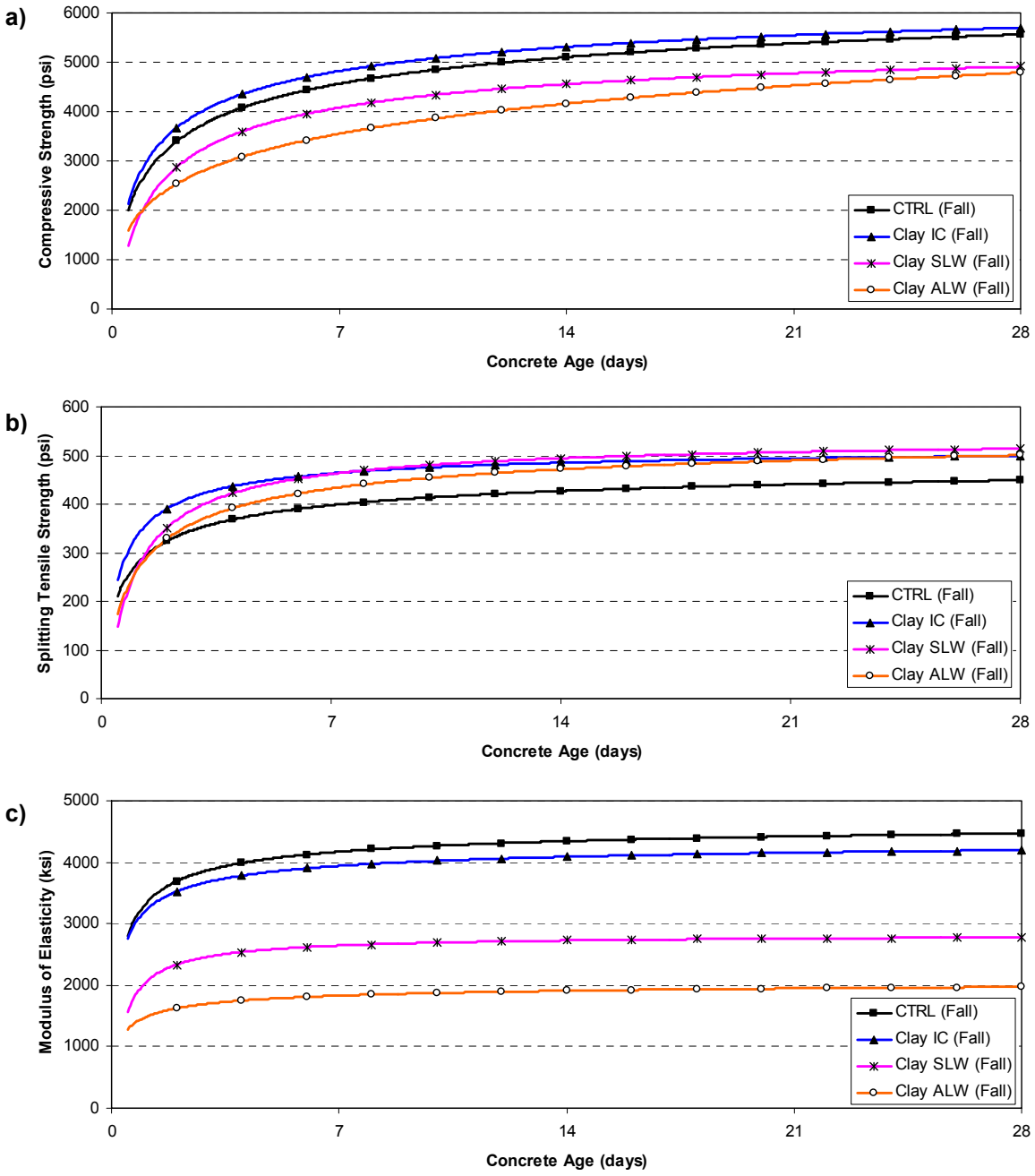

Figure 4-15: Fall placement scenario for clay and control mixtures: a) Compressive strength, b) Splitting tensile strength, and c) Modulus of elasticity development

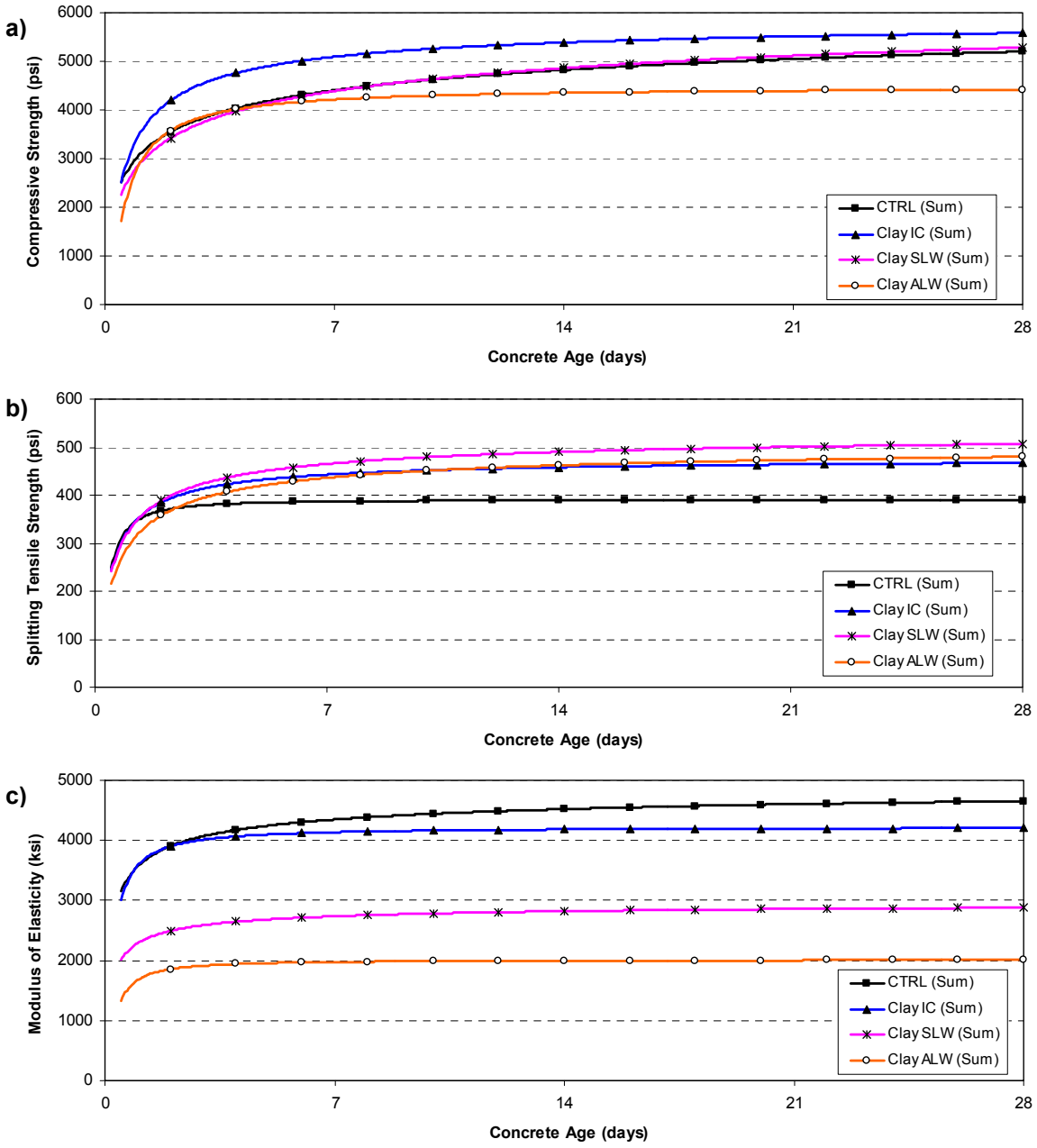

Figure 4-16: Summer placement scenario for clay and control mixtures: a) Compressive strength, b) Splitting tensile strength, and c) Modulus of elasticity development

4.3 EXPANDED SHALE RESULTS

4.3.1 Mixture Gradations and Proportions

Three concretes containing expanded shale LWA were produced and tested at two temperature scenarios. The three concretes used were an internal curing (IC), a sand-lightweight (SWL), and an all-lightweight (ALW) concrete. The proportions for the concretes made with this LWA are shown in Table 3-4. The combined aggregate gradations for the mixtures are presented on a 0.45 power curve in Figures 4-17 and 4-18.

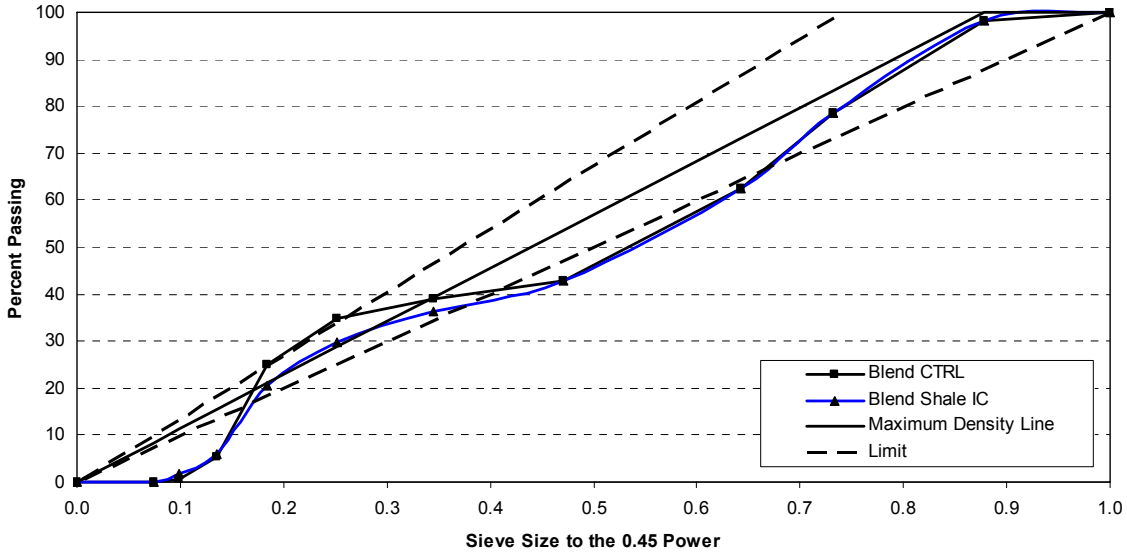

Figure 4-17: Combined gradation of CTRL and Shale IC mixtures on the 0.45 power curve

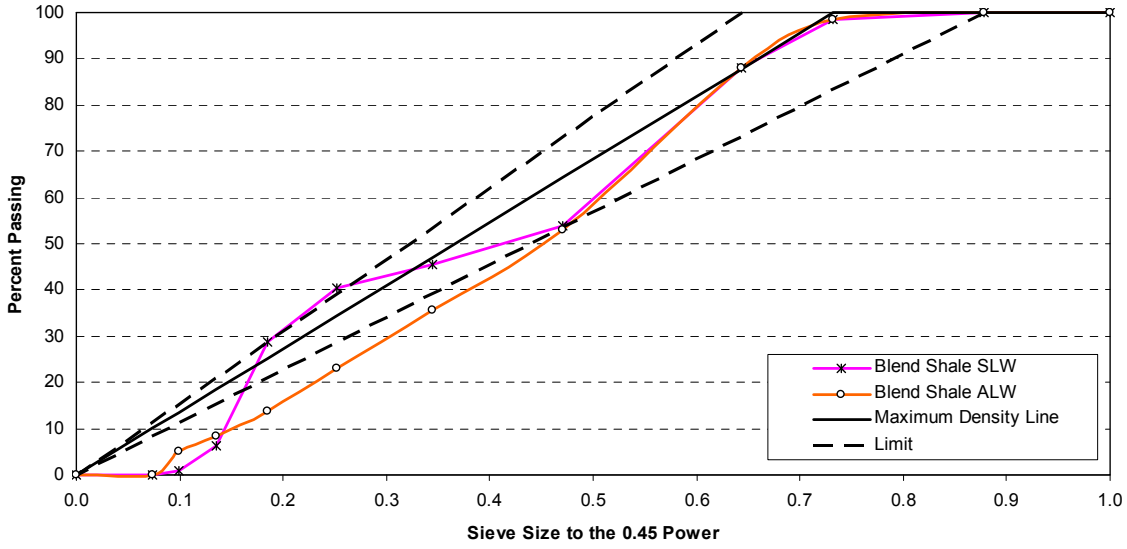

Figure 4-18: Combined gradation of Shale SLW and ALW mixtures on the 0.45 power curve

4.3.2 Fresh Concrete Properties

For each mixture and placement scenario, two batches were produced. The first batch was used to produce the concrete cylinders for mechanical property testing and the second batch was for RCF and FSF testing. The fresh properties for each mixture, batch and placement scenario is presented in Table 4-7. As mentioned previously, the "Δ Density" column in Table 4-7 is the difference between the measured density and the calculated density after correcting for the measured air content of each batch.

Table 4-7: Measured fresh concrete properties of expanded shale and control mixtures

Mixture and Placement Scenario	Batch No.	Fresh Concrete Test Results				Calculated
		Slump (in.)	Temp. (°F)	Air (%)	Density (lb/ft^3)	Δ Density (lb/ft^3)
CTRL (Fall)	1	3.25	74	5.0	143.8	0.3
	2	4.5	73	6.25	141.9	0.6
CTRL (Sum)	1	2.5	100	4.75	143.0	-0.3
	2	2.0	100	5.25	141.9	-0.6
Shale IC (Fall)	1	5.5	69	6.0	138.0	-0.3
	2	5.0	69	4.75	140.1	-0.2
Shale IC (Sum)	1	5.25	93	4.25	141.0	0.7
	2	3.5	97	4.0	141.0	-0.1
Shale SLW (Fall)	1	3.5	74	6.0	117.9	-0.8
	2	3.5	75	6.0	117.8	-1.0
Shale SLW (Sum)	1	2.0	94	4.25	120.5	-0.3
	2	2.0	95	4.25	120.4	-0.5
Shale ALW (Fall)	1	2.75	76	5.5	103.2	-0.4
	2	2.5	75	4.5	104.4	-0.2
Shale ALW (Sum)	1	3.0	94	5.0	104.6	0.5
	2	5.5	97	5.25	103.4	-0.4

4.3.3 Miscellaneous Properties

The calculated equilibrium density as per ASTM C 567, coefficient of thermal expansion measured from the modified AASHTO T 336 setup, and the thermal diffusivity determined from semi-adiabatic calorimetry are summarized in Table 4-8.

Table 4-8: Miscellaneous properties of expanded shale and control mixtures

Property	CTRL	Shale IC	Shale SLW	Shale ALW
Calculated Equilibrium Density (lb/ft^3)	140.0	135.0	110.6	87.1
Coefficient of Thermal Expansion (με/°F)	6.2	6.0	5.2	4.0
Thermal Diffusivity (ft^2/hr)	0.046	0.042	0.035	0.029

4.3.4 Curing Temperatures

The curing temperature profiles from for fall and summer placement scenarios for the expanded shale aggregate concretes and the normalweight control concrete are presented in Figure 4-19. The temperature profiles end when cracking occurred in RCF A.

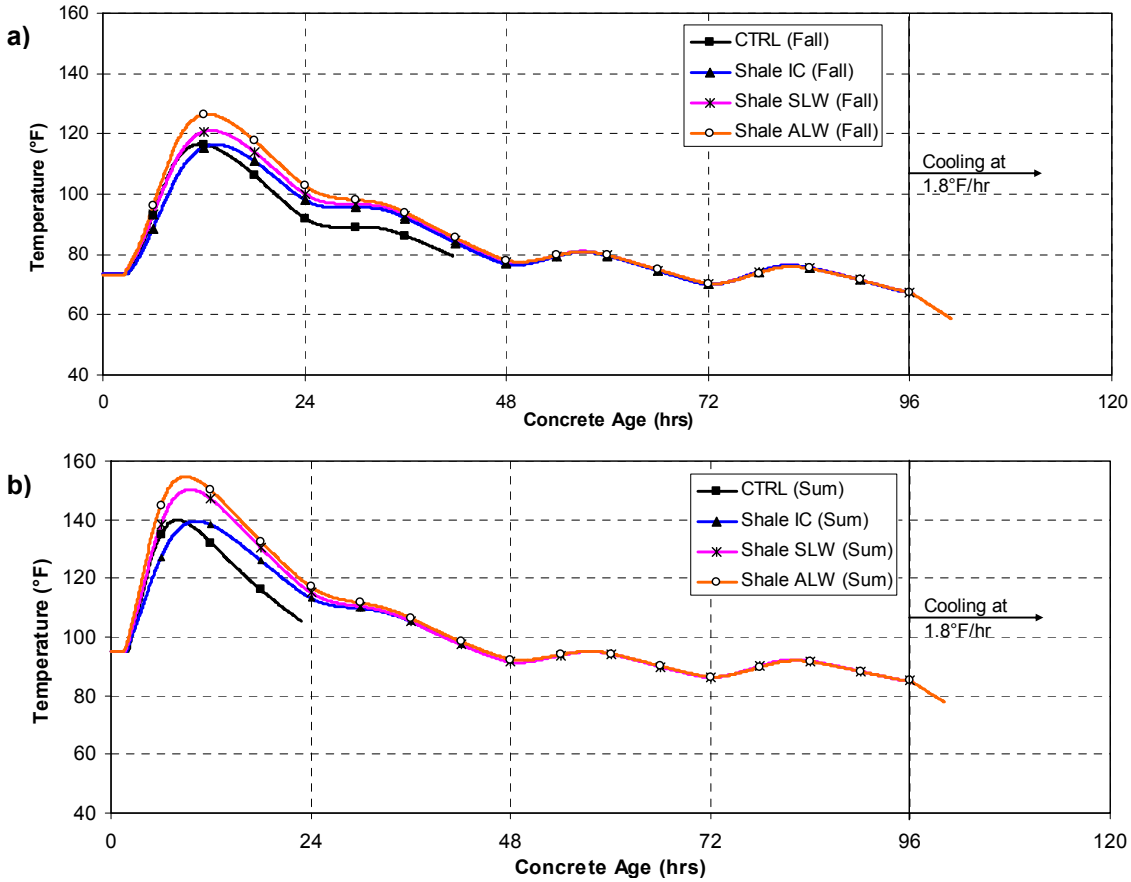

Figure 4-19: Modeled temperature profile for expanded shale and control mixtures: a) Fall and b) Summer placement scenarios

4.3.5 Restrained Stress Development

The restrained stress development is presented in Figure 4-20 and Figure 4-21 for the match cured and isothermal cured conditions, respectively. The restrained stress development data for

the match-cured condition end at the time of cracking. The restrained stress development for the isothermal curing conditions was measured for 96 hours.

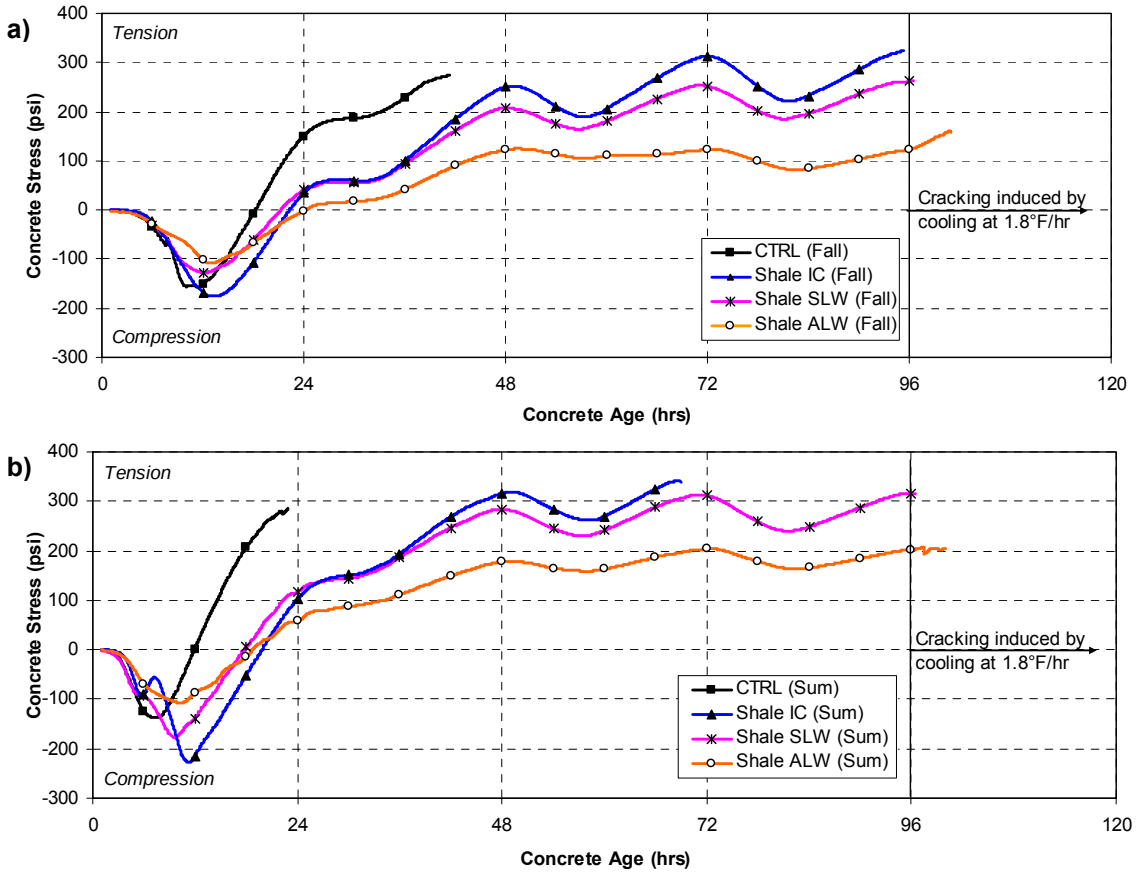

Figure 4-20: Restrained stress development for expanded shale and control mixtures: a) Fall and b) Summer placement scenarios

4.3.5.1 Time to zero stress and cracking

The time and temperature to the zero stress and cracking for each mixture and curing scenario is presented in Table 4-9.

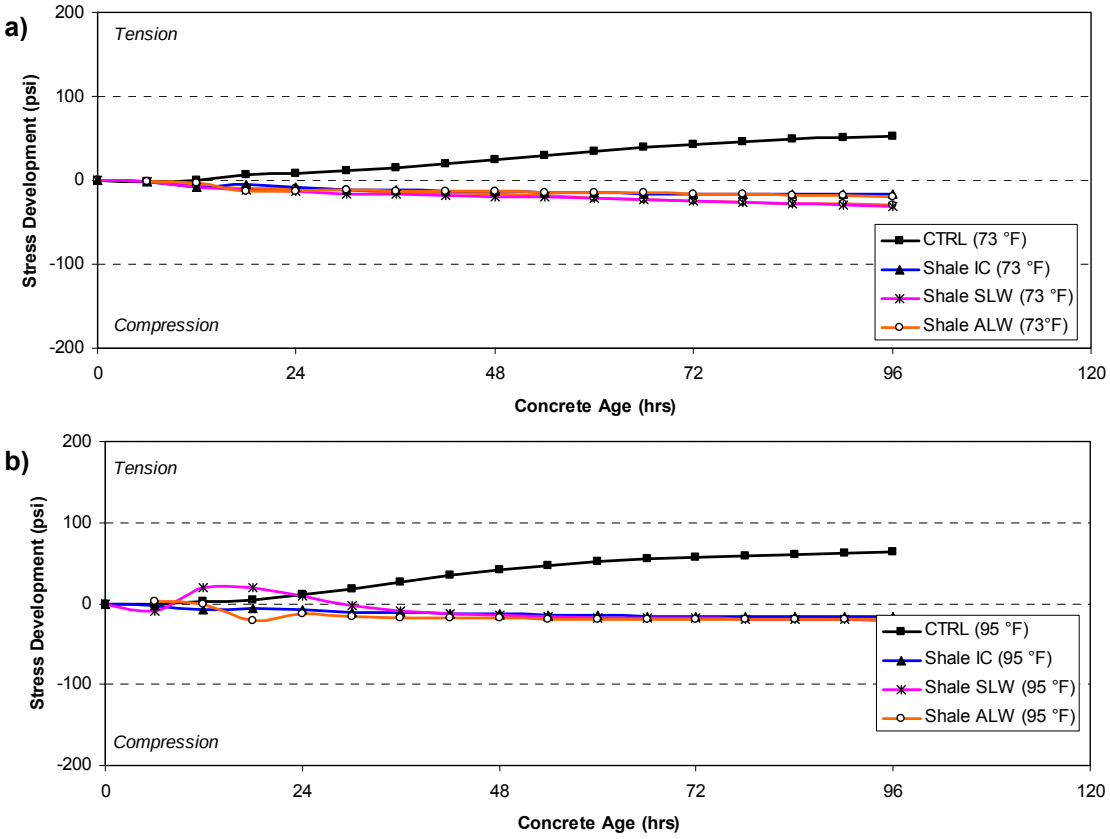

Figure 4-21: Restrained stress development for expanded shale and control mixtures under: a) 73 °F and b) 95°F isothermal conditions

Table 4-9: Time and temperature to zero stress and cracking of shale and control mixtures

Mixture	Zero Stress		Cracking	
	Time (hrs)	Temp. (°F)	Time (hrs)	Temp. (°F)
CTRL (Fall)	18.7	104.8	41.7	79.5
CTRL (Sum)	12.4	131.3	22.8	105.5
Shale IC (Fall)	24.3	99.7	95.3	67.6
Shale IC (Sum)	19.0	127.6	68.9	88.4
Shale SLW (Fall)	21.3	103.9	96.5 *	66.5
Shale SLW (Sum)	17.8	126.6	96.4 *	84.5
Shale ALW (Fall)	22.3	104.6	101.0 *	58.5
Shale ALW (Sum)	19.8	125.6	100.1 *	77.7

* Note: Cracking induced by cooling at 1.8 °F/hr after 96 hours

4.3.6 Measured Unrestrained Length Change

The strain measurements from the unrestrained specimens in the FSF are presented in Figure 4-22. The concrete specimens were match cured to the modeled temperature profile of the 8-in. thick bridge deck. The data are truncated at the time of initial cracking to help illustrate the strain developed in concrete until cracking occurred.

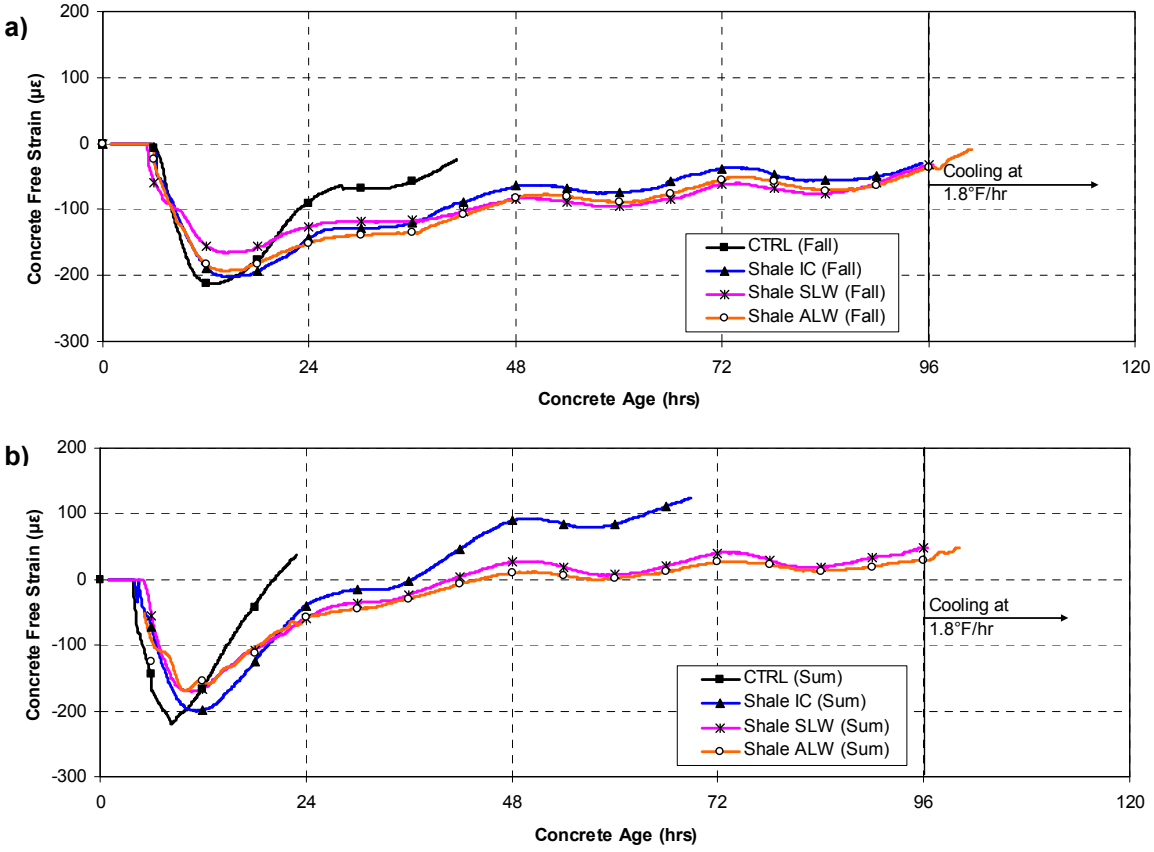

Figure 4-22: Free shrinkage strains for expanded shale and control mixtures: a) Fall and b) Summer placement scenarios

4.3.7 Mechanical Properties

The compressive strength, splitting tensile strength, and modulus of elasticity development were measured by testing cylinders match cured to the bridge deck temperature profile for each mixture and placement scenario. A regression analysis was performed on the discrete data points with the exponential function recommended by ASTM C 1074. The resulting best-fit curves for each property are shown in Figures 4-23 and 4-24 for fall and summer placement scenarios, respectively.

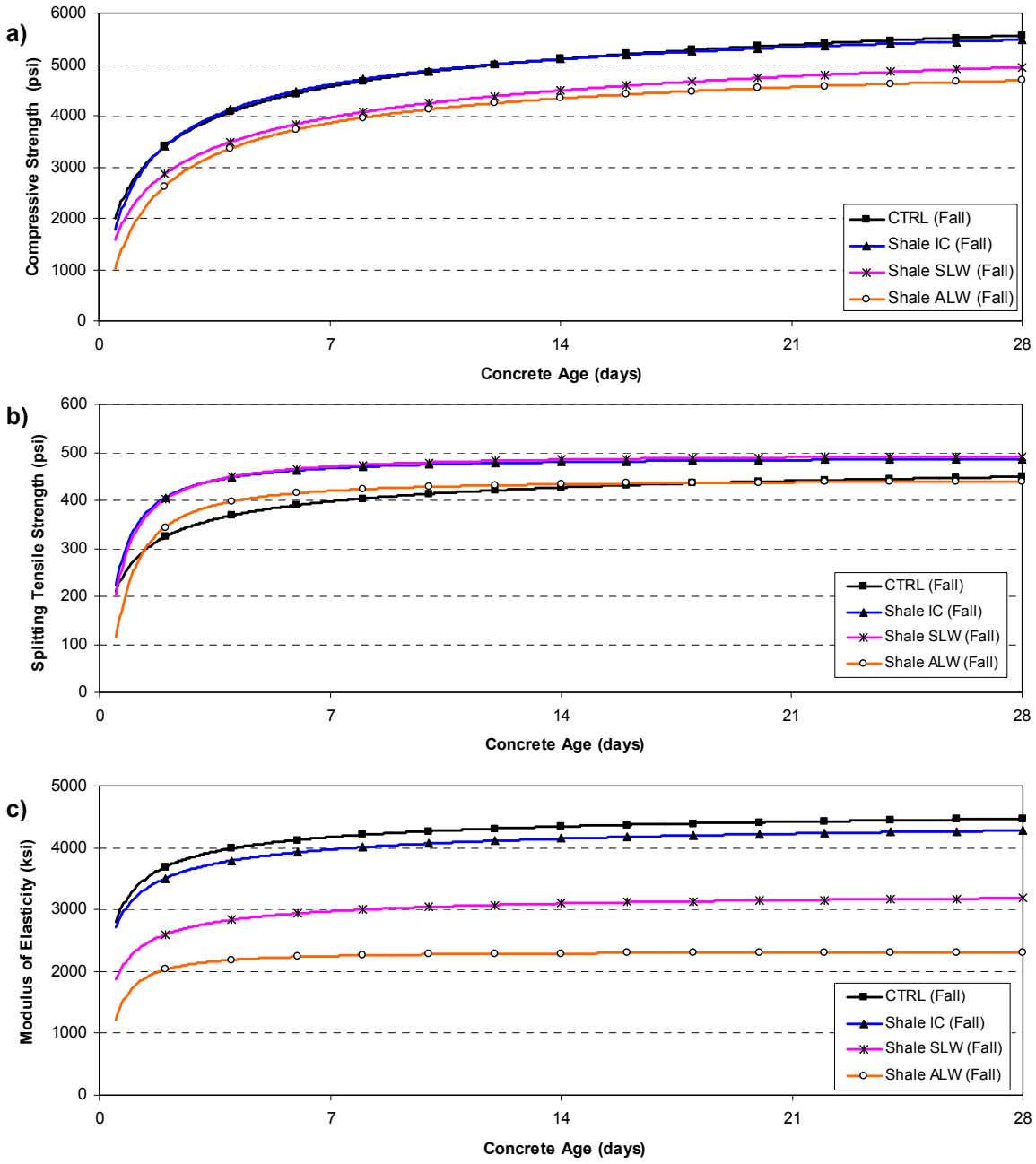

Figure 4-23: Fall placement scenario for shale and control mixtures: a) Compressive strength, b) Splitting tensile strength, and c) Modulus of elasticity development

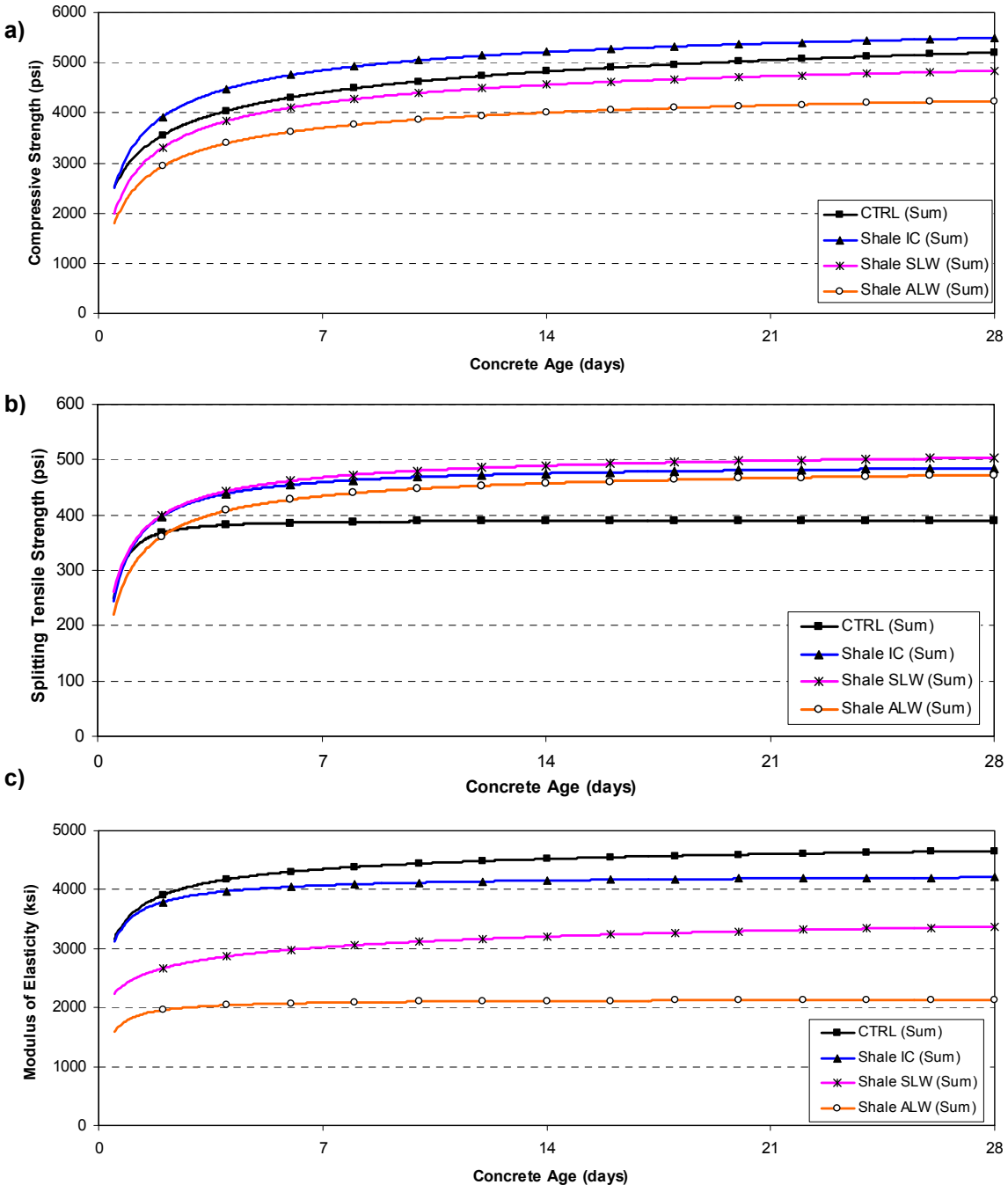

Figure 4-24: Summer placement scenario for shale and control mixtures: a) Compressive strength, b) Splitting tensile strength, and c) Modulus of elasticity development

Chapter 5

Discussion of Results

A discussion and synthesis of the results are presented in this chapter. The changes in concrete properties when lightweight aggregates are introduced are evaluated in Section 5.1 of this chapter. The effects of placement and curing temperature are discussed in Section 5.2. The effect of using various lightweight aggregates on the cracking tendency, autogenous shrinkage, and peak hydration temperature is then evaluated. The mechanisms by which the altered concrete properties affect early-age stress are discussed in Section 5.6. The applicability of the ACI 318 (2008) expression to estimate the modulus of elasticity and ACI 207.2R and ACI 207.1R to estimate the splitting tensile strength of the concretes made with LWAs are assessed at the end of this chapter.

5.1 Effect of Lightweight Aggregates on Concrete Properties

5.1.1 Modulus of Elasticity

The modulus of elasticity development for all concretes and both placement scenarios is presented in Part (c) of Figures 4-7, 4-8, 4-15, 4-16, 4-23, and 4-24. It can be seen that the ALW concrete has a significantly lower modulus of elasticity than the other concretes. In all cases, except for Slate IC (Fall), the modulus of elasticity is reduced when lightweight aggregate is added to the mixture. This reduction in modulus of elasticity is due to the reduced stiffness of the LWA. The reduction in modulus of elasticity was expected, as the addition of LWA lowers the density of the concrete as compared to its control concrete, which as per Equation 2-2 will lower the modulus of elasticity. The results for the Slate IC (Fall) test seem similar to that of the normalweight concrete; however, this is not the case for the Slate IC (Sum) results. Since the Slate IC (Fall) modulus of elasticity results are the only ones not reduced by the addition of LWA, these results may be a slight anomaly and not the norm.

5.1.2 Compressive Strength

The compressive strength development for all concretes are presented in Part (a) of Figures 4-7, 4-8, 4-15, 4-16, 4-23, and 4-24. All internal curing (IC) mixtures, except Shale IC (Fall), have slightly higher compressive strengths at all ages than the normalweight control concrete. The compressive strength of the Shale IC (Fall) is similar to that of the normalweight control concrete. The compressive strength of the SLW concretes is similar to that of the normalweight control concrete. Whereas, the compressive strength for all ALW concretes is approximately 13 to 19% lower when compared to that of the normalweight control concrete. The ALW mixtures could

have been proportioned with a lower water-cement ratio to have strength equivalent to the control concrete. However, since the 28-day compressive strength level of the ALW mixtures sufficiently exceeded 4,000 psi, it was decided to proportion the SLW and ALW concretes with the same water-cement ratio and paste volume.

5.1.3 Splitting Tensile Strength

The splitting tensile strength development for all concretes are presented in Parts (b) of Figures 4-7, 4-8, 4-15, 4-16, 4-23, and 4-24. All internal curing concretes exhibited an increase in tensile strength when compared to the normalweight control concrete. Furthermore, the increase in tensile strength was more for the clay and shale internal curing concretes, which occurs probably because these IC concretes provide more internal curing water, which promotes increased cement hydration. An interesting finding is that the splitting tensile strength of all the SLW concretes is either higher or similar to that of the IC concretes although their compressive strengths are lower. In all cases, the splitting tensile strength of the SLW concretes exceeds that of the normalweight control concrete. The increase in tensile strength of the SLW concrete as compared to the normalweight control concrete is partly attributable to the replacement of river gravel with an angular porous lightweight aggregate as well as increased cement hydration. The increased cement hydration is promoted by the availability of additional water desorbed from the LWA.

Mixed trends can be observed from the splitting tensile strength results of the ALW concretes. The slate ALW concrete has a decreased splitting tensile strength up to an age of approximately 7 days when compared to the normalweight control concrete. Whereas, both the clay and shale ALW concretes have a similar or slightly increased splitting tensile strength when compared to the normalweight control concrete. The difference in the splitting tensile strength results of the ALW concretes may be related to the poor particle packing of the slate ALW mixture, as shown in Figure 4-2. The particle packing was closer to the maximum density line for the clay and shale concretes, as shown in Figures 4-10 and 4-18. Further research is necessary to confirm the cause of the reduced tensile strength of the slate ALW concrete used in this study as compared to the clay and shale ALW concretes.

5.1.4 Coefficient of Thermal Expansion

The measured coefficient of thermal expansion values for all concretes are summarized in Tables 4-2, 4-5, and 4-8. In all cases, the concretes in ascending order of coefficient of thermal expansion are ALW, SLW, IC, and normalweight. There is a significant reduction of about 30 % in coefficient of thermal expansion for all of the all-lightweight concretes when compared to the normalweight control concrete. The coefficient of thermal expansion is reduced by about 15 % for all the sand-lightweight concretes when compared to the normalweight control concrete.

The finding that the addition of lightweight aggregate lowers the coefficient of thermal expansion of concrete made with river gravel aggregate is significant in applications where thermal cracking occurs, as is the case in bridge decks or pavements. Equation 2-1 indicates that the magnitude of thermal stress is proportional to the coefficient of thermal expansion; therefore, any reduction in coefficient of thermal expansion will reduce the magnitude of thermal stress that develops.

5.1.5 Thermal Diffusivity

The measured thermal diffusivity values for all concretes are summarized in Tables 4-2, 4-5, and 4-8. Concrete with high thermal diffusivity, more rapidly adjusts its temperature to that of its surroundings than a concrete with a low thermal diffusivity. In all cases, the concretes in ascending order of thermal diffusivity are ALW, SLW, IC, and CTRL. The thermal diffusivity decreases as the amount of lightweight aggregate added to mixture is increased.

5.2 Effect of Placement Season

The cracking times for each mixture for fall and summer placement scenario are shown in Figures 5-1 and 5-2, respectively. From comparison of the results on Figures 4-4, 4-12, 4-20, 5-1, and 5-2 and the data presented in Tables 4-3, 4-6, and 4-9, it can also be concluded that increasing the placement and curing temperature increases the zero-stress temperature and decreases the time to cracking. As shown in Equation 2-1, the higher the zero-stress temperature, the greater the thermal stresses become. Breitenbücher and Mangold (1994) also found that decreasing the temperature of the fresh concrete significantly increased the time to cracking. These results confirm that the thermal stresses that develop during summer placement conditions are much higher than those that develop during fall placement conditions.

A comparison of the results in Figures 5-1 and 5-2 reveal that the time to cracking for all concretes made with LWA when placed under *summer* placement conditions, is *greater* than the time to cracking of the normalweight concrete when placed under *fall* conditions. This indicates that the use of pre-wetted LWA may be especially beneficial during summer time placement conditions to minimize the occurrence of cracking at early ages in bridge deck applications.

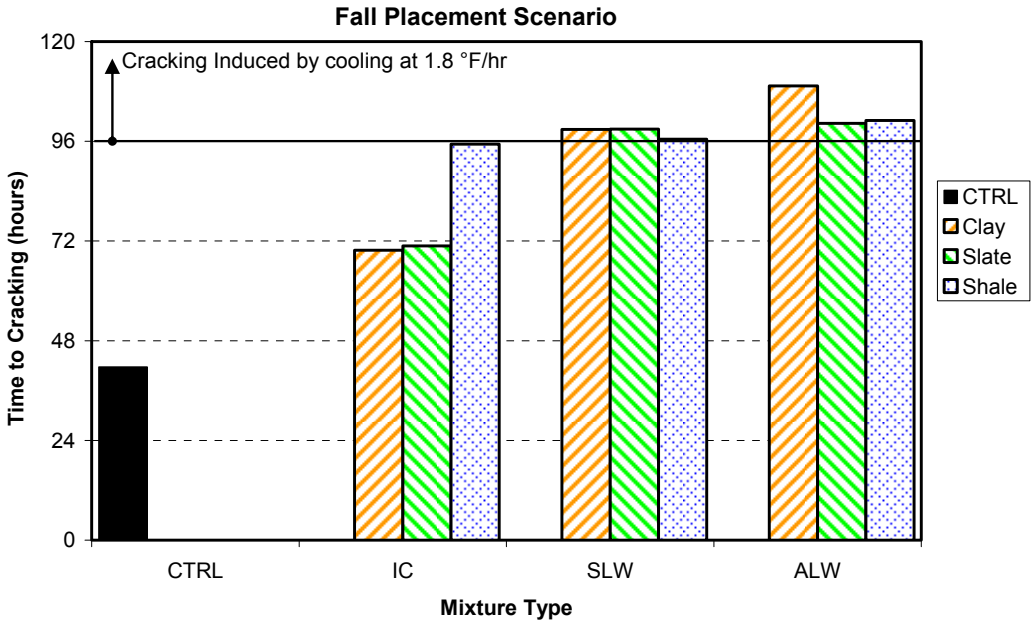

Figure 5-1: Time to cracking for the fall placement scenario

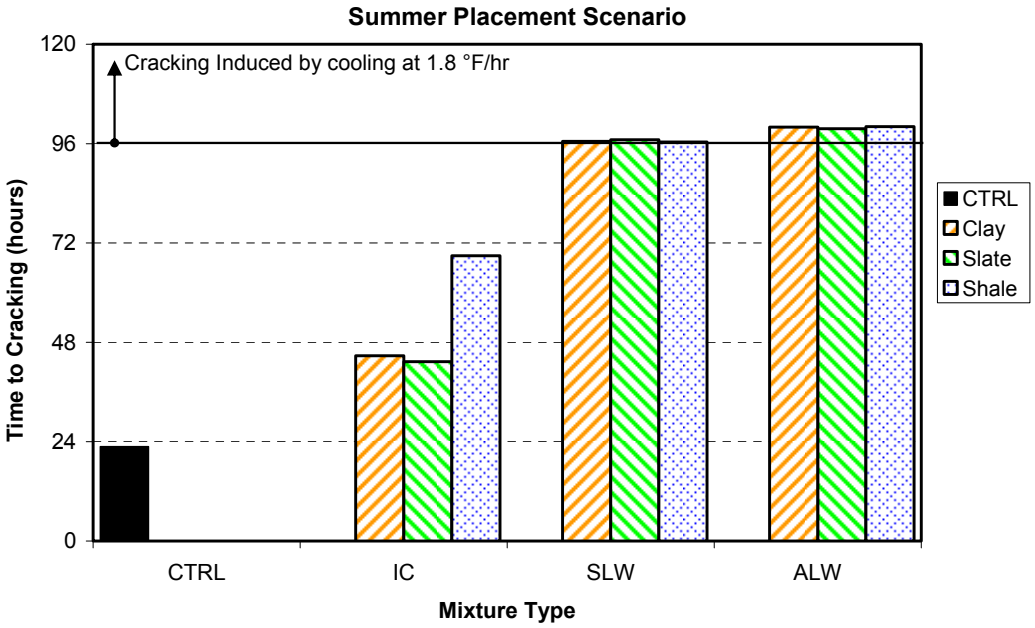

Figure 5-2: Time to cracking for the summer placement scenario

5.3 EFFECT OF INTERNAL CURING WATER ON AUTOGENOUS STRESS DEVELOPMENT

The internal curing water provided by each mixture containing LWA is summarized in Table 3-5. The SLW and ALW concretes have more water available because of the greater proportion of LWA in these mixtures. The stress development due to autogenous shrinkage effects are shown for all concretes in Figures 4-5, 4-13, and 4-21. The stress developed due to autogenous shrinkage effects is in all cases reduced by the introduction of lightweight aggregates when

compared to the behavior of the normalweight control concrete. The decrease in autogenous stresses is due to the availability of water from the LWA to fill capillary voids formed by chemical shrinkage and the reduction in modulus of elasticity. The IC concretes experienced reduced autogenous shrinkage compared to the control concrete due to the fraction of fine LWA replacement and its reduced modulus of elasticity. The SLW and ALW concretes have an even greater reduction in autogenous tensile stress than the IC concretes. It can be concluded that both the SLW and ALW concretes completely prevent the development of tensile stresses caused by autogenous shrinkage effects. These SLW and ALW concretes thus contain sufficient amounts of internal curing water to mitigate the effects of autogenous shrinkage.

5.4 COMPARISON OF THE BEHAVIOR OF VARIOUS TYPES OF LIGHTWEIGHT CONCRETES

The early-age behavior of the internal curing, sand-lightweight, and all-lightweight concretes with the various sources of lightweight aggregate are compared to the behavior of a normalweight control concrete in this section.

5.4.1 Response of Internal Curing Concretes

The modeled temperature profiles, the match-cured restrained stress development, and the isothermal restrained stress development for the internal curing concretes for all three sources of lightweight aggregates are compared to the response of the control concrete for the fall placement scenario in Figure 5-3. The amount of internal curing water provided by each internal curing mixture is shown in Figure 5-3c. The internal curing water provide was calculated using the absorbed water in the LWA and the desorption coefficients presented in Table 2-2. The modeled temperature profiles for the three IC concretes were nearly identical, as shown in Figure 5-3a.

The effect of using LWA for internal curing purposes is evident in Figure 5-3c, which show the stress development under isothermal curing conditions. All three internal curing mixtures experienced *reduced* stress development due to autogenous shrinkage effects when compared to the normalweight concrete (CTRL). The decrease in autogenous stresses is due to the availability of water from the LWA to fill capillary voids formed by chemical shrinkage and the reduction in modulus of elasticity. The Shale IC and Clay IC concretes reduce the autogenous stress more than the Slate IC concrete as they contain more internal curing water available from the LWA. The fact that the stress development of Shale IC remains in compression, simply indicates that sufficient internal curing water is provided to negate the development of tensile stresses.

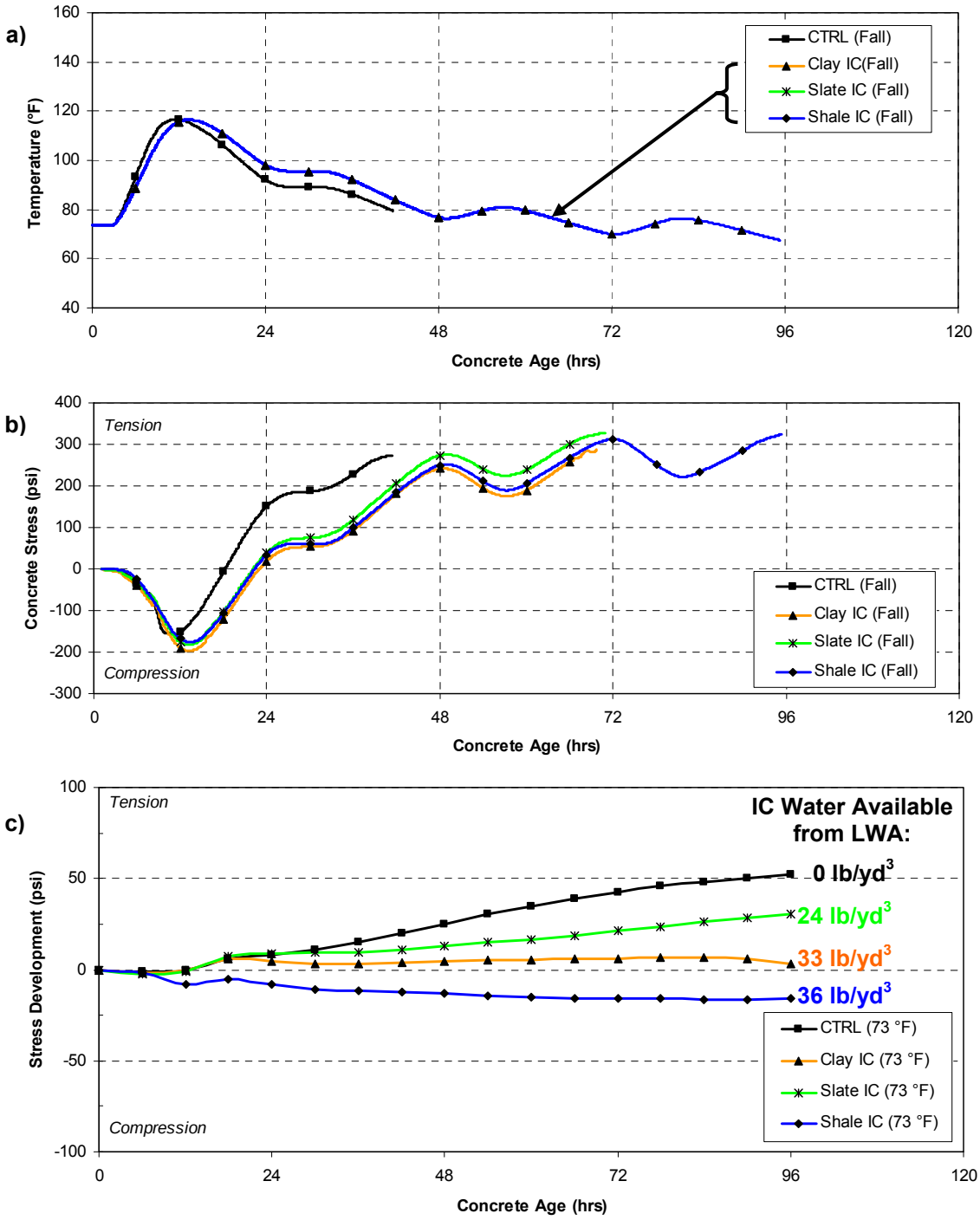

Figure 5-3: Fall placement scenario: a) Temperature profiles, b) Match-cured restrained stress development, and c) Isothermal restrained stress development for internal curing mixtures

It is clear from the results shown in Figure 5-3b that the use of lightweight aggregates in these internal curing concretes delays the occurrence of cracking at early ages in bridge deck concrete applications. As stated in Section 5.2, the results shown in Figures 4-4, 4-12, 4-20, 5-1, and 5-2 also reveal that the use of LWA in *summer* conditions, improves the time to cracking of

the concrete to exceed the time of cracking of the control concrete placed in under *fall* conditions. This improvement in cracking behavior is attributed to the *increased* tensile strength and *decrease* in modulus of elasticity, coefficient of thermal expansion, and autogenous shrinkage of the internal curing concretes when compared to the normalweight control concrete.

It can be seen in Figure 5-3b that all three IC concretes cracked at a similar level of tensile stress; however, the shale concrete did not crack at the 96-hour temperature low, thereby delaying its cracking an additional 24 hours. Of the internal curing concretes, the slate LWA had the lowest absorption capacity and did not fully mitigate the isothermal stress as seen in Figure 5-3c. This difference in the degree of autogenous stress mitigation, may explain the slight difference in measured tensile stress between the Slate IC mixture and the other two IC mixtures

5.4.2 Response of Sand-Lightweight Concretes

The modeled temperature profiles, the match-cured restrained stress development, and the modulus of elasticity development for the sand-lightweight concretes for all three sources of lightweight aggregates are compared to the response of the control concrete for the fall placement scenario in Figure 5-4.

It is clear from the results shown in Figure 5-4b that the use of lightweight aggregates in these sand-lightweight concretes significantly reduces the tensile stress and delays the occurrence of cracking at early ages in bridge deck concrete applications. This improvement in cracking behavior is caused by the *decreased* modulus of elasticity, coefficient of thermal expansion, and autogenous shrinkage of the SLW concretes when compared to the normalweight control concrete.

The SLW concretes have similar coefficient of thermal expansion values and curing temperature profiles. Because of these factors and the fact that autogenous shrinkage effects are not present in these SLW concretes, the difference in stress development shown in Figure 5-4b is primarily attributable to differences in modulus of elasticity values of these SLW concretes as shown in Figure 5-4c. For example, because the Clay SLW concrete has the lowest modulus of elasticity, the stresses that develop from the same change in temperature are the least, as seen in the test results. However, all three SLW concretes cracked at very similar times, which indicate that they provide similar levels of improvement to the cracking response of the normalweight control concrete.

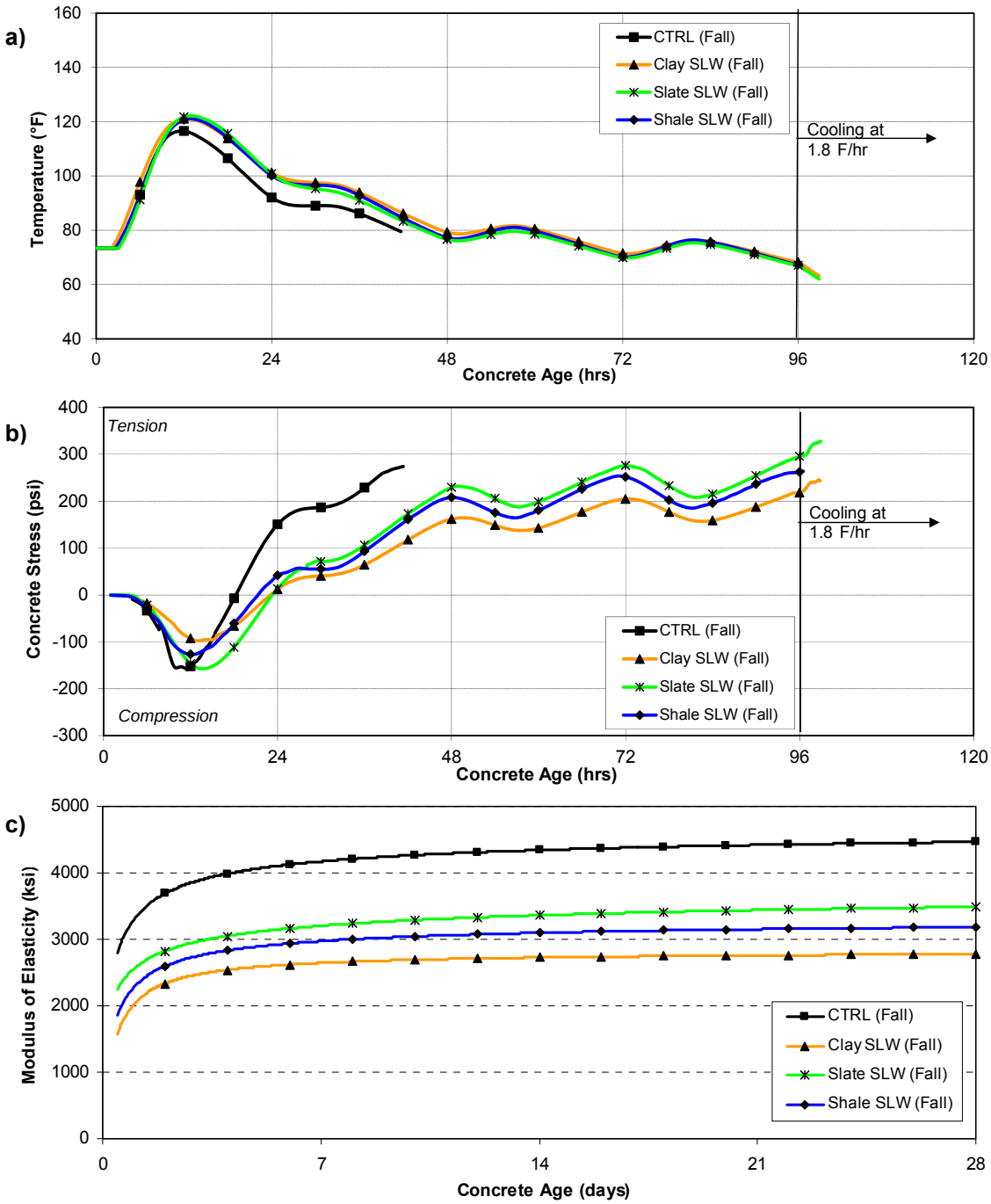

Figure 5-4: Fall placement scenario a) Temperature profiles, b) Match-cured restrained stress development, and c) Modulus of elasticity development for SLW mixtures

5.4.3 Response of All-Lightweight Concretes

The modeled temperature profiles, the match-cured restrained stress development, and the modulus of elasticity development for the all-lightweight concretes are compared to the response of the control concrete for the fall placement scenario in Figure 5-5.

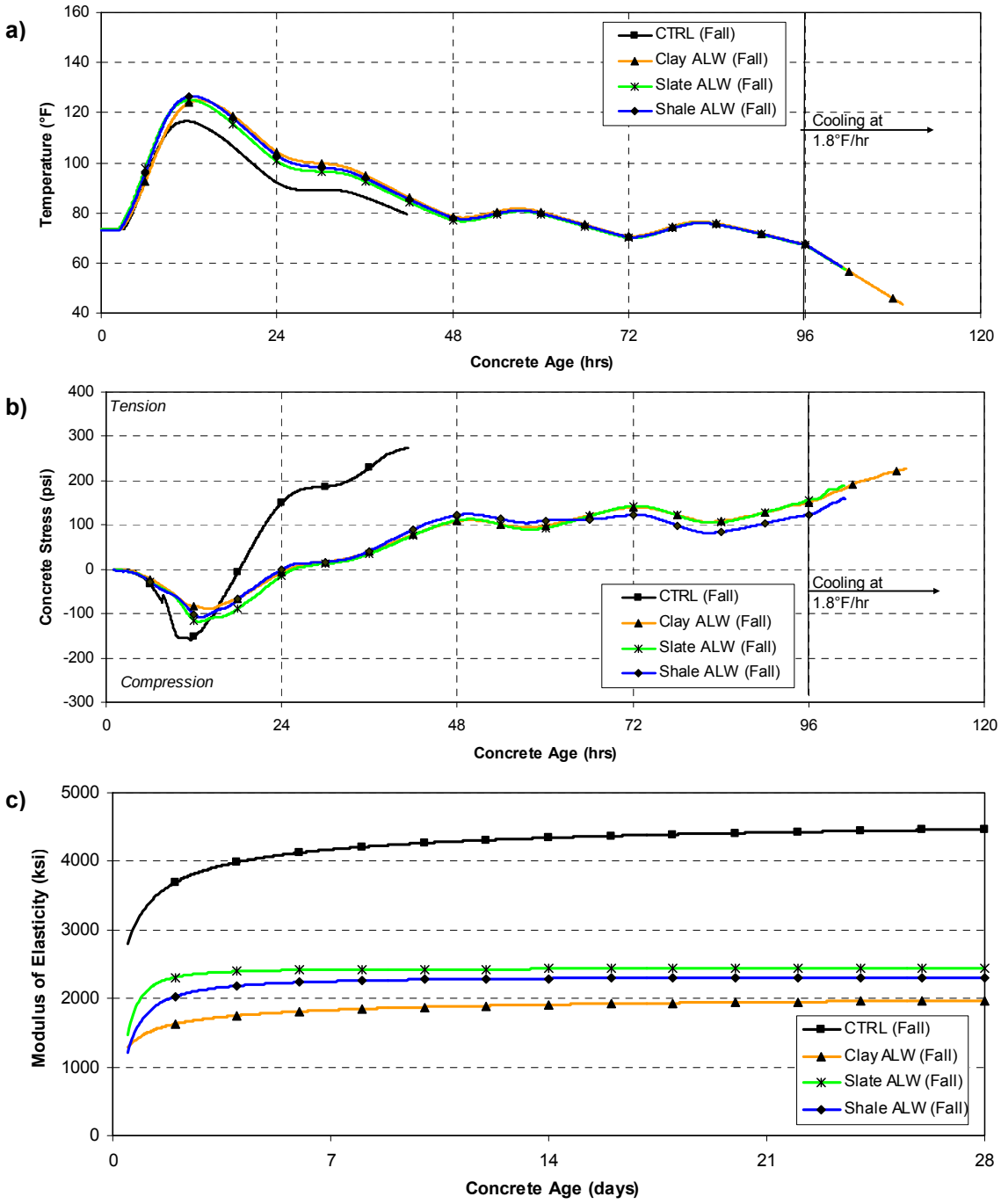

Figure 5-5: Fall placement scenario a) Temperature profiles, b) Match-cured restrained stress development, and c) Modulus of elasticity development for ALW mixtures

The results shown in Figure 5-5b indicate that the use of lightweight aggregates in these all-lightweight concretes significantly delays the occurrence of cracking at early ages in bridge deck concrete applications. The magnitudes of the early-age stresses in all three ALW concretes are significantly reduced when compared to that of the normalweight control concrete. Note that

when the control concrete cracks in tension, the tensile stress developed in the ALW concretes is one-third of the stress in the control concrete. This improvement in cracking behavior is caused by the *significant decrease* in modulus of elasticity, coefficient of thermal expansion, and autogenous shrinkage of the ALW concretes when compared to the normalweight control concrete.

The ALW concretes have similar coefficient of thermal expansion values and curing temperature profiles. As was the case for the SLW concretes, the difference in stress development shown in Figure 5-5b is mostly attributable to differences in modulus of elasticity values of these ALW concretes as shown in Figure 5-5c. For example, because the clay ALW concrete has the lowest stiffness, it requires the most cooling to induce cracking. However, the stress levels measured for all three ALW concretes are very similar, which indicate that they provide similar levels of improvement to the cracking response of the normalweight control concrete.

5.5 EFFECT OF LWA ON PEAK TEMPERATURES

The temperature profiles simulated for an 8-in. thick bridge deck for all the concretes evaluated in this project are shown in Figures 4-3, 4-11, and 4-19. It can be seen that the peak temperatures of the ALW concretes, followed by the SLW concretes, for both placement scenarios and all lightweight aggregate sources are higher than the peak temperatures of the CTRL and IC concretes. This is because the ALW concretes have the lowest thermal diffusivity followed by the SLW concretes, and these concretes have slightly increased portland cement contents. The decrease in thermal diffusivity has an insulating effect that retains the heat of cement hydration causing a greater peak temperature as noted by Maggenti (2007). The temperature peaks of the CTRL and IC concretes are similar, but the peak temperatures of IC concretes are slightly retarded when compared to the CTRL concrete.

5.6 EFFECT OF LIGHTWEIGHT CONCRETE PROPERTIES ON EARLY-AGE STRESS DEVELOPMENT

The restrained stress development results shown in Figures 4-4, 4-12 and 4-20 reveal that the magnitude of the peak temperature alone does not provide a direct indication of the cracking tendency of the concretes. While the magnitude of the peak temperature is important, the decreased coefficient of thermal expansion of the LWA concretes causes a reduced strain per unit temperature change, and the reduced modulus of elasticity of the LWA concretes causes a reduced stress for a given strain. Although the SLW and ALW concretes experience greater peak temperatures, the significant reduction in coefficient of thermal expansion and modulus of

elasticity lead to a reduction in stress and a significant overall delay in early-age cracking in bridge deck concrete applications.

5.7 MODULUS OF ELASTICITY BEHAVIOR COMPARED TO ACI 318 AND AASHTO LRFD ESTIMATES

The ACI 318 (2008) and the AASHTO LRFD Bridge Design Specifications (2007) modulus of elasticity estimation equation was used to calculate the modulus of elasticity of each concrete based on the average measured compressive strength at each testing age and temperature scenario. ACI 318 (2008) clearly states that the density of the concrete should be the calculated based on the equilibrium density, which may be an attempt to obtain a lower-bound estimate of the concrete's modulus of elasticity for design purposes. The estimated compared to the measured modulus of elasticity for the 0.5, 1, 2, 3, 7, and 28-day results, when both the equilibrium density and fresh density are used, are shown in Figures 5-6 and 5-7, respectively.

From the results shown in Figure 5-6, it can be concluded that the ACI 318 (2008) modulus of elasticity equation using the fresh density estimated the stiffness of all the concretes reasonably well. The ACI 318 (2008) modulus of elasticity estimation equation in general under estimates the modulus when the equilibrium density is used, as shown in Figure 5-7. Using the fresh density, the ACI 318 (2008) modulus estimation equation generally under estimates the concretes made with slate, slightly over estimates the stiffness of the concretes made with clay, and estimates the modulus of the shale concrete reasonably well. This is due to the modulus of the slate being the highest, followed by the shale and then the clay.

The unbiased estimate of the standard deviation of the absolute error can be determined as shown in Equation 5-1 (McCuen 1985). The unbiased estimate of the standard deviation of the absolute error when using the ACI 318 (2008) and the AASHTO LRFD Bridge Design Specifications (2007) modulus of elasticity equation using both the fresh and calculated equilibrium density is presented in Tables 5-1 and 5-2. It can be seen from Tables 5-1 and 5-2 that using the *fresh density* in the ACI 318 (2008) and the AASHTO LRFD Bridge Design Specifications (2007) modulus of elasticity estimation equation produces a lower absolute error and thus better predicts the modulus of elasticity of all the mixtures.

$$S_j = \sqrt{\frac{1}{n-1}\sum_{i}^{n}\Delta_i^2} \quad \text{..... Equation 5-1}$$

where, S_j = unbiased estimate of the standard deviation (ksi),

n = number of data points (unitless), and

Δ_i = absolute error (ksi).

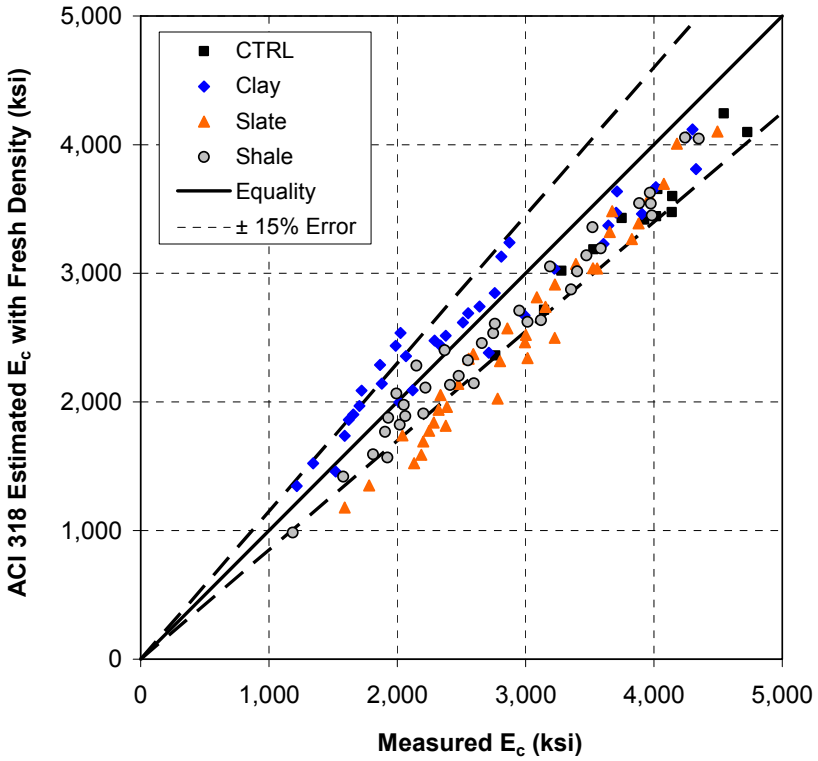

Figure 5-6: Measured modulus of elasticity compared to ACI 318 predicted with *fresh density*

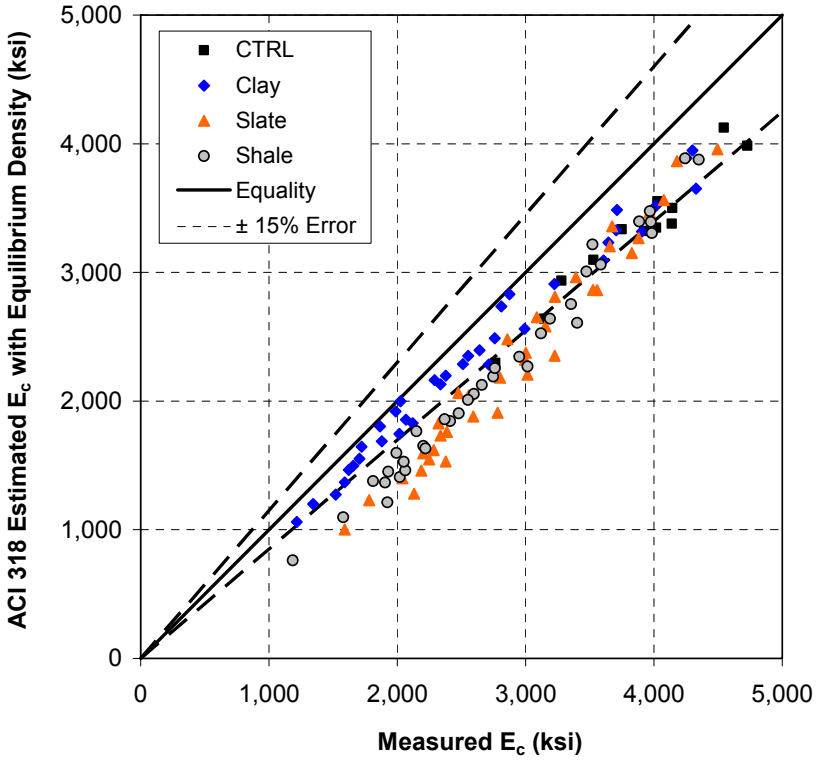

Figure 5-7: Measured modulus of elasticity compared to ACI 318 predicted with *equilibrium density*

Table 5-1: Unbiased estimate of standard deviation of absolute error for modulus of elasticity estimation equations per source material

Density used for E_c Estimate	S_j for E_c Estimate (ksi)			
	CTRL	Slate	Clay	Shale
E_c Estimated with Fresh Density	484	456	277	290
E_c Estimated with Equilibrium Density	579	624	303	553

Table 5-2: Unbiased estimate of standard deviation of absolute error for modulus of elasticity estimation equations per mixture type

Density used for E_c Estimate	S_j for E_c Estimate (ksi)			
	CTRL	IC	SLW	ALW
E_c Estimated with Fresh Density	484	361	364	326
E_c Estimated with Equilibrium Density	579	488	538	629

5.8 SPLITTING TENSILE STRENGTH BEHAVIOR COMPARED TO ACI ESTIMATES

The ACI 207.2R (1995) and ACI 207.1R (1996) splitting tensile strength estimation equations were used to estimate the measured splitting tensile strength based on the measured compressive strength test results. The 1, 2, 3, 7 and 28-day measured splitting tensile strengths compared to the results obtained from both ACI 207 estimation equations are shown in Figure 5-8.

The unbiased estimate of the standard deviation of the absolute error when using both ACI 207 estimation equations are presented in Tables 5-3 and 5-4. Because the control concrete contained coarse aggregate that was smooth river gravel, the splitting tensile strength estimated with both ACI 207 expressions is generally greater than the measured strength. For the same reason, the measured splitting tensile strengths of the IC concrete are also generally overestimated. As the amount of LWA used in the concrete is increased, the predictions of ACI 207.2R and ACI 207.1R improve, as shown in Table 5-4. From Tables 5-3 and 5-4 it can be seen that the splitting tensile strength formulations of ACI 207.2R and ACI 207.1R both provide adequate estimates of the splitting tensile strength of all the concretes made with LWA.

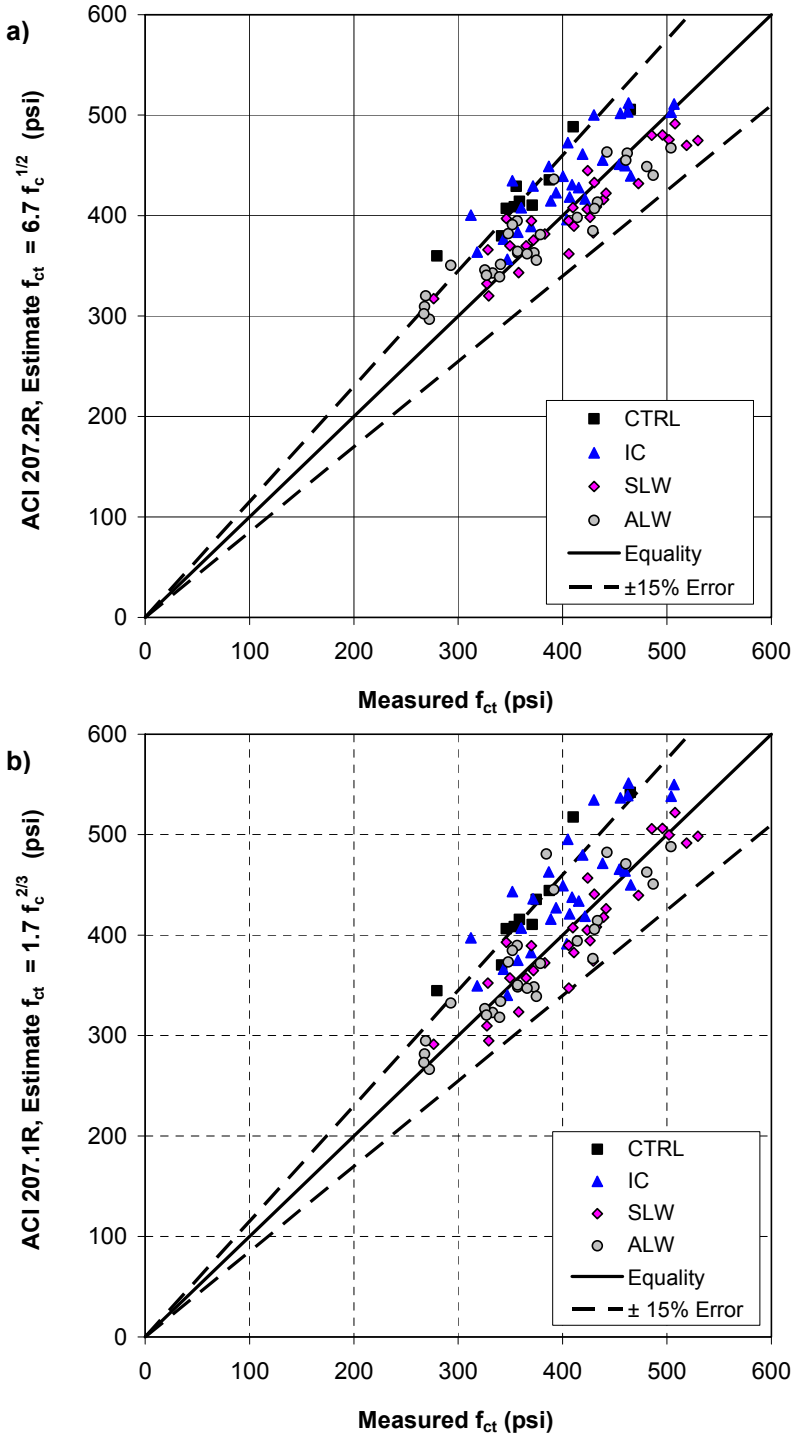

Figure 5-8: Measured splitting tensile strength compared to a) ACI 207.2R and b) ACI 207.1R estimates

Table 5-3: Unbiased estimate of standard deviation of absolute error for splitting tensile strength estimation equations for each source material

Splitting Tensile Strength Estimation Model	S_j for f_{ct} Estimate (psi)			
	CTRL	Slate	Clay	Shale
$6.7\times f_c^{0.5}$	43	26	39	38
$1.7\times f_c^{2/3}$	47	30	40	46

Table 5-4: Unbiased estimate of standard deviation of absolute error for splitting tensile strength estimation equations for each mixtures type

Splitting Tensile Strength Estimation Model	S_j for f_{ct} Estimate (psi)			
	CTRL	IC	SLW	ALW
$6.7\times f_c^{0.5}$	43	42	33	28
$1.7\times f_c^{2/3}$	47	54	31	27

The 1, 2, 3, 7 and 28-day splitting tensile strength data compared to the ACI 318 lightweight modification factor (λ) is presented in Figure 5-9. The lines on Figure 5-9 represent the ACI 318 (2008) and AASHTO (2007) specified lightweight modification factors for SLW (λ = 0.85) and ALW (λ = 0.75) concretes when the splitting tensile strength data are unavailable. From Figure 5-9, it can be seen that the measured splitting tensile strength results for all SLW concretes are above the 0.85 modification factor line and the measured splitting tensile strength results for all ALW concrete are above the 0.75 modification factor line. The average calculated lambda values for each mixture type is shown in Table 5-5. Based on these results, it may be concluded that the ACI 318 (2008) and AASHTO (2007) lightweight modification factors are very conservative for the lightweight aggregate concretes tested in this study.

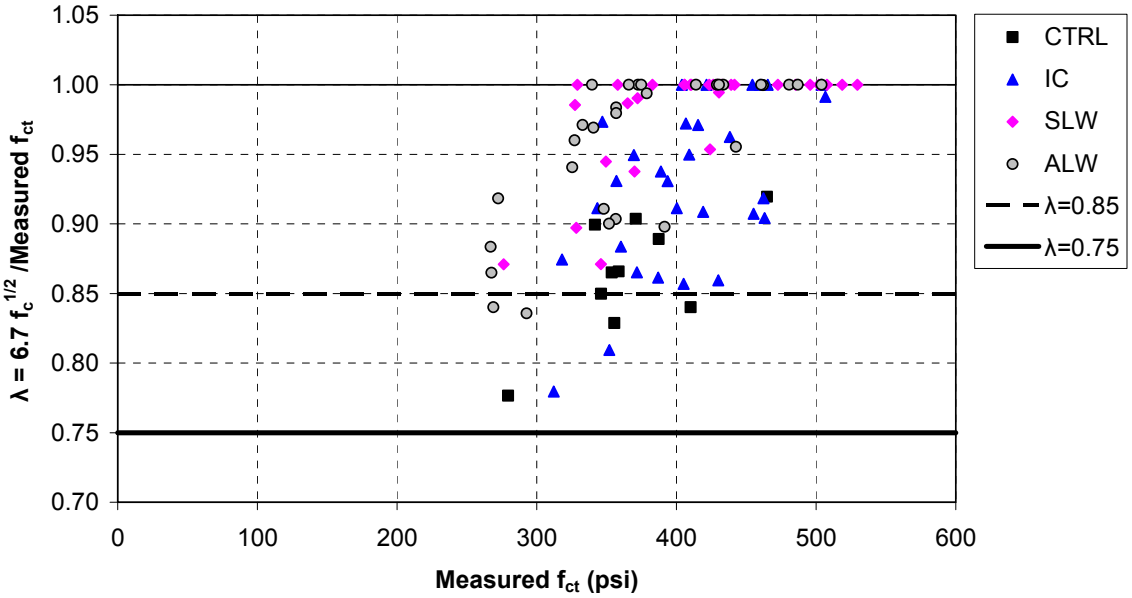

Figure 5-9: Measured splitting tensile strength compared to ACI 318 (2008) and AASHTO (2007) lightweight modification factors

Table 5-5: Average lightweight modification (λ) of each mixture type

Lightweight Modification Factor	Mixture Type			
	CTRL	IC	SLW	ALW
ACI 318 and AASHTO Specified without f_{ct} Data	1.00	1.00	0.85	0.75
Average Lightweight Modification Factor (λ)	0.86	0.93	0.98	0.96

Chapter 6

Conclusions and Recommendations

6.1 SUMMARY OF WORK

Early-age cracking in bridge decks is a severe problem that may reduce functional life of the structure. In this project, the effect of using lightweight aggregate on the cracking tendency of bridge deck concrete was evaluated by cracking frame testing techniques. Cracking frames measure the development of stresses due to thermal and autogenous shrinkage effects from setting until the onset of cracking. Restrained and unrestrained concrete specimens were tested under temperature conditions that match those in an 8-in. thick bridge deck and under isothermal curing conditions.

Expanded shale, clay, and slate lightweight coarse and fine aggregates were evaluated in this study. Normalweight, internal curing (IC), sand-lightweight (SLW), and all-lightweight (ALW) concretes were made in the laboratory and their early-age behavior evaluated. The normalweight concrete used is a typical 0.42 water to cement ratio mixture used in bridge deck applications in the Southeastern United States. The IC mixture is similar to the normalweight mixture, except that a fraction of the normalweight fine aggregate was replaced with pre-wetted lightweight fine aggregate. Note that the amount of lightweight aggregate added to the IC mixture was selected to obtain a concrete with an equilibrium density of 135 lb/ft^3, which allows this mixture to be classified as "normalweight concrete" as per the AASHTO LRFD Bridge Design Specifications (2007).

Each concrete was made and cured under conditions that simulate summer and fall placement conditions in the southeastern parts of the United States. Ten different concretes were produced and tested at two different curing conditions. Additionally, for each mixture and placement condition, 24 cylinders were cast and tested for compressive strength, splitting tensile strength, and modulus of elasticity to assess the development of these properties over time. The coefficient of thermal expansion of the hardened concrete was also assessed with a test setup similar to that required by AASHTO T 336 (2009).

6.2 CONCLUSIONS

6.2.1 Effect of Using Lightweight Aggregates on Concrete Properties

From this research, the following conclusions can be made about the effect of using lightweight aggregate on concrete properties:

1. Increasing the amount of pre-wetted lightweight aggregate in the concrete systematically decreases the density and thus the modulus of elasticity of the concrete. By using the *fresh* density and Equation 2-2 found in ACI 318 (2008), the density and compressive strength can be used to estimate, with reasonable accuracy, the modulus of elasticity of all the concretes made with lightweight aggregate.
2. In general, the compressive strength of the internal curing concretes was slightly higher at all ages than that of the normalweight control concrete. The compressive strength development of the sand-lightweight concretes was similar to that of the normalweight control concrete. Whereas, the compressive strength for the all-lightweight concretes were approximately 13 to 19% lower when compared to that of the normalweight control concrete.
3. All internal curing and sand-lightweight concretes exhibited an increase in splitting tensile strength when compared to the normalweight control concrete.
4. The slate all-lightweight concrete has a decreased splitting tensile strength up to an age of approximately 7 days when compared to the normalweight control concrete. Whereas, both the clay and shale all-lightweight concretes have a similar or slightly increased splitting tensile strength when compared to the normalweight control concrete. The difference in the splitting tensile strength results of the all-lightweight concretes may be related to the particle packing of the slate all-lightweight mixture used in this study.
5. The equations of ACI 207.2R (1995) and ACI 207.1R to estimate the splitting tensile both provide accurate estimates for all of the concretes made with lightweight aggregate.
6. The ACI 318 (2008) and AASHTO (2007) lightweight modification factor (λ factor) to estimate the splitting tensile strength from a known compressive strength is very conservative for the lightweight aggregate concretes tested in this study.
7. Increasing the amount of pre-wetted lightweight aggregate in the concrete systematically decreases the coefficient of thermal expansion. There is a reduction of 15 % and 30 % in coefficient of thermal expansion for the sand-lightweight and all-lightweight concretes, respectively, when compared to the normalweight control concrete.
8. Increasing the amount of lightweight aggregate in the mixture decreases the concrete's thermal diffusivity, which resulted in an increase in peak hydration temperatures.

6.2.2 Early-Age Concrete Behavior

From this research, the following conclusions can be made about the effect of using lightweight aggregate on the cracking tendency and autogenous shrinkage of concrete:

1. Higher placement and curing temperatures result in higher thermal stresses. Decreasing the placement and curing temperature can reduce tensile stresses and delay cracking.

2. The time to cracking for all concretes made with LWA when placed under *summer* placement conditions is *greater* than the time to cracking of the normalweight concrete when placed under *fall* conditions. This indicates that the use of pre-wetted LWA may be especially beneficial during summer time placement conditions to minimize the occurrence of cracking at early ages in bridge deck applications.
3. The use of pre-wetted lightweight aggregates in concrete can reduce or eliminate the stress development caused by autogenous shrinkage. The decrease in autogenous stresses is due to internal curing, because water is desorbed from the lightweight aggregates to fill capillary voids formed by chemical shrinkage.
4. Internal curing concrete made with pre-wetted lightweight aggregate experienced *reduced* stress development due to autogenous shrinkage effects when compared to the normalweight concrete. Since the sand-lightweight and all-lightweight concretes can supply more internal curing water, they cause a greater reduction in tensile stresses due to autogenous shrinkage effects than the internal curing concretes. The sand-lightweight and all-lightweight concretes used in this study completely prevented the development of tensile stresses due to autogenous shrinkage effects.
5. The use of lightweight aggregates to produce internal curing concretes with a density of 135 lb/ft^3 delays the occurrence of cracking at early ages in bridge deck concrete applications when compared to the normalweight control concrete. This improvement in cracking behavior is attributed to the *increased* tensile strength and *decrease* in modulus of elasticity, coefficient of thermal expansion, and autogenous shrinkage of the internal curing concretes when compared to the normalweight control concrete.
6. The use of sand-lightweight and all-lightweight concretes significantly delays the occurrence of cracking at early ages in bridge deck concrete applications when compared to the normalweight control concrete. Although the sand-lightweight and all-lightweight concretes experience greater peak temperatures, the significant reduction in coefficient of thermal expansion and modulus of elasticity lead to a significant overall delay in early-age cracking in bridge deck concrete applications.
7. When compared to a normalweight control concrete, the introduction of lightweight aggregates in concrete effectively delays the occurrence of cracking at early ages in bridge deck applications.

6.3 RECOMMENDATIONS FOR FUTURE RESEARCH

The following recommendations are offered for future research:

1. It is possible that the difference in splitting tensile strength results of the all-lightweight concretes is related to differences in the particle packing the all-lightweight mixtures evaluated. The effect of particle packing on the properties of all-lightweight concrete should be evaluated to determine its effect.
2. The thermal properties of the concretes made with lightweight aggregates were back-calculated from semi-adiabatic calorimeter results and were thus not directly measured. If it is deemed necessary to model the in-place temperature of various types of lightweight concretes, then it is recommended that the thermal properties of these concretes be determined by standardized ASTM test methods.
3. The experimental program used in this study did not evaluate the effect that the use of lightweight aggregate will have on drying shrinkage and its effect on the long-term performance of bridge decks should be evaluated.

References

AASHTO T 336. 2009. *Standard Method of Test for Coefficient of Thermal Expansion of Hydraulic Cement Concrete*. Washington D.C.: American Association of State Highway and Transportation Officials.

AASHTO. 2007. *LRFD Bridge Design Specifications*. 4th Edition with 2009 interim revisions. Washington D.C.: American Association of State Highway and Transportation Officials.

ACI 318. 2008. *Building Code Requirements for Structural Concrete and Commentary.* Farmington Hills, MI, American Concrete Institute.

ACI 207.1R. 1996. *Mass Concrete.* Farmington Hills, MI, American Concrete Institute.

ACI 207.2R. 1995. *Effect of Restraint, Volume Change, and Reinforcement on Cracking of Mass Concrete.* Farmington Hills, MI, American Concrete Institute.

ACI 211.1R. 1991. *Standard Practice for Selecting Proportions for Normal, Heavyweight, and Mass Concrete.* Farmington Hills, MI, American Concrete Institute.

Bentz, D.P., P. Lura, and J.W. Roberts. 2005. Mixture Proportioning for Internal Curing. *Concrete International,* Vol. 27, No. 2, pp. 35-40.

Bjøntegaard, Ø. 1999. *Thermal Dilation and Autogenous Deformation as Driving Forces to Self-Induced Stresses in High Performance Concrete*. Doctoral Thesis. Norwegian University of Science and Technology, Division of Structural Engineering,

Breitenbücher, R., and M. Mangold. 1994. Minimization of Thermal Cracking in Concrete at Early Ages. In RILEM Proceedings 25*, Thermal Cracking in Concrete at Early Ages*, ed. R. Springenschmid, London, E & FN Spon, pp. 205-212.

Byard, B.E, A.K. Schindler, and R.W. Barnes. 2010. Cracking Tendency of Lightweight Concrete in Bridge Deck Applications, *Proceedings of the Concrete Bridge Conference*, Phoenix, AZ.

Byard, B.E, A.K. Schindler, R.W. Barnes, and A. Rao. 2010. Cracking Tendency of Bridge Deck Concrete, *Journal of the Transportation Research Board*, TRR No. 2164, pp. 122-131.

Castro, J., L. Keiser, M. Golias, and W.J. Weiss. 2011. Absorption and Desorption of Fine Lightweight Aggregate for Applications to Internally Cured Concrete Mixtures. *Cement and Concrete Composites,* submitted for review.

Chandra, S., and L. Berntsson. 2002. *Lightweight Aggregate Concrete.* Noyes Publications, Norwich, NY.

Darwin, D., and J. Browning. 2008. Construction of Low Cracking High Performance Concrete (LC-HPC) Bridge Decks: Field Experience. *Proceedings of the Concrete Bridge Conference*, St. Louis, MO.

Delatte, N., D. Crowl, E. Mack, and J. Cleary. 2008. Evaluating High Absorptive Materials to Improve Internal Curing of Concrete. In ACI Special Publication 256*, Internal Curing of High-Performance Concretes*, ed. D. Bentz and B. Mohr. Farmington Hills, MI. 2008

Emborg, M. 1989. *Thermal Stresses in Concrete Structures at Early Ages*. Doctoral Thesis. Luleå University of Technology, Division of Structural Engineering.

FHWA. 2008. *Cast-in-Place High Performance Concrete.* Federal Highway Administration High Performance Concrete Website, http://knowledge.fhwa.dot.gov/cops/hpcx.nsf/home?openform&Group=HPC%20Cast-in-Place%20Construction&tab=WIP, accessed 2008.

Harmon, K.S. 2000. Physical Characteristics of Rotary Kiln Expanded Slate Lightweight Aggregate, *Proceeding of the 2nd International Symposium on Structural Lightweight Aggregate Concrete*, Kristiansand, Norway, June 18-22, pp. 574- 583.

Henkensiefken, R. 2008. *Internal Curing in Cementitious Systems made using Saturated Lightweight Aggregate.* Masters Thesis. Purdue University.

Holt, E. 2001. *Early Age Autogenous Shrinkage of Concrete*. Doctoral Thesis. The University of Washington in Seattle.

Krauss, P.D., and E.A. Rogalla. 1996. *Transverse Cracking in Newly Constructed Bridge Decks*. NCHRP Report 380, Transportation Research Board, National Research Council, Washington, D.C.

Lamond, J.F., and J.H. Pielert. 2006. *Significance of Tests and Properties of Concrete and Concrete-Making Materials*. ASTM Publication STP 169D. American Society of Testing Materials, West Conshohocken, PA.

Lura, P. 2003. *Autogenous Deformation and Internal Curing of Concrete.* Doctoral Thesis. Technical University of Delft.

Maggenti, R. 2007. From Passive to Active Thermal Control. *Concrete International,* Vol. 29, No. 2, pp. 24-30.

Mangold, M. 1998. Methods for Experimental Determination of Thermal Stresses and Crack Sensitivity in the Laboratory. In RILEM Report 15, *Prevention of Thermal Cracking in Concrete at Early Ages*, ed. R. Springenschmid, London, E & FN Spon, pp. 26-39.

McCuen, R.H. 1985. *Statistical Methods for Engineers*, Prentice-Hall. Upper Saddle River, NJ.

Meadows, J.L. 2007. *Early-Age Cracking of Mass Concrete Structures.* Master of Science Thesis. Auburn University.

Mehta, P.K., and P.J.M. Monteiro. 2006. *Concrete: Microstructure, Properties, and Materials*. 3rd Edition, McGraw-Hill, Inc. New York, NY.

Mindess, S., J.F. Young, and D. Darwin. 2002. *Concrete*. 2nd Edition, Prentice Hall, Upper Saddle River, NJ.

Poole, J.L, K.A. Riding, R.A. Browne, and A.K. Schindler. 2006. Temperature Management of Mass Concrete Structures. *Concrete Construction Magazine*.

RILEM Technical Committee 119-TCE. 1998. Testing of the Cracking Tendency of Concrete at Early Ages in the Cracking Frame Test. In RILEM Report 15, *Prevention of Thermal Cracking in Concrete at Early Ages*, ed. R. Springenschmid, London, E & FN Spon, pp. 315-339.

RILEM Technical Committee 196-ICC. 2007. *Internal Curing of Concrete*. ed. K. Kovler and O.M. Jensen, Bagneux, RILEM Publications S.A.R.L.

Schindler, A.K., and B.F. McCullough. 2002. The Importance of Concrete Temperature Control During Concrete Pavement Construction in Hot Weather Conditions. *Journal of the Transportation Research Board*, TRR No. 1813, pp. 3-10.

Schindler, A.K. 2002. Prediction of Concrete Setting. Proceedings of the RILEM International Symposium on Advances in Concrete through Science and Engineering, Edited by J. Weiss, K. Kovler, J. Marchand, and S. Mindess, RILEM Publications SARL, Illinois.

Schindler, A.K., and K.J. Folliard. 2005. Heat of Hydration Models for Cementitious Materials. *ACI Materials Journal*, Vol. 102, No. 1, pp. 24-33.

Weakley, R.W. 2009. *Evaluation of Semi-Adiabatic Calorimetry to Quantify Concrete Setting.* Master of Science Thesis. Auburn University, Alabama.

Wight, J.K., and J.G. MacGregor. 2009. *Reinforced Concrete.* 5th Edition Prentice Hall, Upper Saddle River, NJ.

Appendix A

Aggregate Gradations

Table A-1: Coarse aggregate gradations

Sieve Size	Percent Passing			
	Normalweight Shorter Alabama	**Slate** Gold Hill North Carolina	**Clay** Frazier Park California	**Shale** New Market Missouri
1 in.	100.0	–	–	–
¾ in.	96.9	100.0	–	100.0
½ in.	63.7	32.7	100.0	99.3
3/8 in.	36.5	11.4	90.6	76.3
# 4	3.7	1.9	38.0	13.7
# 8	0.5	1.6	13.2	2.0
# 16	–	–	1.0	1.1

Table A-2: Fine aggregate gradations

Sieve Size	Percent Passing					
	Normalweight Shorter Alabama	**Slate**		**Clay**		**Shale** New Market Missouri
		MS 16	D Tank	Source 1	Maximizer	
½ in.	100.0	–	–	–	100.0	–
3/8 in.	100.0	100.0	100.0	100.0	99.9	100.0
# 4	99.8	100.0	96.0	100.0	80.6	97.6
# 8	94.9	99.6	67.7	93.1	48.4	77.0
# 16	84.8	64.1	43.6	55.0	22.3	53.4
# 30	60.8	35.3	27.8	27.3	9.6	33.0
# 50	13.3	12.8	18.6	13.7	4.7	21.7
# 100	1.6	3.6	12.2	5.8	2.2	15.2
Pan	0.0	1.4	0.3	0.3	0.2	0.0

Appendix B

Mechanical Property Results

Table B-1: Match-cured compressive strength results for all mixtures

Mixture	Compressive Strength (psi)					
	½ day	1 day	2 days	3 days	7 days	28 days
Control RG (Fall)	1770	2890	3690	3720	4230	5700
Control RG (Sum)	2330	3210	3750	3820	4100	5310
Slate IC (Fall)	1590	2950	3700	3980	4740	5840
Slate IC (Sum)	2300	3280	3830	4210	4490	5580
Slate SLW (Fall)	1590	2280	3050	3470	4170	5140
Slate SLW (Sum)	2090	2980	3380	3540	4410	5130
Slate ALW (Fall)	1180	1960	2560	2790	2860	4760
Slate ALW (Sum)	1540	2130	2670	3250	3560	4610
Clay IC (Fall)	1950	3160	3900	4130	4530	5820
Clay IC (Sum)	2450	3570	4110	4620	4980	5640
Clay SLW (Fall)	1090	2240	3050	3240	3850	5020
Clay SLW (Sum)	2050	3140	3510	3710	4160	5380
Clay ALW (Fall)	1370	2280	2620	2930	3300	4860
Clay ALW (Sum)	1750	2730	3470	4200	3960	4490
Shale IC (Fall)	1580	2830	3500	3870	4310	5610
Shale IC (Sum)	2380	3380	4080	4300	4510	5640
Shale SLW (Fall)	1370	2460	2920	3260	3720	5040
Shale SLW (Sum)	1970	2620	3470	3680	3970	4920
Shale ALW (Fall)	800	2040	2750	2960	3690	4780
Shale ALW (Sum)	1670	2590	2920	3240	3530	4320

Table B-2: Match-cured splitting tensile strength results for all mixtures

Mixture	Splitting Tensile Strength (psi)					
	½ day	1 day	2 days	3 days	7 days	28 days
Control RG (Fall)	200	280	345	355	385	465
Control RG (Sum)	245	340	370	360	375	410
Slate IC (Fall)	205	320	360	395	420	465
Slate IC (Sum)	245	355	390	350	385	430
Slate SLW (Fall)	200	330	350	370	430	495
Slate SLW (Sum)	225	330	410	425	425	485
Slate ALW (Fall)	170	270	340	375	375	462
Slate ALW (Sum)	210	270	325	350	350	460
Clay IC (Fall)	235	345	405	410	455	505
Clay IC (Sum)	250	310	370	440	440	460
Clay SLW (Fall)	130	275	365	385	440	530
Clay SLW (Sum)	230	355	370	410	475	510
Clay ALW (Fall)	165	270	335	355	430	505
Clay ALW (Sum)	215	295	355	390	435	480
Shale IC (Fall)	215	345	405	420	465	495
Shale IC (Sum)	230	370	400	400	440	505
Shale SLW (Fall)	200	325	405	430	460	500
Shale SLW (Sum)	250	360	405	425	440	520
Shale ALW (Fall)	105	265	340	355	430	445
Shale ALW (Sum)	205	325	365	380	415	485

Table B-3: Match-cured modulus of elasticity results for all mixtures

Mixture	Modulus of Elasticity (ksi)					
	½ day	1 day	2 days	3 days	7 days	28 days
Control RG (Fall)	2750	3300	3900	3750	4050	4550
Control RG (Sum)	3150	3550	4000	4150	4150	4750
Slate IC (Fall)	2500	3250	3850	3900	4100	4500
Slate IC (Sum)	2850	3400	3650	3650	3950	4200
Slate SLW (Fall)	2200	2600	2900	3050	3150	3500
Slate SLW (Sum)	2300	2800	3000	3000	3100	3550
Slate ALW (Fall)	1450	2100	2300	2300	2450	2450
Slate ALW (Sum)	1750	2100	2250	2350	2400	2650
Clay IC (Fall)	2700	3200	3650	3700	3700	4300
Clay IC (Sum)	3000	3600	3900	4000	4050	4250
Clay SLW (Fall)	1500	2100	2350	2400	2650	2800
Clay SLW (Sum)	2000	2300	2500	2550	2750	2850
Clay ALW (Fall)	1200	1600	1600	1700	1700	2050
Clay ALW (Sum)	1350	1650	1750	2050	1950	2000
Shale IC (Fall)	2600	3350	3600	3500	3900	4350
Shale IC (Sum)	3100	3450	3800	4000	3950	4250
Shale SLW (Fall)	1800	2400	2550	2650	3000	3200
Shale SLW (Sum)	2200	2500	2750	2750	2950	3400
Shale ALW (Fall)	1200	1800	2000	2050	2200	2350
Shale ALW (Sum)	1600	1800	1950	2050	2050	2150